UNIVERSITY OF OKLAHOMA

GRADUATE COLLEGE

PERFORMANCE AND ENVIRONMENTAL IMPACT ASSESSMENT OF AGRICULTURAL WASTE-BASED SORBENTS FOR PHOSPHORUS RECOVERY AND REUSE

A DISSERTATION

SUBMITTED TO THE GRADUATE FACULTY

in partial fulfillment of the requirements for the

Degree of

DOCTOR OF PHILOSOPHY

By

YIFAN DING
Norman, Oklahoma
2023

PERFORMANCE AND ENVIRONMENTAL IMPACT ASSESSMENT OF AGRICULTURAL WASTE-BASED SORBENTS FOR PHOSPHORUS RECOVERY AND REUSE

A DISSERTATION APPROVED FOR THE

SCHOOL OF CIVIL ENGINEERING AND ENVIRONMENTAL SCIENCE

BY THE COMMITTEE CONSISTING OF

Dr. Elizabeth C. Butler, Chair

Dr. David A. Sabatini, Co-chair

Dr. Andrew Elwood Madden

Dr. Robert W. Nairn

Dr. Jason Vogel

DEDICATION

This dissertation is dedicated to the memory of my late grandfather.

Acknowledgements

During the first days of my program, new and friendly faces asked me a same question: why Oklahoma? I think now I have the definite answer for them all. But before that, I would like to express my sincerest gratitude to my advisor Dr. Elizabeth Butler and my co-advisor Dr. David Sabatini. This research and my program would not be possible without the advice, mentoring, and encouragement from them.

Dr. Butler has been leading me through the power of example since day one. Her professionalism and incredible work ethic will always be inspiring to me, and I would use them to drive myself through my future endeavor. I thank Dr. Butler for her undivided attention and dedication in these five years. Through the questions for me to dig deeper, the solutions to obstacles to move forward, the comments for drafts to polish to their best, the resources of knowledge to explore broader, and the ultimate patience for progress, I learned how to be a leader and how to be a better researcher. Through the extremely well-organized course materials and the timely attentiveness to students' problems, I can only hope I gathered the skills that I can apply if I have the privilege to be a professor in the future. Honor is all mine to be one of her students.

I owe many thanks to Dr. Sabatini. I will always admire his profuse knowledge, rich experience, colorful stories, multi-dimensional lectures, life wisdom, and the deep love to the world. His work on water issues in the developing world has been an eye-opener for me. It is a noble work where I found much inspiration and hope one day, I can contribute my own force. I

appreciate Dr. Sabatini for the heartwarming hospitality, the exciting invitation to the sport event, and the endless encouragement. It was my privilege to study and work with him.

I am very grateful for Dr. Andrew Elwood Madden, Dr. Robert Nairn, and Dr. Jason Vogel taking the time serving as my committee members and refining my dissertation. I thank Dr. Madden for his training in me on conducting mineralogical characterization. I appreciate his trust and permission allowing me to use the XRD lab equipment and his kind help on analyzing XRD data remotely during the COVID-19 pandemic lockdown. Dr. Nairn and Dr. Vogel's research broadened my horizon through seminars and conference presentations. I admire Dr. Nairn's work on ecosystem restoration both from a technical perspective and how his work is involved with the people within the ecosystem. It is always bigger than remediation itself. I also found Dr. Vogel's work relating wastewater with epidemiology such as coronavirus very inspiring, and his way of presenting academic research to broad audience will always be an excellent example. I enjoyed every each of the personal encounter with all my committee members, as they always exude care, kindness, and warmth.

I am indebted to all the CEES staff members, with particular thanks to Marlene "Molly" Smith, Laura Swan, Deanna Amidon. Molly has been there for me for all kinds of workplace issues since the moment I started, and her infectious smile lit my soul numerous times. I am also grateful for having Laura and Deanna, for they have made my work much easier and enjoyable through their prompt efforts. Thank them all and I enjoyed every trip to their offices and every email exchange.

I would like to give a special mention to all the professors and personnel offering help to me on completing my program. Thank Dr. Tohren Kibbey for allowing me to use the spectrophotometer in his lab for four years; thank Dr. Mark Nanny for his great lecture on

aquatic chemistry enhancing my knowledge; thank Dr. Preston Larson for his training on SEM, SEM-EDS; thank Dr. Scott Russell for his guidance on using TEM; and thank Dr. Gerald Miller for the access to the sifter in his lab. Thank Dr. Tiantian Yang for giving me academic and career advice. Thank Anna McClung and Laduska Sells at the USDA Dale Bumpers National Rice Research Center in Stuttgart, Arkansas for providing the biomass.

I would like to acknowledge the financial support by Agriculture and Food Research Initiative (AFRI) grant number 2018-67020-27805 from the USDA National Institute of Food and Agriculture.

In five years of living here, my fellow graduate students and my friends have been the source of encouragement, joy, sense of relaxation, and most of all, feeling of home on a foreign land. I was very lucky to have Anisha Nijhawan, Phaodee “Tam” Parichat, Nusrat Sharmin, Philip Deal, Ian Thom, and Sarah Jones as my partners. I would ask no better people to fight by my side. I wish all the best to them. I also cherish the friendship offered by Ruichun Liu, Huang Chen, Shijun Chen, Sirawit “Singto” Thanomsap, Shang Gao, and many others. They were my “wings” when I first moved here with no personal transportation and my buddies whenever there were things to share and witness. I look forward to meeting with them again. And I like to send my best wishes to all my basketball teammates, the weekly basketball game with them was one of my most expected things throughout the week. Speaking of basketball, allow me to single out my friend Huang Chen. The whole year we spent on outdoor court playing 1v1 was nothing less than the best medicine during the depressing pandemic. Last but certainly not least, my dearest friends back in China were my “cloud-harbor” and my origin of limitless happiness and cure, and I cannot wait to hug them all again: Shunyu Yao, Kaiwen Ping, Tianqi Zhang, Zhengqiu Yang, Shouchuan Zhang, Meng Ma, and many others I wish I had the capacity to list them all.

I wish I could have the proper estimation of how much gratitude I have towards my parents. They constantly offer their endless unconditional love and support to me and show their confidence in me to reach for higher and further. I could never wish to return with the same amount, but I will never cease to try. My dearest and bravest mother endured great pain from cancer during the years I could not have spent by her side, and she never doubted me for a second for what I can achieve. And I also have no doubt that she can overcome the hardest hardship in the universe. My most loving and toughest father is the rock of our family, and single-handedly keeps on bringing hope and joy to us every second of the day. I wish I could be half of a man he has been and I would be satisfied. I have the best parents a child can ever ask for, and with every heartbeat in my chest, I shall carry the love and faith they have in me to eternity.

Lastly, I would love to express my unending gratitude to my elixir my loving wife, Mengyao Lyu, who has suffered for a great deal both mentally and physically over the years but never stopped believing in me and giving me the unwavering support. She is the reason why I always have a smile on my face walking home from work and have the strength to conquer adversity. Her heart is as pure as a crystal and as inspiring as her own arts. I am so grateful to have her along the journey.

Now, back to the question why Oklahoma. My answer is: why not?

Table of Contents

List of Tables

List of Figures

Abstract

Phosphorus is an essential resource, yet global phosphorous reserves are limited, and increasing quantity of high-grade ore is being mined and turned into fertilizers to meet the increasing demand of food. However, since currently the phosphorus cycle is not closed loop, considerable amounts of excessive phosphorus are discharged from agricultural activities to environment causing eutrophication and wasting the resource. Hence, recovering and reusing phosphorus are key to building a sustainable phosphorus cycle. Materials derived from agricultural wastes such as biochar showed great potential of serving as a matrix for sorbents. Therefore, this research focused on sorbents prepared from agricultural wastes for recovering phosphorus from animal wastewater and reuse as fertilizer. Batch isotherm sorption phosphorus recovery studies and continuous flow column phosphorus release studies were conducted, as well as the life cycle assessment and cost analysis of producing the sorbents.

Biochars with magnesium amendments (referred as Mg-chars hereafter) from $MgCl_2$ were tested in model animal wastewater at different pH conditions. Results showed precipitation as struvite was responsible for phosphorus recovery in model wastewater containing phosphate and ammonium, as confirmed through X-ray Diffraction (XRD). Additionally, since the solubility of struvite decreases with increasing pH, pH 8.0 and 9.0 were more beneficial for struvite formation. Furthermore, alkalinity in wastewater was found to compete with dissolved phosphorus on the sorbent.

Magnesium amendments such as using $MgCl_2$ would often account for the major portion of the total cost producing the sorbents. To find cheaper solutions with similar phosphorus recovery performance, this research tested low-price magnesium sources including natural minerals and industrial by-products. Correspondingly, mineral magnesium hydroxide and bittern,

a residue from sea salt evaporation, were identified as two alternatives for commercial $MgCl_2$ salt. In concentrated animal wastewater at pH 8.0, Mg-char ($Mg(OH)_2$) and Mg-char (bittern) both obtained phosphate recovery capacities over 220 mg P/g through struvite formation.

Additional to biochar, this research also tested materials synthesized from crop waste ashes. First, magnesium silicate minerals were prepared by extracting silicate from rice straw and wheat straw ash and then precipitated using magnesium salt. Even though magnesium silicate worked only slightly poorer than Mg-chars in terms of phosphorus recovery, the interference from dissolved silicate in concentrated wastewater on phosphate analysis was too high. Thus, magnesium silicate minerals were not tested further. Next, calcium silicate hydrate (CSH) was prepared using rice husk ash and calcium hydroxide. Unlike Mg-chars' precipitation dominant phosphorus recovery mechanism, CSH fixed dissolved phosphate through a Langmuir type adsorption with maximum adsorption capacity of 55 mg P/g.

Next, post-phosphorus-exposure Mg-char ($Mg(OH)_2$), Mg-char (bittern), and CSH were selected for phosphorus release test in continuous flow column studies considering the effects of pH and soil minerals goethite and kaolinite. Post-phosphorus-exposure sorbents, or spent sorbents, were collected from phosphorus recovery studies, then added to columns. Spent Mg-char ($Mg(OH)_2$) and Mg-char (bittern) had phosphorus content of 182 and 198 mg P/g, respectively, and spent CSH had 46 mg P/g. Results showed that, first, both spent Mg-chars effectively released over 80 % of the recovered phosphorus within five pore volumes at pH 5.5, 7.0 and 8.5, but CSH needed significantly more pore volumes (time). Second, pH 5.5 and 7.0 yielded similar release characteristics while pH 8.5 was notably slower, which could be attributed to the lower solubility of struvite at higher pH. Third, soil minerals affect dissolved phosphate concentration greatly and goethite had more impact on phosphate availability than

kaolinite. Further, at lower pH conditions, both minerals retained phosphate more than higher pH conditions, which was due to the fact that the further pH was lower than point of zero charge, the more affinity the mineral surface has for attracting phosphate ions.

Finally, this research evaluated the environmental impact of using Mg-char ($Mg(OH)_2$), Mg-char (bittern), and CSH for phosphorus recovery and reuse comparing to commercial fertilizer monoammonium phosphate (MAP) through life cycle assessment (LCA), as well as cost analysis. While results suggested that both Mg-chars had lower environmental impact than MAP, CSH had the greatest environmental impact due to its high chemical inputs and biomass required. Further, Mg-char (bittern) had less impact than Mg-char ($Mg(OH)_2$), illustrating the advantage of using bittern. Moreover, since Mg-chars achieved higher phosphorus release efficiency at lower pH soil, or when greater quantities of phosphorus release were needed for farmland with the same transportation distance, using Mg-chars for phosphorus management and fertilization could be even more advantageous than MAP. Finally, the two Mg-chars can be less expensive than MAP when the transportation cost was minimized or greater amount of phosphorus was needed.

Overall, this research provided knowledge on the use of several sorbents including magnesium amended biochars and silicate minerals that were derived from agricultural wastes for phosphorus recovery and reuse. These sorbents showed high potential as keys to a closed phosphorus cycle, and as substitutions to commercial fertilizers with less environmental impact and lower cost.

Chapter 1 Introduction

1.1 Phosphorus resources

Phosphorus is a nutrient essential and non-substitutable to life on earth (Geissler et al. 2020). The vast majority of phosphorus in use by human activities is through the production and application of fertilizers (Van Vuuren et al. 2010). The availability of phosphorus in soil is critical to crop health and is often the growth-limiting factor (Roy 2017) and thus referred to as "life's bottleneck (Cordell and White 2011)". The crop health is tightly tied with the yield in the world with growing food needs (Cordell et al. 2009, van den Berg et al. 2016, Van Vuuren et al. 2010). In 2021, around 10% of the world population was faced with hunger and 8% was projected to struggle with food insecurity in 2030 (FAO 2022). There is a long history of using phosphorus as an amendment for food growing, and before the industrialization of fertilizer production, wastes such as organic urban wastes, animal excrement, animal bones, and volcanic ash were often applied to the field (Reijnders 2014, Van Vuuren et al. 2010). Correspondingly, guano, a type of bird excrement deposition, contains high content of acid extractable phosphorus (around 21 to 57 g/kg) and has long been used as a valuable resource (Irick et al. 2015, Reijnders 2014). Currently, high grade phosphorus mines are the main source of phosphorus for human activities (Roy 2017), with the majority of phosphorus reserves located in countries such as Morocco, China, and Egypt (USGS 2022).

Awareness that phosphorus is a finite resource sprouted as early as the 19th century, and in the 20th century (Reijnders 2014), examples of depletion were spotted around the globe. For instance, well known is the Pacific island of Nauru which exploited and exported around 80 million tons of guano, leading to the depletion of the resource and the devastation of the local

ecosystem due to over-mining (Reijnders 2014, Scholz and Wellmer 2013, Zowada et al. 2020). Over the years, studies have shown different perspectives on the quantity of global phosphorus reserve and possible depletion timeline as reviewed in (Scholz et al. 2013). Despite the discrepancies, the consensus is that the high-grade sources will continually decline until a closed phosphorus cycle is established (Cooper et al. 2011, Cordell and White 2011, Edixhoven et al. 2014, Scholz et al. 2013, Scholz and Wellmer 2016).

In contrast to the declining high-grade phosphorus resource, the agricultural need for phosphorous continues to increase over the years, and the annual P_2O_5 consumption in 2018 came to over 49 million tons (IFA 2022). However, with such great quantities of phosphorus being utilized, there are phosphorus losses in every step from mining to fertilizer production, crop utilization, and food processing (Cordell and White 2011, Rittmann et al. 2011). It was estimated that over 80% of the mined phosphorus was applied to farmland, out of which 10-40% was incorporated into the harvested crop, and even less reached the end user of food such as humans (Rittmann et al. 2011, Sattari et al. 2012). This means the major portion of the mined phosphorus becomes residual soil phosphorus and lost through the runoff and wastes. Residual soil phosphorus, or some may refer to “legacy phosphorus”, is still available to plants over the years depending on the soil pH, redox conditions, and minerals such as iron and aluminum oxides (Jarvie et al. 2013, Sattari et al. 2012, Sharpley et al. 2013). But the accumulation of soil phosphorus through over-fertilization not only is a waste of resource, but also increases the potential for phosphorus loss and leads to inaccurate phosphorus management responses (Jarvie et al. 2013, Sharpley et al. 2013). With current low-efficiency agricultural practices, soil phosphorus accumulation is around 7 million ton of phosphorus per year (Nagarajan et al. 2020). As for the portion lost to natural waterbodies through runoff and other sources of discharge, it is

no longer available to plants and eventually causes the dilution of the phosphorus resource and series of environmental issues (Nedelciu et al. 2018, Withers et al. 2020). Specifically, eutrophication caused by excessive nutrients supports the growth of algae, which is harmful to the aesthetics of the water and most importantly, lethal to aquatic organisms through the depletion of oxygen and the release of toxins (Li et al. 2020a, Sena et al. 2020). In the past decades, eutrophication is one of the reoccurring environmental issues in countries with highly active agricultural activities such as China (Li et al. 2020a), USA (Turner and Rabalais 1994), and India (Sinha et al. 2017).

With a closer look at agricultural phosphorus, possible losses include farmland leachate and the manure produced by livestock (Nixon 1995). Recoverable phosphorus from global animal production can be more than 17 million tons, which can supply 90% of the global agricultural phosphorus need on a 2015 basis (Kok et al. 2018). Similar to the low utilization efficiency of crops, livestock incorporates dietary phosphorus with low efficiency (~20%) as well (Li et al. 2014). Thus, animal manure wastewater often contains high levels of phosphorus, for instance, a swine wastewater had mean value of 654 mg phosphorus/L reported in (Capdevielle et al. 2013). In addition to the high phosphorus concentration, animal wastewater can have ammonium concentrations as high as over 1,100 mg as nitrogen/L (Foletto et al. 2013, He et al. 2014). Mismanagement of the animal wastes would exacerbate the phosphorus resource dissipation and impact environmental quality.

1.2 Phosphorus recovery and reuse technologies

In efforts to solve the dilemma where phosphorus resource is finite but human activities continue to pull excessive phosphorus into the environment, and to form a sustainable phosphorus cycle, developing effective phosphorus recovery technologies is key so that fertilizer

would eventually depend on the recycled phosphorus rather than the mined high-grade phosphorus rock (Withers et al. 2020). Strategies including adsorption, precipitation, ion exchange, or a combination of processes, have been studied widely (Rittmann et al. 2011). There are other phosphorus recovery technologies involving biological recovery such as in (Zubair et al. 2020), however, biological processes often convert phosphorus into organic form, hence the subsequent reuse might need additional pretreatment (Rittmann et al. 2011). Biological recovery is beyond the scope of this research and thus is not discussed further.

Interactions of phosphate with metal (hydr)oxides is very common in soil (Robles et al. 2020) and many phosphorus recovery materials were inspired based on similar mechanisms (Jiang et al. 2019). Specifically, metal (hydr)oxides can bind phosphate through electrostatic attraction (Lü et al. 2017). Additionally, interactions between phosphate and metal-OH can possibly trigger the ion exchange of surface -OH functional groups and the formation of inner-sphere complexes contributing to adsorption (Ioannou and Dimirkou 1997, Kamiyango et al. 2009, Li et al. 2016, Nobaharan et al. 2021, Sigg and Stumm 1981). Furthermore, metal cations can be released from the minerals and facilitate the precipitation of phosphate (Penn and Warren 2009); however, depending on the metal, the ease of reusing the recovered phosphorus is highly affected by the metal phosphate mineral solubility (Rittmann et al. 2011).

Adsorption-based phosphorus recovery has the advantage that fixed phosphorus can be released through desorption and the sorbents can be regenerated (Robles et al. 2020). Oxides of magnesium (Mg), calcium (Ca), iron (Fe), and aluminum (Al) have been widely tested for the purpose such as in (Gérard 2016, Li et al. 2020b, Zhang et al. 2012). Metal oxides have a range of point of zero charge (pH_{pzc}) values, for instance iron oxides normally have pH_{pzc} values with a range of 7 to 9 (Schwertmann and Fechter 1982) and for aluminum (hydr)oxides the pH_{pzc} ranges

from 5 to 9 (Guaya et al. 2015). Hence, the pH condition is a determining factor for the adsorption to take place. Specifically, the lower the pH relative to the pH_{pzc}, the more positively charged surface will recover more phosphate. In addition, changing pH alters the speciation of phosphate, and with higher pH, phosphate is more deprotonated showing stronger affinity towards positively charged surfaces.

Precipitation-based phosphorus recovery has largely focused on the formation of struvite ($MgNH_4PO_4 \cdot 6H_2O$). This is a clever attempt for nutrient management in that the animal and urban wastewater often contains phosphate and ammonium, and using the Mg-based materials can recover both phosphorus and N (Ye et al. 2014). In fact, some developed regions have already incorporated struvite recovery as a step during wastewater treatment (Cieslik and Konieczka 2017, Nagy et al. 2019). Additionally, numerous studies have tested struvite as an alternative phosphorus and nitrogen fertilizer showing great potential (Darwish et al. 2016, Talboys et al. 2016). Mg in the amended biochar is often in form of MgO (Yao et al. 2013b), since the hydration and dissolution of MgO in water can produce magnesium cations that facilitate the precipitation of struvite. Solution pH is a determining factor for the effectiveness of precipitation by controlling the solubility of struvite, and by controlling the speciation of phosphate and ammonium affecting the availability of ions for struvite formation.

1.3 Agricultural waste-based sorbents

Multiple million tons of agricultural wastes from corn and rice farming are being produced every year (Berber-Villamar et al. 2018, Pinzi and Dorado 2011), but due to their low nutrient level and high silica content (Khan et al. 2004, Nakhshiniev et al. 2014), feeding livestock is not a plausible solution for disposal of this waste. Hence the most traditional disposal is through slash and burn. However, the emissions from the burning cannot be ignored and often

comes with detrimental public health issues in agricultural countries such as India (Lan et al. 2022, Moraes et al. 2014). Therefore, using agricultural wastes as a material could not only provide a solution for better waste management but also provide a low-cost raw material for practices such as phosphorus recovery.

Biochar gained much attention for green engineering and phosphorus recovery (Sud et al. 2008). While biochar can remove phosphate (Zeng et al. 2013, Zhang and Wang 2016), its adsorption performance is limited due to its negatively charged surface (Roy 2017). For this reason, many studies have tested chemical amendments for enhancing the phosphorus recovery effectiveness, and Mg-based amendments are among the most popular (Chen et al. 2018, Cui et al. 2016, Fang et al. 2014, Li et al. 2016, Yao et al. 2013b, Zhang et al. 2012, Zhou et al. 2011). These research studies found that both adsorption and precipitation were responsible for phosphorus recovery and the increase in phosphorus recovery performance by the chemical amendment was pronounced.

Another frequently tested family of materials is silicate minerals. Silicate can be provided by silicon rich ash from crop wastes such as rice straw, wheat straw, and rice husk through chemical extraction (Terzioglu and Yucel 2012). Calcium silicate hydrate (CSH) is one of the materials showing potential for both phosphorus recovery and reuse (Okano et al. 2013, Si et al. 2018). The precipitation of calcium-phosphorus minerals induced by the Ca^{2+} dissolved from CSH is found to be a mechanism (Sharmin et al. 2021) in addition to the CaO initiated adsorption. Although the phosphorus recovery mechanism is similar to calcium silicate minerals, and there were studies testing magnesium silicate minerals for the same task such as in (Smith and Hwang 1978), the attention on the latter is largely insignificant.

1.4 Life cycle and cost assessment of phosphorus fertilizers

Phosphorus recovery and reuse is an effort to find alternatives for substituting the current and traditional mining-based phosphorus fertilizer industry. The advantages are minimizing the need for mining of the high-grade phosphorus rock and lowering the upstream phosphorus loading into the environment consequently, alleviating the environmental issues induced by the excessive phosphorus, and potentially mitigating the environmental impact from the traditional phosphorus fertilizer industry. Traditional phosphorus fertilizer production is tightly linked with phosphorus mining and sulfuric acid production, which are two processes with great environmental impacts in categories such as climate change, fossil fuel depletion, and land transformation (Farjana et al. 2019, Kiss et al. 2006). Through life cycle assessment (LCA), many studies have come to the conclusion that energy and chemical inputs are two major sources of impact from the current phosphorus recovery strategies (Bradford-Hartke et al. 2015). Although some studies demonstrated that phosphorus recovery and reuse might have more environmental impact than the traditional fertilizer productions (Goel et al. 2021, Pradel and Aissani 2019, Zhang et al. 2017), research that strives to find optimization in terms of energy consumption, chemical inputs, and related infrastructural and operational inputs should be emphasized when evaluating the new technologies for phosphorus recovery and reuse and striving for the better phosphorus sustainability (Sena and Hicks 2018).

The optimization of chemical input type not only affects the related environmental impacts, but also influences the overall cost of one strategy. For example, the lab-scale evaluation of a Mg-based sorbent often uses commercial chemical such as $MgCl_2$ (Yao et al. 2013a), however, many natural occurring materials such as brucite, dolomite, and sea bittern might be alternatives with much lower environmental impacts and cost, without compromising

the phosphorus recovery performance (Bradford-Hartke et al. 2021, Jarosinski et al. 2020, Shirazinezhad et al. 2021). Therefore, the detailed environmental impact and cost evaluation on phosphorus recovery materials using agricultural wastes and alternative chemical sources can add more knowledge into the field and help decision-making in the future.

1.5 Overview of this dissertation

The overarching objective of this research was to evaluate agricultural waste-based materials for phosphorus recovery and reuse and to quantify the corresponding environmental impacts and cost. To achieve the objective, this research was composed of three tasks (Figure 1.1).

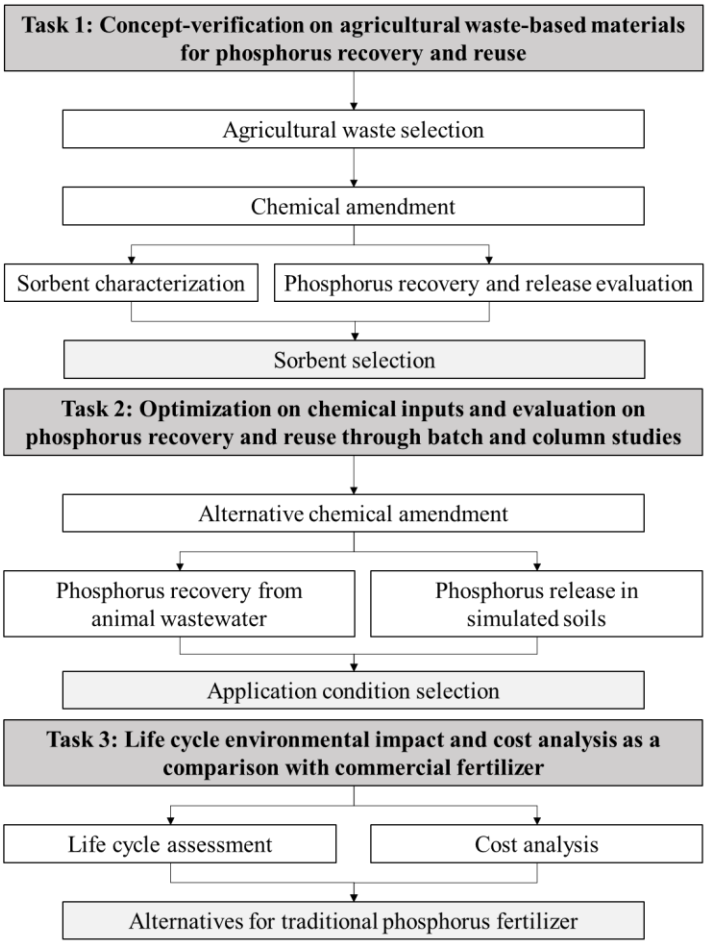

Figure 1.1 Overview of research tasks

Task 1: Concept-verification on agricultural waste-based materials for phosphorus recovery and reuse

The objective of this task was to evaluate the performance of phosphorus recovery and release by agricultural waste-based materials. Six different agricultural wastes were tested for phosphorus recovery: corn cobs, rice straw, wheat straw, rice husk, pine shavings, and wheat bran. Two categories of materials were synthesized: Mg amended biochars (Mg-chars) and magnesium silicate minerals ($MgSiO_3$). The Mg source was commercial $MgCl_2 \cdot 6H_2O$. Simple phosphate deionized water solution and model animal wastewater containing phosphate, ammonium, and bicarbonate alkalinity were used for testing the performance of phosphorus recovery in batch settings. Experimental conditions including pH and wastewater composition were evaluated to find optimal materials at a suitable condition. Surface and elemental characterizations of the materials before and after the exposure to wastewater were conducted. phosphorus release was also tested under standard soil tests at different pH conditions. And the possible phosphorus recovery and release mechanisms were discussed. This task is addressed in Chapter 2.

Task 2: Optimization on chemical inputs and evaluation on phosphorus recovery and reuse through batch and column studies

The objective of this task was to test the alternative chemical amendment sources and to test phosphorus release from the post-phosphorus-exposure materials in simulated soils. Based on the material selections from Task 1, Mg amended corn cob biochar from $Mg(OH)_2$ (Mg-char ($Mg(OH)_2$) and Mg amended corn cob biochar from model sea bittern (Mg-char (bittern)) were tested in batch settings with model animal wastewater to verify the plausibility of using less expensive alternatives to $MgCl_2$ for char amendment. Calcium silicate hydrate (CSH) prepared

from rice husk ash and using hydrated lime ($Ca(OH)_2$) as an alternative to more expensive $CaCl_2$ as a Ca source were also tested for phosphorus recovery. Phosphorus release was evaluated in sand columns considering the effects from soil pH and the soil minerals goethite and kaolinite. The soil pH selection covered acidic, neutral, and alkaline conditions aiming to provide insights on a wide spectrum of soil types. The addition of goethite and kaolinite aimed to model soil conditions containing natural phosphorus "sinks", and to make recommendations when the post-phosphorus -exposure sorbents were used as fertilizers. This task is addressed in Chapter 3.

Task 3: Life cycle environmental impact and cost analysis as a comparison with commercial fertilizer

The objective of this task was to evaluate and compare the environmental impacts and the costs of the selected materials with commercial fertilizer. Previous tasks fine-tuned the selections of sorbents and application conditions for phosphorus recovery from animal wastewater and reuse as fertilizers. However, whether they were better options than traditional fertilizer production in terms of environmental impact and cost was still a question yet to be answered. Therefore, in Task 3, life cycle assessment and cost analysis were conducted to compare the resource inputs and waste emissions from producing Mg-char ($Mg(OH)_2$, Mg-char (bittern), and CSH versus the commercial fertilizer monoammonium phosphate (MAP). The comparison selected a realistic annual personal phosphorus demand as the benchmark. Scenarios and corresponding experimentally measured data from Task 2 were used in the assessments. Transportation was considered as an additional parameter in analysis of different scenarios. Specifically, scenarios including pH 8.5, 7.5, 5.5, and pH 8.5 plus transportation were used in the life cycle assessment and cost analysis. Furthermore, the current cost of each input was considered in the cost analysis. Categories with environmental impact hotspots were identified in

each scenario, which could provide potential optimization of the overall process. This task is addressed in Chapter 4.

This research provides strategies for using agricultural wastes and low-cost chemical amendments for the synthesis of sorbents for phosphorus recovery and reuse. The conclusions from Task 1, 2, and 3 are summarized in Chapter 5. Chapter 5 identifies important finding suggests future research recommendations. This research contributes to knowledge on phosphorus sustainability and could be used to the further realization of closing the phosphorus cycle.

1.6 References

Berber-Villamar, N.K., Netzahuatl-Munoz, A.R., Morales-Barrera, L., Chavez-Camarillo, G.M., Flores-Ortiz, C.M. and Cristiani-Urbina, E. (2018) Corncob as an effective, eco-friendly, and economic biosorbent for removing the azo dye Direct Yellow 27 from aqueous solutions. Plos One 13(4).

Bradford-Hartke, Z., Lane, J., Lant, P. and Leslie, G. (2015) Environmental Benefits and Burdens of Phosphorus Recovery from Municipal Wastewater. Environmental Science & Technology 49(14), 8611-8622.

Bradford-Hartke, Z., Razmjou, A. and Gregory, L. (2021) Factors affecting phosphorus recovery as struvite: Effects of alternative magnesium sources. Desalination 504, 114949.

Capdevielle, A., Sýkorová, E., Biscans, B., Béline, F. and Daumer, M.-L. (2013) Optimization of struvite precipitation in synthetic biologically treated swine wastewater—Determination of the optimal process parameters. Journal of Hazardous Materials 244, 357-369.

Chen, Q.C., Qin, J.L., Cheng, Z.W., Huang, L., Sun, P., Chen, L. and Shen, G.Q. (2018) Synthesis of a stable magnesium-impregnated biochar and its reduction of phosphorus leaching from soil. Chemosphere 199, 402-408.

Cieslik, B. and Konieczka, P. (2017) A review of phosphorus recovery methods at various steps of wastewater treatment and sewage sludge management. The concept of "no solid waste generation" and analytical methods. Journal of Cleaner Production 142, 1728-1740.

Cooper, J., Lombardi, R., Boardman, D. and Carliell-Marquet, C. (2011) The future distribution and production of global phosphate rock reserves. Resources Conservation and Recycling 57, 78-86.

Cordell, D., Drangert, J.-O. and White, S. (2009) The story of phosphorus: global food security and food for thought. Global environmental change 19(2), 292-305.

Cordell, D. and White, S. (2011) Peak phosphorus: clarifying the key issues of a vigorous debate about long-term phosphorus security. Sustainability 3(10), 2027-2049.

Cui, X.Q., Dai, X., Khan, K.Y., Li, T.Q., Yang, X.E. and He, Z.L. (2016) Removal of phosphate from aqueous solution using magnesium-alginate/chitosan modified biochar microspheres derived from Thalia dealbata. Bioresource Technology 218, 1123-1132.

Darwish, M., Aris, A., Puteh, M.H., Abideen, M.Z. and Othman, M.N. (2016) Ammonium-Nitrogen Recovery from Wastewater by Struvite Crystallization Technology. Separation and Purification Reviews 45(4), 261-274.

Edixhoven, J., Gupta, J. and Savenije, H. (2014) Recent revisions of phosphate rock reserves and resources: a critique. Earth System Dynamics 5(2), 491-507.

Fang, C., Zhang, T., Li, P., Jiang, R.F. and Wang, Y.C. (2014) Application of Magnesium Modified Corn Biochar for Phosphorus Removal and Recovery from Swine Wastewater. International Journal of Environmental Research and Public Health 11(9), 9217-9237.

FAO, I., UNICEF, WFP and WHO. (2022) The State of Food Security and Nutrition in the World 2022. Repurposing food and agricultural policies to make healthy diets more affordable., FAO. , Rome.

Farjana, S.H., Huda, N., Parvez Mahmud, M.A. and Saidur, R. (2019) A review on the impact of mining and mineral processing industries through life cycle assessment. Journal of Cleaner Production 231, 1200-1217.

Foletto, E.L., Santos, W.R.B.d., Jahn, S.L., Bassaco, M.M., Mazutti, M.A., Cancelier, A. and Gündel, A. (2013) Organic pollutants removal and recovery from animal wastewater by

mesoporous struvite precipitation. Desalination and Water Treatment 51(13-15), 2776-2780.

Geissler, B., Mew, M.C., Matschullat, J. and Steiner, G. (2020) Innovation potential along the phosphorus supply chain: A micro and macro perspective on the mining phase. Science of the Total Environment 714, 10.

Gérard, F. (2016) Clay minerals, iron/aluminum oxides, and their contribution to phosphate sorption in soils—A myth revisited. Geoderma 262, 213-226.

Goel, S., Kansal, A. and Pfister, S. (2021) Sourcing phosphorus for agriculture: Life cycle assessment of three options for India. Resources Conservation and Recycling 174.

Guaya, D., Valderrama, C., Farran, A., Armijos, C. and Cortina, J.L. (2015) Simultaneous phosphate and ammonium removal from aqueous solution by a hydrated aluminum oxide modified natural zeolite. Chemical Engineering Journal 271, 204-213.

He, Q.M., Peng, X.Y. and Li, Z.Y. (2014) The treatment of animal manure wastewater by coupled simultaneous methanogenesis and denitrification (SMD) and shortcut nitrification - denitrification (SND). Journal of Chemical Technology and Biotechnology 89(11), 1697-1704.

IFA (2022) Fertilizer use by crop and country for the 2017-2018 period, Paris, France.

Ioannou, A. and Dimirkou, A. (1997) Phosphate Adsorption on Hematite, Kaolinite, and Kaolinite–Hematite (k–h) Systems As Described by a Constant Capacitance Model. Journal of Colloid and Interface Science 192(1), 119-128.

Irick, D.L., Gu, B., Li, Y.C., Inglett, P.W., Frederick, P.C., Ross, M.S., Wright, A.L. and Ewe, S.M.L. (2015) Wading bird guano enrichment of soil nutrients in tree islands of the Florida Everglades. Science of the Total Environment 532, 40-47.

Jarosinski, A., Radomski, P., Lelek, L. and Kulczycka, J. (2020) New Production Route of Magnesium Hydroxide and Related Environmental Impact. Sustainability 12(21), 8822.

Jarvie, H.P., Sharpley, A.N., Spears, B., Buda, A.R., May, L. and Kleinman, P.J.A. (2013) Water Quality Remediation Faces Unprecedented Challenges from "Legacy Phosphorus". Environmental Science & Technology 47(16), 8997-8998.

Jiang, Y.H., Li, A.Y., Deng, H., Ye, C.H., Wu, Y.Q., Linmu, Y.D. and Hang, H.L. (2019) Characteristics of nitrogen and phosphorus adsorption by Mg-loaded biochar from different feedstocks. Bioresource Technology 276, 183-189.

Kamiyango, M.W., Masamba, W.R.L., Sajidu, S.M.I. and Fabiano, E. (2009) Phosphate removal from aqueous solutions using kaolinite obtained from Linthipe, Malawi. Physics and Chemistry of the Earth, Parts A/B/C 34(13), 850-856.

Khan, M.A., Sarwar, M., Nisa, M.-u. and Khan, M.S. (2004) Feeding value of urea treated corncobs ensiled with or without enzose (corn dextrose) for lactating crossbred cows. Asian-Australasian Journal of Animal Sciences 17(8), 1093-1097.

Kiss, A.A., Bildea, C.S. and Verheijen, P.J. (2006) Computer Aided Chemical Engineering, pp. 737-742, Elsevier.

Kok, D.J.D., Pande, S., van Lier, J.B., Ortigara, A.R.C., Savenije, H. and Uhlenbrook, S. (2018) Global phosphorus recovery from wastewater for agricultural reuse. Hydrology and Earth System Sciences 22(11), 5781-5799.

Lan, R., Eastham, S.D., Liu, T., Norford, L.K. and Barrett, S.R.H. (2022) Air quality impacts of crop residue burning in India and mitigation alternatives. Nature Communications 13(1), 6537.

Li, B., Li, P., Zeng, X.C., Yu, W., Huang, Y.F., Wang, G.Q. and Young, B.R. (2020a) Assessing the sustainability of phosphorus use in China: Flow patterns from 1980 to 2015. Science of the Total Environment 704, 12.

Li, G.H., Li, H.G., Leffelaar, P.A., Shen, J.B. and Zhang, F.S. (2014) Characterization of Phosphorus in Animal Manures Collected from Three (Dairy, Swine, and Broiler) Farms in China. Plos One 9(7).

Li, R.H., Wang, J.J., Zhou, B.Y., Awasthi, M.K., Ali, A., Zhang, Z.Q., Lahori, A.H. and Mahar, A. (2016) Recovery of phosphate from aqueous solution by magnesium oxide decorated magnetic biochar and its potential as phosphate-based fertilizer substitute. Bioresource Technology 215, 209-214.

Li, X.Y., Xie, Y.H., Jiang, F., Wang, B., Hu, Q.L., Tang, Y., Luo, T. and Wu, T. (2020b) Enhanced phosphate removal from aqueous solution using resourceable nano-CaO2/BC composite: Behaviors and mechanisms. Science of the Total Environment 709, 12.

Lü, C., Yan, D., He, J., Zhou, B., Li, L. and Zheng, Q. (2017) Environmental geochemistry significance of organic phosphorus: An insight from its adsorption on iron oxides. Applied Geochemistry 84, 52-60.

Moraes, C.A., Fernandes, I.J., Calheiro, D., Kieling, A.G., Brehm, F.A., Rigon, M.R., Berwanger Filho, J.A., Schneider, I.A. and Osorio, E. (2014) Review of the rice production cycle: By-products and the main applications focusing on rice husk combustion and ash recycling. Waste Management & Research 32(11), 1034-1048.

Nagarajan, D., Lee, D.J., Chen, C.Y. and Chang, J.S. (2020) Resource recovery from wastewaters using microalgae-based approaches: A circular bioeconomy perspective. Bioresource Technology 302, 15.

Nagy, J., Mikola, A., Pradhan, S.K. and Zseni, A. (2019) The Utilization of Struvite Produced from Human Urine in Agriculture as a Natural Fertilizer: A Review. Periodica Polytechnica-Chemical Engineering 63(3), 478-484.

Nakhshiniev, B., Biddinika, M.K., Gonzales, H.B., Sumida, H. and Yoshikawa, K. (2014) Evaluation of hydrothermal treatment in enhancing rice straw compost stability and maturity. Bioresource Technology 151, 306-313.

Nedelciu, C.-E., Ragnarsdóttir, K. and Stjernquist, I. (2018) From waste to resource: A systems dynamics and stakeholder analysis of phosphorus recycling from municipal wastewater in Europe. Ambio 48, 741 - 751.

Nixon, S.W. (1995) Coastal marine eutrophication: A definition, social causes, and future concerns. Ophelia 41(1), 199-219.

Nobaharan, K., Bagheri Novair, S., Asgari Lajayer, B. and van Hullebusch, E.D. (2021) Phosphorus Removal from Wastewater: The Potential Use of Biochar and the Key Controlling Factors. Water 13(4), 517.

Okano, K., Uemoto, M., Kagami, J., Miura, K., Aketo, T., Toda, M., Honda, K. and Ohtake, H. (2013) Novel technique for phosphorus recovery from aqueous solutions using amorphous calcium silicate hydrates (A-CSHs). Water research 47(7), 2251-2259.

Penn, C.J. and Warren, J.G. (2009) Investigating Phosphorus Sorption onto Kaolinite Using Isothermal Titration Calorimetry. Soil Science Society of America Journal 73(2), 560-568.

Pinzi, S. and Dorado, M.P. (2011) Handbook of Biofuels Production. Luque, R., Campelo, J. and Clark, J. (eds), pp. 61-94, Woodhead Publishing.

Pradel, M. and Aissani, L. (2019) Environmental impacts of phosphorus recovery from a "product" Life Cycle Assessment perspective: Allocating burdens of wastewater treatment in the production of sludge-based phosphate fertilizers. Science of the Total Environment 656, 55-69.

Reijnders, L. (2014) Phosphorus resources, their depletion and conservation, a review. Resources Conservation and Recycling 93, 32-49.

Rittmann, B.E., Mayer, B., Westerhoff, P. and Edwards, M. (2011) Capturing the lost phosphorus. Chemosphere 84(6), 846-853.

Robles, A., Aguado, D., Barat, R., Borras, L., Bouzas, A., Gimenez, J.B., Marti, N., Ribes, J., Ruano, M.V., Serralta, J., Ferrer, J. and Seco, A. (2020) New frontiers from removal to recycling of nitrogen and phosphorus from wastewater in the Circular Economy. Bioresource Technology 300, 18.

Roy, E.D. (2017) Phosphorus recovery and recycling with ecological engineering: A review. Ecological Engineering 98, 213-227.

Sattari, S.Z., Bouwman, A.F., Giller, K.E. and van Ittersum, M.K. (2012) Residual soil phosphorus as the missing piece in the global phosphorus crisis puzzle. Proceedings of the National Academy of Sciences of the United States of America 109(16), 6348-6353.

Scholz, R.W., Ulrich, A.E., Eilitta, M. and Roy, A. (2013) Sustainable use of phosphorus: A finite resource. Science of the Total Environment 461, 799-803.

Scholz, R.W. and Wellmer, F.-W. (2013) Approaching a dynamic view on the availability of mineral resources: What we may learn from the case of phosphorus? Global environmental change 23(1), 11-27.

Scholz, R.W. and Wellmer, F.W. (2016) Comment on: "Recent revisions of phosphate rock reserves and resources: a critique" by Edixhoven et al. (2014) - clarifying comments and thoughts on key conceptions, conclusions and interpretation to allow for sustainable action. Earth System Dynamics 7(1), 103-117.

Schwertmann, U. and Fechter, H. (1982) The point of zero charge of natural and synthetic ferrihydrites and its relation to adsorbed silicate. Clay Minerals 17(4), 471-476.

Sena, M. and Hicks, A. (2018) Life cycle assessment review of struvite precipitation in wastewater treatment. Resources Conservation and Recycling 139, 194-204.

Sena, M., Morris, M.R., Seib, M. and Hicks, A. (2020) An exploration of economic valuation of phosphorus in the environment and its implications in decision making for resource recovery. Water research 172, 8.

Sharmin, N., Sabatini, D.A. and Butler, E.C. (2021) Phosphorus Recovery and Reuse Using Calcium-Silicate Hydrate Made from Rice Husk. Journal of Environmental Engineering 147(6), 04021015.

Sharpley, A., Jarvie, H.P., Buda, A., May, L., Spears, B. and Kleinman, P. (2013) Phosphorus Legacy: Overcoming the Effects of Past Management Practices to Mitigate Future Water Quality Impairment. Journal of Environmental Quality 42(5), 1308-1326.

Shirazinezhad, M., Faghihinezhad, M., Baghdadi, M. and Ghanbari, M. (2021) Phosphate removal from municipal effluent by a porous MgO-expanded graphite composite as a novel adsorbent: Evaluation of seawater as a natural source of magnesium ions. Journal of Water Process Engineering 43, 102232.

Si, Q.S., Zhu, Q. and Xing, Z.P. (2018) Simultaneous removal of nitrogen and phosphorus by magnesium-modified calcium silicate core-shell material in water. Ecotoxicology and Environmental Safety 163, 656-664.

Sigg, L. and Stumm, W. (1981) The interaction of anions and weak acids with the hydrous goethite (α-FeOOH) surface. Colloids and Surfaces 2(2), 101-117.

Sinha, E., Michalak, A.M. and Balaji, V. (2017) Eutrophication will increase during the 21st century as a result of precipitation changes. Science 357(6349), 405-408.

Smith, R.W. and Hwang, M.-Y. (1978) Phosphate adsorption of magnesium silicates. Journal (Water Pollution Control Federation), 2189-2197.

Sud, D., Mahajan, G. and Kaur, M.P. (2008) Agricultural waste material as potential adsorbent for sequestering heavy metal ions from aqueous solutions - A review. Bioresource Technology 99(14), 6017-6027.

Talboys, P.J., Heppell, J., Roose, T., Healey, J.R., Jones, D.L. and Withers, P.J.A. (2016) Struvite: a slow-release fertiliser for sustainable phosphorus management? Plant and Soil 401(1-2), 109-123.

Terzioglu, P. and Yucel, S. (2012) Synthesis of magnesium silicate from wheat husk ash: effect of parameters on structural and surface properties. Bioresources 7(4), 5435-5447.

Turner, R.E. and Rabalais, N.N. (1994) Coastal eutrophication near the Mississippi river delta. Nature 368(6472), 619-621.

USGS (2022) Mineral commodity summaries 2022, p. 202, Reston, VA.

van den Berg, M., Neumann, K., van Vuuren, D.P., Bouwman, A.F., Kram, T. and Bakkes, J. (2016) Exploring resource efficiency for energy, land and phosphorus use: Implications

for resource scarcity and the global environment. Global Environmental Change-Human and Policy Dimensions 36, 21-34.

Van Vuuren, D.P., Bouwman, A.F. and Beusen, A.H.W. (2010) Phosphorus demand for the 1970-2100 period: A scenario analysis of resource depletion. Global Environmental Change-Human and Policy Dimensions 20(3), 428-439.

Withers, P.J.A., Forber, K.G., Lyon, C., Rothwell, S., Doody, D.G., Jarvie, H.P., Martin-Ortega, J., Jacobs, B., Cordell, D., Patton, M., Camargo-Valero, M.A. and Cassidy, R. (2020) Towards resolving the phosphorus chaos created by food systems. Ambio 49(5), 1076-1089.

Yao, Y., Gao, B., Chen, J., Zhang, M., Inyang, M., Li, Y., Alva, A. and Yang, L. (2013a) Engineered carbon (biochar) prepared by direct pyrolysis of Mg-accumulated tomato tissues: characterization and phosphate removal potential. Bioresource Technology 138, 8-13.

Yao, Y., Gao, B., Chen, J.J. and Yang, L.Y. (2013b) Engineered Biochar Reclaiming Phosphate from Aqueous Solutions: Mechanisms and Potential Application as a Slow-Release Fertilizer. Environmental Science & Technology 47(15), 8700-8708.

Ye, Z.L., Shen, Y., Ye, X., Zhang, Z.J., Chen, S.H. and Shi, J.W. (2014) Phosphorus recovery from wastewater by struvite crystallization: Property of aggregates. Journal of Environmental Sciences 26(5), 991-1000.

Zeng, Z., Zhang, S.D., Li, T.Q., Zhao, F.L., He, Z.L., Zhao, H.P., Yang, X.E., Wang, H.L., Zhao, J. and Rafiq, M.T. (2013) Sorption of ammonium and phosphate from aqueous solution by biochar derived from phytoremediation plants. Journal of Zhejiang University-Science B 14(12), 1152-1161.

Zhang, F., Wang, Q., Hong, J., Chen, W., Qi, C. and Ye, L. (2017) Life cycle assessment of diammonium-and monoammonium-phosphate fertilizer production in China. Journal of Cleaner Production 141, 1087-1094.

Zhang, J.S. and Wang, Q.Q. (2016) Sustainable mechanisms of biochar derived from brewers' spent grain and sewage sludge for ammonia-nitrogen capture. Journal of Cleaner Production 112, 3927-3934.

Zhang, M., Gao, B., Yao, Y., Xue, Y.W. and Inyang, M. (2012) Synthesis of porous MgO-biochar nanocomposites for removal of phosphate and nitrate from aqueous solutions. Chemical Engineering Journal 210, 26-32.

Zhou, J.B., Yang, S.L. and Yu, J.G. (2011) Facile fabrication of mesoporous MgO microspheres and their enhanced adsorption performance for phosphate from aqueous solutions. Colloids and Surfaces a-Physicochemical and Engineering Aspects 379(1-3), 102-108.

Zowada, C., Gulacar, O., Siol, A. and Eilks, I. (2020) Phosphorus – a “political” element for transdisciplinary chemistry education. Chemistry Teacher International 2(1).

Zubair, M., Wang, S., Zhang, P., Ye, J., Liang, J., Nabi, M., Zhou, Z., Tao, X., Chen, N. and Sun, K. (2020) Biological nutrient removal and recovery from solid and liquid livestock manure: Recent advance and perspective. Bioresource Technology 301, 122823.

Chapter 2 Phosphorus recovery and recycling from model animal wastewaters using materials prepared from rice straw and corn cobs[*]

2.1 Abstract

Anthropogenic loss of phosphorus to surface waters not only causes environmental problems but depletes valuable phosphorus reserves. In this study, magnesium amended biochars and magnesium silicate, synthesized from corn cobs and rice straw, respectively, were evaluated for phosphorus uptake including the effects of pH and alkalinity. The overall goal was to close the phosphorus loop by recovering phosphorus from animal waste and reusing it as fertilizer. After phosphorus uptake, spent materials were tested for phosphorus release using modified soil tests representing different soil pH and alkalinity conditions. In experiments using model animal wastewaters containing both ammonia and bicarbonate alkalinity, dissolved phosphorus was removed by struvite ($MgNH_4PO_4 \cdot 6H_2O$) formation, whereas in deionized water, dissolved phosphorus was removed by adsorption. Alkalinity in the model animal wastewaters competed with phosphate for dissolved or solid-associated magnesium thereby reducing phosphorus uptake. Spent materials released significant phosphorus in waters with bicarbonate alkalinity. This work shows that abundant agricultural wastes can be used to synthesize solids for phosphorus uptake, with the spent materials having potential application as fertilizers.

[*] Ding, Y., Sabatini, D.A. and Butler, E.C. (2021) Phosphorus recovery and recycling from model animal wastewaters using materials prepared from rice straw and corn cobs. Water Science and Technology 83(8), 1893-1906.

2.2 Introduction

Phosphorus is introduced into the environment through runoff and seepage from agricultural activities such as crop and livestock production, as well as from municipal wastewater treatment plants and landfills (Nixon 1995). Not only does excess phosphorus introduction to surface waters cause eutrophication (Nixon 1995), it wastes a nutrient that is essential for agriculture, and for which reserves of high grade ores are limited (Roy 2017). In order to close the phosphorus cycle, therefore, efforts should be made not only to reduce consumption of new phosphorus ores, but also to recover and reuse phosphorus from wastes and wastewaters (Mukherjee et al. 2020, Withers et al. 2020). Potentially recoverable phosphorus from global livestock production waste is estimated to be 17.4 Mt per year, which could in theory meet 90% of the total phosphorus needed for agriculture (Kok et al. 2018). While animal manure has served directly as a fertilizer for centuries, it has several disadvantages, many of which also apply to composted manure or thermally treated biosolids. These include a phosphorus to nitrogen ratio greater than necessary for plant growth, which essentially wastes phosphorus when applied to soil, an unstable nitrogen content due to microbial denitrification, the potential for pathogen transmission, and aesthetic and regulatory concerns (Bacelo et al. 2020, Szogi et al. 2015). Recovery of phosphorus in a stable mineral form that can be easily stored and transported, as is studied here, is novel and poses an advantage over composted or thermally treated animal waste.

Phosphorus can be removed from wastewaters by precipitation as iron and aluminum phosphates, which results in formation of highly insoluble minerals that are unsuitable for use as fertilizers. Adsorption and precipitation using calcium-based (Mitrogiannis et al. 2017) and magnesium-based (Zhang et al. 2020) solids, on the other hand, yields solid phase phosphorus

more suitable for use as fertilizer (e.g., Zhang et al. 2020). For instance, magnesium silicate minerals such as serpentine and chrysotile can effectively remove phosphate by interaction with $Mg(OH)_2$ surface groups (Smith and Hwang 1978), and layered double hydroxides can release dissolved Mg^{2+} and Ca^{2+} that can remove phosphorus by precipitation (Seida and Nakano 2002).

Nitrogen and phosphorus coexist in wastewaters, so their simultaneous precipitation as struvite ($MgNH_4PO_4 \cdot 6H_2O$) in the presence of dissolved Mg^{2+} is commonly used to remove both. While struvite precipitation for phosphorus recovery is well established (Rittmann et al. 2011), it can be hindered by high ionic strength and bicarbonate alkalinity (Huchzermeier and Tao 2012), so phosphorus recovery as struvite should be tested in high ionic strength and high alkalinity wastewaters, as in this study.

Solution pH affects phosphorus uptake and subsequent release in several ways. First, it can strongly influence mineral surface charge, and therefore adsorption of charged species. For example, phosphate sorption to biochars with magnesium (hydr)oxide surfaces is favored at pH values below their pH_{pzc} values, which range from 8.9 to 10.5 (Jiang et al. 2019), and sorption to magnesium silicate minerals is favored below their pH_{pzc} values of 8.4-10.1 (Smith and Hwang 1978). Second, pH can strongly influence the tendency for phosphate removal by precipitation, by controlling the degree of protonation/deprotonation of cations (such as ammonium) and anions (such as HPO_4^{2-}). For instance, struvite solubility has a minimum around pH 9, due to acid-base equilibria among ammonia and phosphate species, with solubility increasing above and below this pH value (Hanhoun et al. 2011). At high pH values, hydroxide can compete with phosphate for magnesium to form $Mg(OH)_2(s)$ (Darwish et al. 2016).

A total of 144 million tons of corn cobs (Berber-Villamar et al. 2018) and 731 million tons of rice straw (Pinzi and Dorado 2011) are produced globally each year. Such wastes have

limited nutritional value for livestock (Khan et al. 2004), and the high silica content of rice straw makes it especially unsuitable as animal feed (Nakhshiniev et al. 2014). Fields are often cleared of crop residues by burning due to lack of low-cost alternatives (Ellis-Petersen 2019). For example, in Asia, 248 million tons of crop wastes are burned each year (Streets et al. 2003), leading to CO_2, nitrogen oxides (NO_x), SO_2, and particulate emissions (Moraes et al. 2014).

As an alternative, crop wastes can be put to beneficial use as feedstock for novel water treatment materials. For example, crop wastes used to produce biochar can be amended with magnesium salts for phosphorus removal. To do this, wastes are typically treated with a soluble Mg salt, then pyrolyzed (Chen et al. 2018). During pyrolysis (> 530 ℃) solid $Mg(OH)_2(s)$ on the biomass surface is transformed to MgO(s) (Choudhary et al. 1992). Since $Mg(OH)_2(s)$ precipitation is favored at high pH (Huang et al. 2012), raising the solution pH when treating biomass with a Mg salt could yield a greater quantity of MgO after pyrolysis.

Agricultural wastes that are rich in silica (e.g., wheat husk, wheat straw, rice husk, and rice straw) can also be used to prepare magnesium silicate through extraction and dissolution of silica, followed by precipitation with Mg^{2+} (Terzioglu and Yucel 2012). The term “magnesium silicate” includes a series of minerals with different magnesium oxide and silica stoichiometric ratios, including chrysotile, olivine, and serpentine.

The overall goal of this study was to test two waste-produced materials, Mg-treated char and magnesium silicate, both synthesized in part from agricultural wastes, for their ability to uptake phosphorus and release it under varying conditions of pH and alkalinity. The specific objectives were: (1) to determine the optimum conditions, in terms of phosphorus uptake, for preparation of Mg-treated char and magnesium silicate, (2) measure phosphorus uptake by these materials in simple model animal wastewaters containing both ammonia and carbonate, and (3)

measure phosphorus release from spent (post-phosphorus-exposure) materials under simulated soil pH conditions. Batch experiments were used to measure phosphorus uptake at a range of pH values and in the presence of both deionized water and two simple model animal wastewaters. Phosphorus release from spent materials was tested using modified soil extraction procedures to gain insight into the pH conditions favorable for phosphorus release and to understand the reactivity of solid associated phosphorus.

2.3 Materials and Methods

2.3.1 Material characterization

Scanning Electron Microscopy (SEM) and Energy Dispersive X-ray Spectroscopy (EDS) were conducted using a JEOL JSM-840 scanning electron microscope at 20 kV coupled with Kevex X-ray analyzer or a Zeiss NEON 40 EsB scanning electron microscope at 15 kV and INCA Energy 250 Energy Dispersive X-ray Microanalysis system. Selected images are shown in Supplementary Material. X-ray Diffraction (XRD) was conducted using a Rigaku Ultima IV diffractometer with Cu-K-alpha radiation (40 kV, 44 mA). Data analysis was done with MDI JADE with the American Mineralogist Crystal Structure Database.

2.3.2 Agricultural waste pretreatment

Agricultural wastes investigated include corn cobs (Kaytee, Chilton, Wisconsin), wheat straw (Thunder Acres, Conway Springs, Kansas), corn stalks (DriedDecor.com, West Jordan, Utah), wheat bran (Bob's Red Mill, Milwaukie, Oregon), pine shavings (Living World brand, Rolf C. Hagen Corp, Mansfield, Massachusetts), and rice straw (a mixture of *Oryza sativa* and *Tropical japonica*). The rice straw was donated by the Dale Bumpers National Rice Research Center, Stuttgart, Arkansas. First, all stalks or straw were cut using ceramic scissors to approximately 5 cm pieces and corn cobs were ground using a manual grain grinder (Azadx

Model 500#, Amazon.com) to 0.125-0.180 mm (120-80 mesh) (derived from (Zhu et al. 2020)). Next, biomass was washed in deionized (DI) water six times to remove residual soil. Then, biomass was soaked in 1 M HNO_3 (Certified ACS Plus, Fisher Chemical, Fair Lawn, New Jersey) for 30 minutes and rinsed with DI water until the rinsate reached pH 6 (Adam and Thankappan 2010). Finally, the biomass was oven-dried overnight at 60 ℃ (Fang et al. 2014).

2.3.3 Preparation of Mg-amended biochars

A total of 15-30 g agricultural waste was placed in capped 100 mL porcelain crucibles and pyrolyzed in a programmable kiln (Caldera, Paragon Industries, Mesquite, Texas). Crucibles were capped to limit air exposure and thereby preserve carbon in the product. The temperature program was as follows: ramp at 300 ℃ per hour to 600 ℃, isothermal at 600 ℃ for six hours, then cool naturally to room temperature (Brunson and Sabatini 2016, Ippolito et al. 2015). Initial experiments indicated that corn cobs had the highest mass recovery of biochar (Table 2.1), so corn cobs were used for biochar preparation thereafter. Other chars with comparable mass recoveries, such as corn stalk char (Table 2.1), could not be readily separated from the aqueous phase due to physical properties or particle size, and interfered with phosphate spectrophotometric analysis.

All unamended chars contained negligible magnesium (Table 2.1), therefore corn cob biochar was augmented with magnesium in one of three ways (Supplementary Material). In all cases, 30 g corn cobs were first soaked in 90 mL of a solution of 3.7 M $MgCl_2 \cdot 6H_2O$ (≥ 99%, Fisher Bioreagents, Ottawa, Ontario) with constant stirring, where the procedures were adapted from (Zhang et al. 2012). This was done in capped plastic bottles to reduce CO_2 dissolution from the atmosphere. “Mg-char” was stirred for ten hours without pH adjustment (pH 6), oven dried at 60 ℃, then pyrolyzed and used without further treatment (Supplementary Material). “Mg-char

(pH 13, post-pyrolysis)" was prepared in the same way, except that after pyrolysis it was rinsed in a pH 13 solution of NaOH (ACS, EMD, Gibbstown, New Jersey) (Supplementary Material). Finally, "Mg-char (pH 13, pre-pyrolysis)" was stirred in a solution of 3.7 M $MgCl_2 \cdot 6H_2O$ at pH 6 for four hours, then adjusted to pH 13 by addition of NaOH pellets and stirred for another four hours, oven dried at 60 ℃, and then pyrolyzed (Supplementary Material).

Table 2.1 Pyrolysis yield and elemental composition of biochar and ash

	Mass recovery and elemental composition[3] (wt %)	Rice straw	Wheat straw	Corn stalks	Corn cobs	Pine shavings	Wheat bran
Biochar[1]	Mass recovery	14	7	14	16	10	7
	C	15	80	74	89	85	88
	O	36	18	17	11	15	12
	Si	48	1	6	BDL[4]	0	BDL
	Mg	0	0	0	BDL	BDL	BDL
	P	0	0	0	BDL	BDL	0
	K	0	0	2	BDL	BDL	BDL
	Ca	1	0	1	0	0	BDL
Ash[2]	Mass recovery	1	3	10	0	0	0
	C	BDL	6	21	NM[5]	NM	NM
	O	43	38	33	NM	NM	NM
	Si	53	23	19	NM	NM	NM
	Mg	0	2	2	NM	NM	NM
	P	0	0	1	NM	NM	NM
	K	0	23	14	NM	NM	NM
	Ca	2	1	5	NM	NM	NM
	Cl	BDL	BDL	4	NM	NM	NM
	S	1	7	2	NM	NM	NM

[1] Biochar was produced by pyrolyzing biomass at 600 ºC for six hours in capped crucibles, which limited oxygen supply.
[2] Ash was produced by pyrolyzing biomass at 600 ºC for six hours in open crucibles.
[3] Mass recovery = (mass after pyrolysis ÷ mass before pyrolysis) × 100%. Elemental composition was determined using scanning electron microscope-energy dispersive X-ray spectroscopy (SEM-EDS) with an estimated detection limit of 0.01 wt%.
[4] BDL: below detection limits.
[5] NM: not measured due to the low mass recoveries for ash from corn cobs, pine shavings, and wheat bran.

All biochars were ground using a mortar and pestle, then sieved through a set of standard sieves (120 and 400 mesh) for 70 minutes on an electric sieve shaker (Houghton Manufacturing Co., Vicksburg, Michigan) (ASTM 2015). Particles with diameters between 38 and 125 µm (400-120 mesh) were retained and used in the phosphorus uptake experiments (Yao et al. 2011).

2.3.4 Preparation of magnesium silicate

Rice straw and wheat straw, both rich in silicon (Table 2.1) were pyrolyzed to obtain silicon-rich ash in a kiln using the same temperature program as above, but with uncapped crucibles to promote the oxidation and loss of carbon as CO_2, leaving only an inorganic, silicon rich ash. A molar ratio of NaOH to Si of 2:1, based on the ash silicon content (Table 2.1), was used to dissolve the ash (Terzioglu and Yucel 2012). Specifically, 10 g rice straw ash was mixed with 590 mL of 0.64 M NaOH, or 2 g wheat straw ash was mixed with 50 mL of 0.64 M NaOH, both for three days with constant stirring. After this, the estimated dissolved Si concentration in both solutions, based on Table 2.1, was 0.32 M. The final pH values were 13.2 (rice straw ash) and 13.5 (wheat straw ash). Plastic bottles were used to avoid silica dissolution from glass and were kept closed to avoid dissolution of CO_2 from the atmosphere. Residual undissolved ash particles were filtered gravimetrically (Grade 1 filter paper, GE Healthcare Whatman, Fisher Scientific, Pittsburgh, Pennsylvania). Then, the remaining filtrate (approximately 590 mL for rice straw ash and approximately 50 mL for wheat straw ash) was added dropwise to an equal volume of 0.32 M $MgCl_2 \cdot 6H_2O$ to obtain an estimated Mg:Si molar ratio of 1:1 to precipitate magnesium silicate (Ali et al. 2010). The slurry was stirred for thirty minutes, then allowed to settle overnight. Then the supernatant was discarded and the solids were oven dried at 60 ℃ (Ali et al. 2010), then ground and sieved as described above.

2.3.5 Phosphate analysis

For experiments with biochar, phosphate was quantified by Method 4500-P. E (Ascorbic acid method) (American Public Health Association 1992) using a Shimadzu UV-1601 spectrophotometer with a wavelength of 880 nm. Blanks containing sorbent materials (i.e., chars) but no phosphorus were tested in every experiment for absorbance at 880 nm due to scattering by fine particles or dissolved species that may have reacted with colorimetric reagents. No absorbance at 880 nm was found for these solid blanks in experiments with biochar. Therefore, in phosphate analysis for biochar samples, a blank containing neither solids nor phosphorus was placed in the reference cell of the spectrophotometer. For experiments with magnesium silicate, solid blanks (containing only magnesium silicate and no phosphorus) did have a small absorbance at 880 nm after reaction with the colorimetric reagents. This was most likely due to the presence of dissolved silica, which forms silicomolybdate (Chalmers and Sinclair 1966) with an intense blue color that absorbs at 880 nm and interferes with phosphate quantification. This was corrected by placing a solid blank, diluted in the same ratio as the samples, in the reference cell of the spectrophotometer.

In addition, to reduce the interference from silicate, a modified analysis method was used when quantifying phosphorus for experiments with magnesium silicate (Galhardo and Masini 2000). Addition of oxalic acid to the molybdate reagent prevents the formation of silicomolybdate, so that upon the later addition of the ascorbic acid reagent, the formed molybdenum blue is solely from phosphomolybdate (Galhardo and Masini 2000). In this modified method, the volume ratio of colorimetric reagents to sample was changed to 0.16:1 to maintain the same final molybdate concentration as in the ascorbic acid method (American Public Health Association 1992) and therefore to attain a similar degree of phosphate sensitivity.

All other conditions, including the order of reagent addition and waiting times, were as reported elsewhere (Galhardo and Masini 2000).

2.3.6 Model wastewater composition

In order to test the effect of ammonium/ammonia and bicarbonate alkalinity, phosphorus uptake was measured in two simple model systems representing wastewaters from production of swine and dairy cattle (Huchzermeier and Tao 2012, Vanotti et al. 2003). Concentrations in the model swine and cattle wastewaters were 24 mM total ammonia, up to 68.5 mg/L phosphate as phosphorus, and alkalinity values ranging from approximately 1,500 to 5,000 mg/L as $CaCO_3$ (Table 2.2).

Table 2.2 Composition of the model wastewaters[1]

Amount added	Model swine wastewater[3]	Model cattle wastewater[4]
$(NH_4)_2CO_3$ (mM)	11.8	12.0
$NaHCO_3$ (mM)	23.6	84.5
NaH_2PO_4 (as mg/L of phosphorus)	68.5	68.5
Resulting alkalinity (as mg/L of $CaCO_3$, considering ionic strength corrections[2])	1535 (pH 7) 1823 (pH 8) 1955 (pH 9)	4605 (pH 7) 4718 (pH 8) 4997 (pH 9)

[1] Chemicals and their sources were as follows: $NaHCO_3$ and NaH_2PO_4 (ACS, Fisher Chemical, Fair Lawn, New Jersey) and $(NH_4)_2CO_3$ (ACS, Alfa Aesar, Tewksbury, Massachusetts).
[2] Ionic strength corrections were calculated using MINEQL+ 5.0 (Environmental Research Software Hallowell, Maine).
[3] Composition was derived from (Vanotti et al. 2003).
[4] Composition was derived from (Huchzermeier and Tao 2012).

2.3.7 Phosphorus uptake experiments

Phosphorus uptake was measured in DI water as well as in the two model animal

wastewaters. Solution pH was adjusted with 5 M HCl (Certified ACS Plus, Fisher Chemical, Fair Lawn, New Jersey) or 5 M NaOH (ACS, EMD Chemicals Inc., Gibbstown, New Jersey) before adding the solids and again before sampling. Isotherm batch tests contained 0.05 g or 0.075 g solid and 25 mL of DI or model wastewater (2 g/L or 3 g/L, respectively), with initial phosphate concentrations ranging from 0.7 to 68.5 mg P/L. Samples were equilibrated for 24 hours on a Cole-Parmer Ping-Pong TM #51504-00 shaker (Cole-Parmer, Vernon Hills, Illinois) at 60 excursions per minute, which was established as sufficient time for aqueous concentrations to reach a constant level (Supplementary Material). All samples were prepared in duplicate.

After equilibration, reaction bottles were centrifuged at a relative centrifugal force of 3661 × g for 30 minutes, followed by filtration of a portion of the supernatant using 0.22 μm pore size hydrophilic polyvinylidene fluoride (PVDF) non-sterile syringe filters (Simsii Inc., Irvine, California) for phosphorus analysis (Section 2.5). After isotherm experiments, solids were separated from the remaining supernatant by gravity filtration (GE Healthcare Whatman Grade 5 qualitative filter paper), air dried, and kept in a desiccator for further analysis.

2.3.8 Phosphorus release

After reaction with Mg-char or magnesium silicate, selected samples were tested for phosphorus release using three phosphorus extraction tests: Bray and Kurtz P1, Mehlich 3, and Olsen P (i.e., Estimation of available phosphorus in soils by extraction with sodium bicarbonate) (Bray and Kurtz 1945, Mehlich 1984, Olsen 1954), with the following minor modifications based on “Methods of phosphorus analysis for soils, sediments, residuals, and waters” (Pierzynski 2000): (1) samples analyzed by the Bray and Kurtz P1 method were shaken for five minutes instead of one minute and (2) no charcoal was added to the samples for decolorization, since no color was observed. In addition, since these samples contained no soil, the solid to

extracting solution ratio for all methods was adjusted to 1:800 (0.025 g solid was added to 20 mL of extracting solution) to better simulate the extractant to phosphorus ratio found in a soil test in which phosphorus is a minor constituent. Finally, the pH of the Mehlich 3 extracting solution (0.2 M CH_3COOH, 0.25 M NH_4NO_3, 0.015 M NH_4F, 0.013 M HNO_3, 0.001 M EDTA) was adjusted from 2.3 to 6.9 using NH_4OH (ACS, 28.0-30.0 % NH_3 basis, Sigma-Aldrich, St. Louis, Missouri) to simulate neutral soil water containing ligands that could compete with phosphate for adsorption sites. The extracting solutions for Bray & Kurtz P1 (0.03 M NH_4F and 0.025 M HCl) and Olsen P (0.5 M $NaHCO_3$) had pH values of 2.5 and 8.4, respectively. After extraction, solids were removed using a 0.22 μm hydrophilic PVDF non-sterile syringe filter and phosphorus was measured as described above.

2.4 Results and Discussion

2.4.1 Effect of pH on phosphorus uptake in DI water

Initial experiments with Mg-char (pH 13, post pyrolysis) and magnesium silicate made from rice straw were conducted in DI water at pH 7, 8, and 9 to identify the optimum pH for subsequent experiments. For both materials, there was more phosphorus uptake at pH 8 and 9 than at pH 7, particularly for Mg-char (pH 13, post pyrolysis) (Figure 2.1). There was not, however, a large increase in phosphorus uptake for either material upon changing the pH from 8 to 9 (Figure 2.1). This overall trend could be due to phosphate speciation, since between pH 7 and 8, there is a significant increase in the concentration of the divalent anion HPO_4^{2-} due to deprotonation of $H_2PO_4^-$ (pK_a=7.2), but a much smaller increase between pH 8 and 9. Electrostatic attractive forces are greater for divalent anions (e.g., HPO_4^{2-}) versus monovalent ions (e.g., $H_2PO_4^-$) of the same size (Valisko et al. 2007).

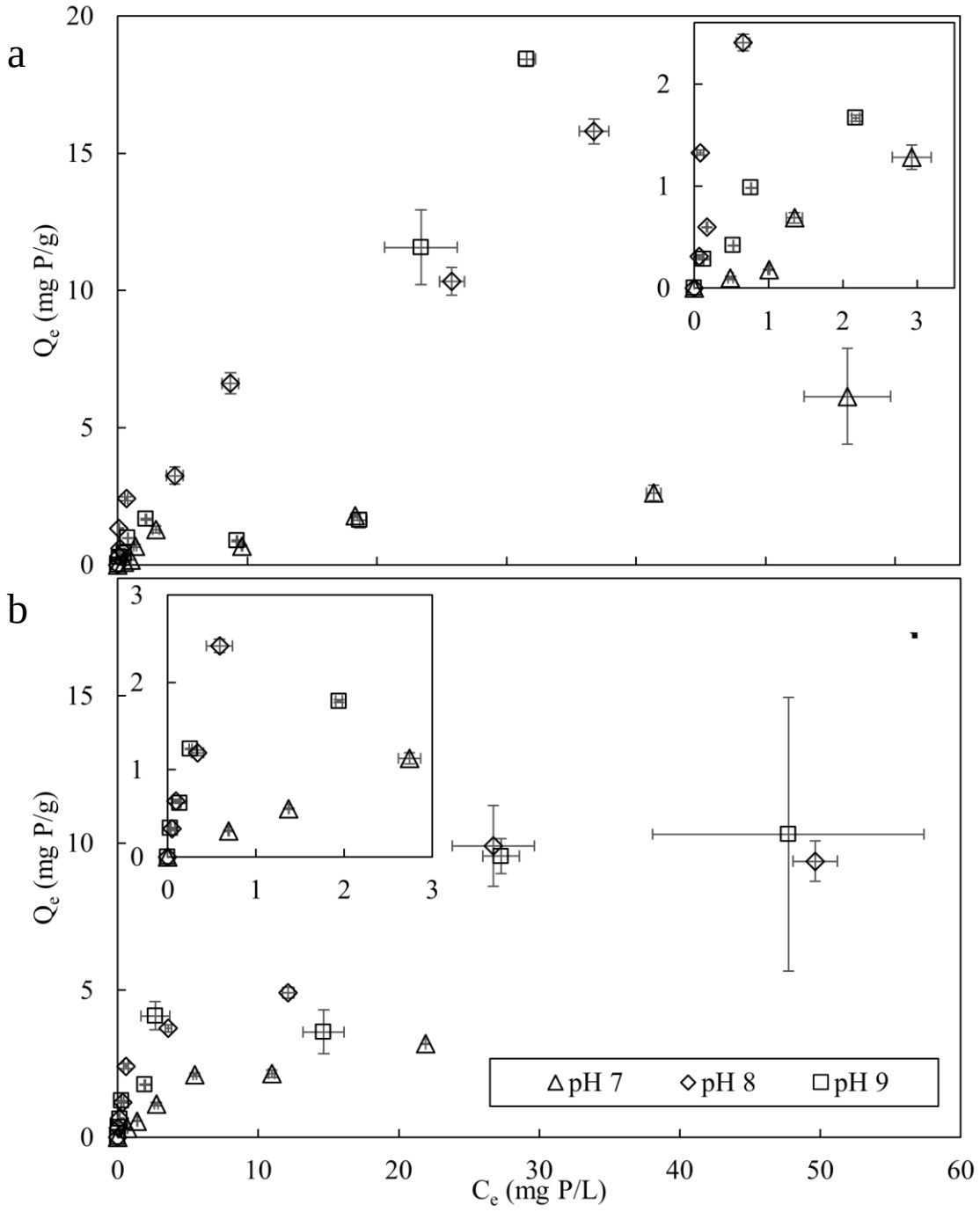

Figure 2.1 Phosphate removal by 2 g/L of (a) Mg-char (pH 13, post-pyrolysis) and (b) magnesium silicate synthesized from rice straw in DI water. C_e is the equilibrium concentration in solution and Q_e is the equilibrium adsorbed concentration. The error bars show standard deviations of duplicate measurements

2.4.2 Comparison of phosphorus uptake by different materials in DI water

A pH of 8 was selected for the comparison of the four chars (Supplementary Material) since this pH value showed good uptake and was similar to that of animal wastewaters (Huchzermeier and Tao 2012, Vanotti et al. 2003). Unamended char showed very little capacity for phosphorus uptake at pH 8 (Figure 2.2a, $Q_{e,max}$=1.4±0.5 mg/g) which was attributed to the absence of magnesium (Table 2.3), and the Mg-char prepared without pH control ("Mg-char" in Supplementary Material) also showed poor phosphorus uptake (Figure 2.2a, $Q_{e,max}$=1.39±0.06 mg/g). On the other hand, the $Q_{e,max}$ values of the two Mg-amended chars treated at pH 13 were 15.8±0.4 and 31.9±0.7 mg/g for post-pyrolysis and pre-pyrolysis, respectively (Figure 2.2a), which are ten to twenty times larger than Mg-char prepared without pH control. In addition, Mg-char (pH 13, pre-pyrolysis) removed 93±2% of added phosphorus at the highest initial concentration of 68.5 mg P/L. Furthermore, this material had an isotherm characteristic of phosphorus uptake by precipitation (i.e., low uptake at low initial phosphorus concentrations, followed by a region where Q_e values increased dramatically and the phosphorus C_e values were independent of initial concentrations (Figure 2.2a)). Phosphorus uptake on Mg-char (pH 13, post-pyrolysis), on the other hand, had an isotherm characteristic of adsorption (Figure 2.2a), similar to other reports (Jiang et al. 2019). The magnesium in the pH 13, pre-pyrolysis char may have been more soluble than that in the pH 13, post-pyrolysis char, facilitating phosphate removal by precipitation. Consistent with this, the pH 13, pre-pyrolysis char contained not only periclase (MgO(s)), but also the soluble salt magnesium salt bischofite ($MgCl_2 \cdot 6H_2O$) (Figure 2.3a).

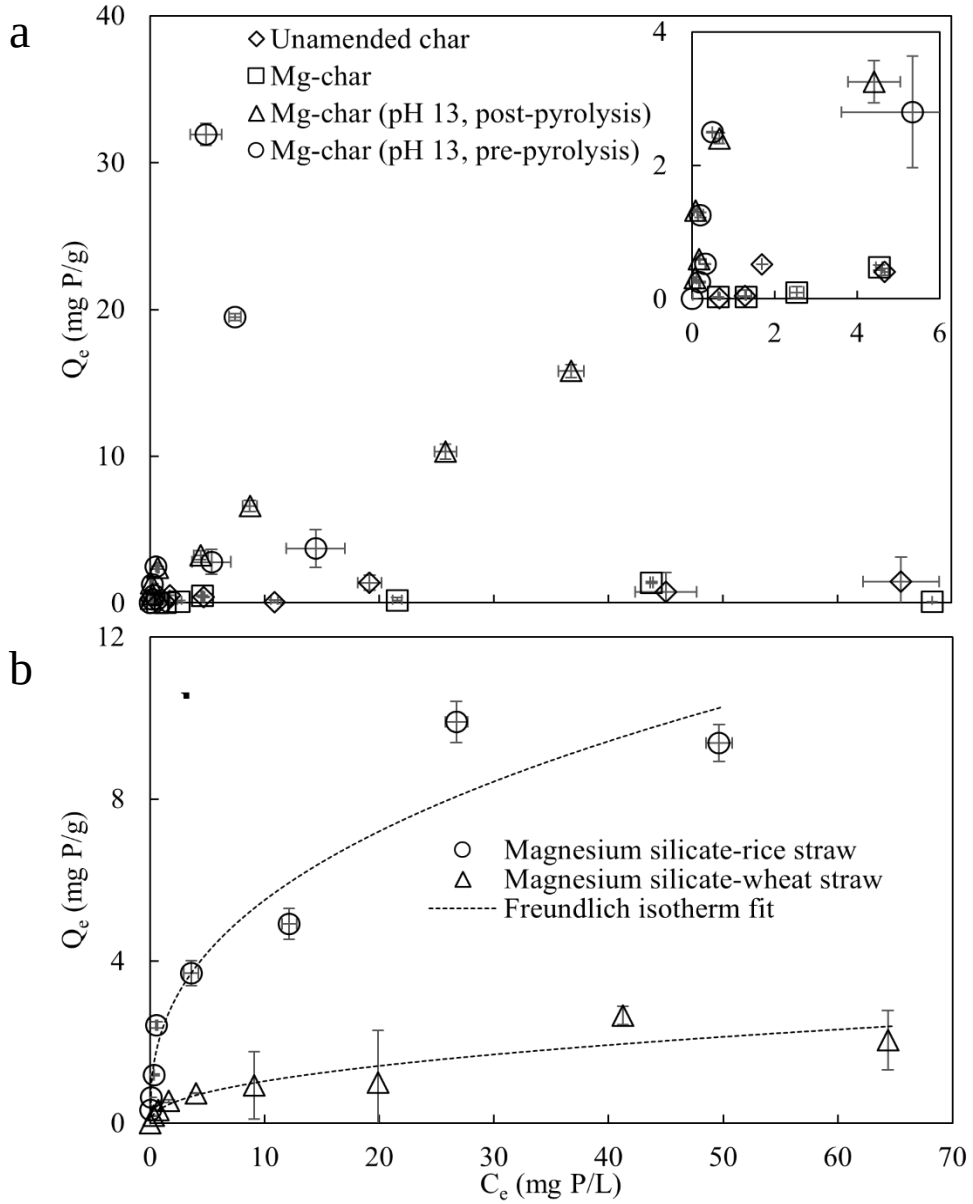

Figure 2.2 Phosphorus uptake by (a) biochars and (b) magnesium silicates in DI water with a solid concentration of 2 g/L at pH 8. C_e is the equilibrium concentration in solution and Q_e is the equilibrium adsorbed concentration. The error bars show standard deviations of the means of Q_e and C_e values obtained from duplicate measurements. Freundlich isotherm parameters are K=0.37±0.13; n=0.45±0.10; R^2=0.87 and K=2.25±0.43; n=0.39±0.06; R^2=0.95 for magnesium silicate-rice straw and magnesium silicate-wheat straw, respectively. Uncertainties associated are standard errors. Freundlich parameters were calculated using nonlinear regression with the Levenberg Marquardt algorithm, using OriginPro 2017 (Origin Lab Corporation, Northampton, Maine)

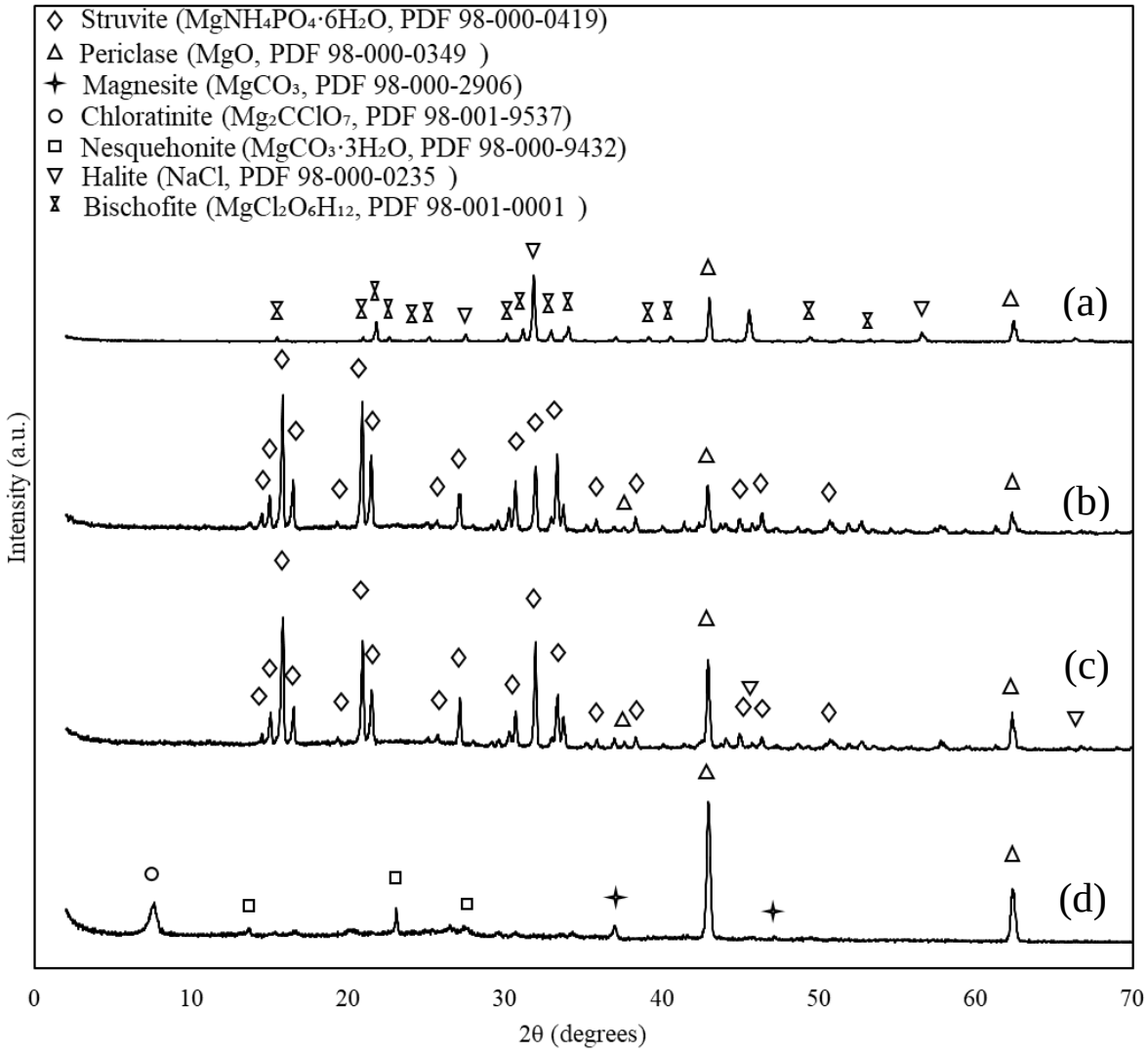

Figure 2.3 XRD patterns of Mg-char (pH 13, pre-pyrolysis) under the following conditions: (a) after synthesis and before exposure to any wastewater; (b) after exposure to pH 8 swine wastewater with phosphorus; (c) after exposure to pH 9 swine wastewater with phosphorus; and (d) after exposure to pH 8 swine wastewater without phosphorus

The Figure 2.2a trend of increased phosphorus uptake by Mg-char (pH 13, post-pyrolysis, 28 wt % Mg (Table 2.3)) compared to the unamended char (no Mg (Table 2.3)) and Mg-char (10 wt% Mg (Table 2.3)) is likely due to greater precipitation of $Mg(OH)_2(s)$ on the char matrix due to low solubility at very high pH. The better phosphorus uptake by Mg-char (pH 13, pre-

pyrolysis, 9 wt % Mg) compared to Mg-char (10 wt % Mg), however, cannot be explained by magnesium mass concentration (Table 2.3), and could be due instead to the nature of the magnesium precipitate. At temperatures above 530 ^{o}C, the $Mg(OH)_2$(s) precipitated at high pH is transformed to MgO(s) (Choudhary et al. 1992). The powder XRD pattern of Mg-char (pH 13, pre-pyrolysis) correlates well with periclase (MgO(s), PDF# 98-000-0349) (specifically the peaks at 37.1°, 43.0°, and 62.4° 2θ) (Figure 2.3a) confirming the conversion from $Mg(OH)_2$(s) to MgO(s) in the Mg-char (pH 13, pre-pyrolysis). The post-pyrolysis pH adjustment in the Mg-char (pH 13, post-pyrolysis), on the other hand, may have led to formation of a greater abundance of less soluble $Mg(OH)_2$(s), promoting uptake.

Table 2.3 Elemental analysis of corn cob biochars[1]

Elements (wt %)	Unamended char	Mg-char	Mg-char (pH 13, post-pyrolysis)	Mg-char (pH 13, pre-pyrolysis)
C	89	79	29	38
Mg	BDL[2]	10	28	9
O	11	9	34	28
P	BDL	0	BDL	BDL
Cl	BDL	2	8	20
Na	BDL	BDL	1	5

[1]Relative standard deviations for reported values are estimated to be 2-6% based on selected replicate measurements.
[2] BDL: below detection limit. The detection limit of EDS is approximately 0.01 wt %.

Magnesium silicate synthesized from rice straw showed better phosphorus uptake ($Q_{e,max}$=9.9±1.4 mg/g) than magnesium silicate synthesized from wheat straw ($Q_{e,max}$=2.7±0.2 mg/g, Figure 2.2b). In both cases, phosphorus uptake data fit well to the Freundlich isotherm (Figure 2.2b), suggesting that adsorption was primarily responsible for phosphorus uptake by these materials. Prior to phosphorus exposure both magnesium silicates were poorly crystalline,

with similar XRD patterns that had broad peaks with 2θ values between approximately 20° and 30°, and at approximately 35° and 60° (Figure 2.4 a and b). Fitting the XRD patterns with MDI JADE software identified antigorite ($Mg_{3-x}(Si_2O_5)(OH)_{4-2x}$, PDF# 00-002-0095) and enstatite ($MgSiO_3$, PDF# 98-000-6296) as possible magnesium silicate minerals with peaks in these regions.

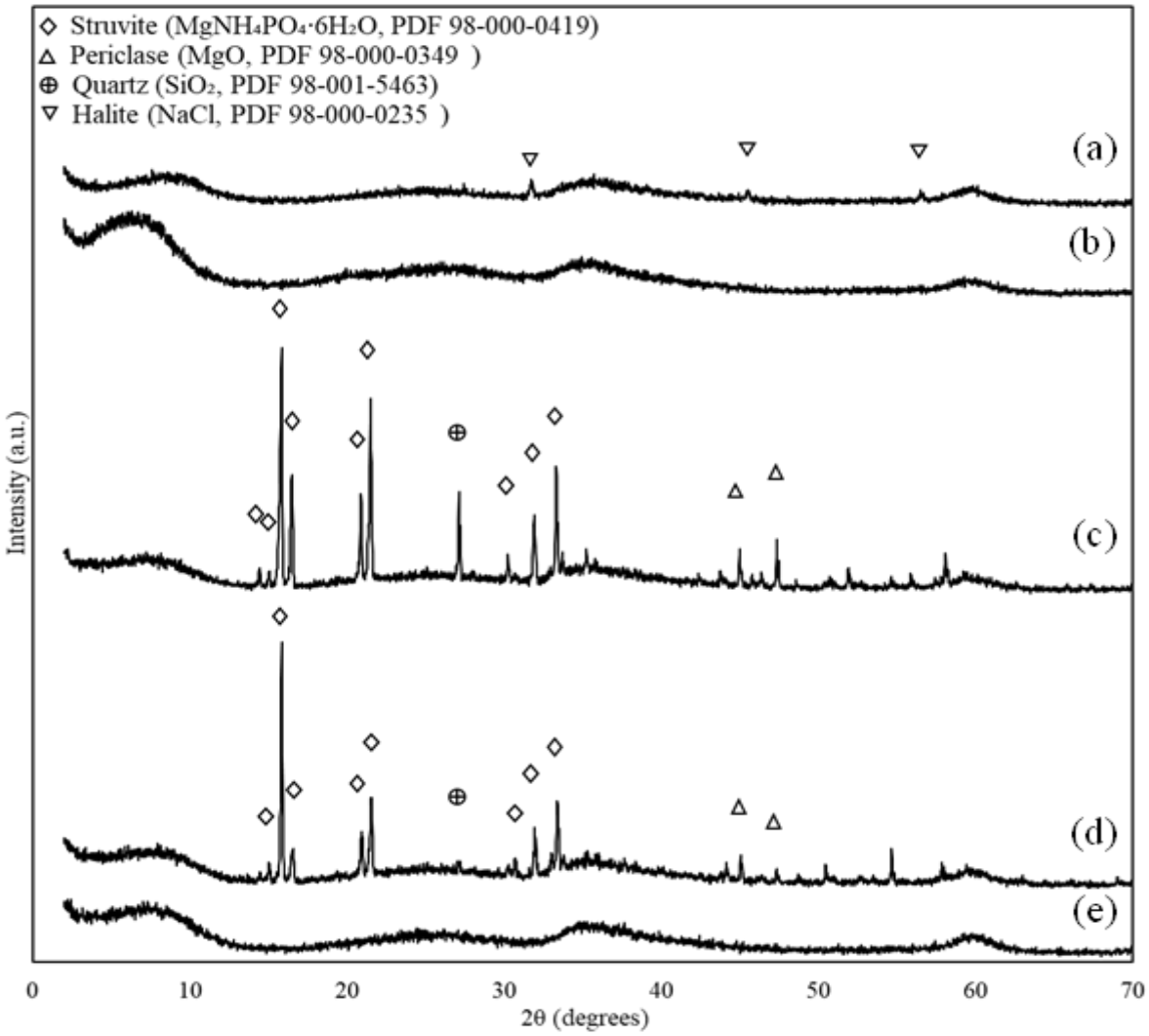

Figure 2.4 XRD patterns of magnesium silicate synthesized from rice straw and wheat straw. Patterns are: (a) magnesium silicate-rice straw and (b) magnesium silicate-wheat straw after synthesis and before wastewater exposure; magnesium silicate-rice straw after exposure to (c) pH 8 and (d) pH 9 model swine wastewater with phosphorus; (e) magnesium silicate-rice straw after exposure to pH 8 model swine wastewater without phosphorus

The magnesium silicate synthesized from rice straw also had three narrow peaks (31.7°, 45.5°, and 56.4° 2θ) corresponding to halite (NaCl) that likely formed from the presence of excess sodium (from NaOH) and chloride (from $MgCl_2 \cdot 6H_2O$) (Figure 2.4a). The XRD patterns for magnesium silicate from rice straw (Figure 2.4a) and wheat straw (Figure 2.4b) differed in the region below 10^o 2θ, with a larger peak centered at a lower value for magnesium silicate from wheat straw (Figure 2.4b) that could be explained by the presence of sepiolite ($Mg_4Si_6O_{23}H_{14}$, PDF# 98-002-0209) or vermiculite ($Mg_3Si_4O_{10}(OH)_2$, PDF# 98-000-1066). For magnesium silicate from rice straw, MDI JADE identified mutinaite (SiO_2, PDF# 98-001-1851) as a match for the broad peak around 10^o 2θ (Figure 2.4a). The differences in magnesium silicate minerals present in the two materials may explain the differences in phosphorus uptake for the magnesium silicate prepared from rice straw and wheat straw (Figure 2.2b).

2.4.3 Phosphorus uptake in simple model animal wastewaters

Next, the best performing materials from experiments in DI water (Mg-char (pH 13, pre-pyrolysis) and magnesium silicate-rice straw) were studied in simple model animal wastewaters containing both ammonia and carbonate alkalinity (Table 2.2). Experiments were conducted at both pH 8 and 9 due to better phosphorus uptake in DI water compared to pH 7 (Figure 2.1). These experiments were conducted with a solid concentration of 3 g/L to ensure sufficient magnesium for phosphorus uptake in the presence of competing ions such as bicarbonate.

The resulting uptake isotherms (Figure 2.5) did not correspond to a plateau shape typical of an adsorption isotherm where solute uptake is ultimately limited by surface functional groups for adsorption sites. Instead, the results are consistent with phosphate uptake by precipitation. Specifically, at low concentrations, C_e is approximately equal to the initial added concentration (C_0), and Q_e remains at approximately zero and is independent of C_0 (Figure 2.5). Then, above a

threshold value of C_0, which likely corresponds to a solubility limit, C_e becomes nearly independent of C_0 (it remains approximately constant) and all added solute is taken up by the solid, sharply increasing Q_e (Figure 2.5). In such a system, the transition from the zone where Q_e is independent of C_0 to that where C_e is independent of C_0 corresponds to the point where the ion activity product equals the solubility constant of the mineral that controls solubility. While uptake of phosphorus by adsorption may also have taken place, trends in Figure 2.5 data indicate that precipitation was the predominant process for phosphorus removal. XRD data indicate that the mineral struvite ($MgNH_4PO_4 \cdot 6H_2O$) was formed upon reaction of both Mg-char (pH 13, pre-pyrolysis) (Figure 2.3 b and c) and magnesium silicate-rice straw (Figure 2.4 c and d) with swine model wastewaters at both pH 8 and 9. (Only one of the model wastewaters was chosen for XRD analysis.)

Several other phosphorus uptake trends were observed with model animal wastewaters. First, at higher concentrations where C_e values were constant and independent of added phosphorus concentration, Mg-char (pH 13, pre-pyrolysis) (Figure 2.5) achieved lower phosphate concentrations for each kind of wastewater at both pH 8 and 9 than magnesium silicate-rice straw (Figure 2.5). Another way of saying this is that the C_e value where phosphorus concentration became independent of C_0 (likely due to precipitation) was lower for Mg-char (pH 13, pre-pyrolysis) than for magnesium silicate-rice straw (Figure 2.5). This could be due to a greater soluble concentration of Mg^{2+} in equilibrium with char-associated $MgO(s)/Mg(OH)_2(s)$ versus magnesium silicate at pH 8 and 9, which would have the effect of increasing the struvite ion activity product above the solubility limit for a lower total concentration of phosphate.

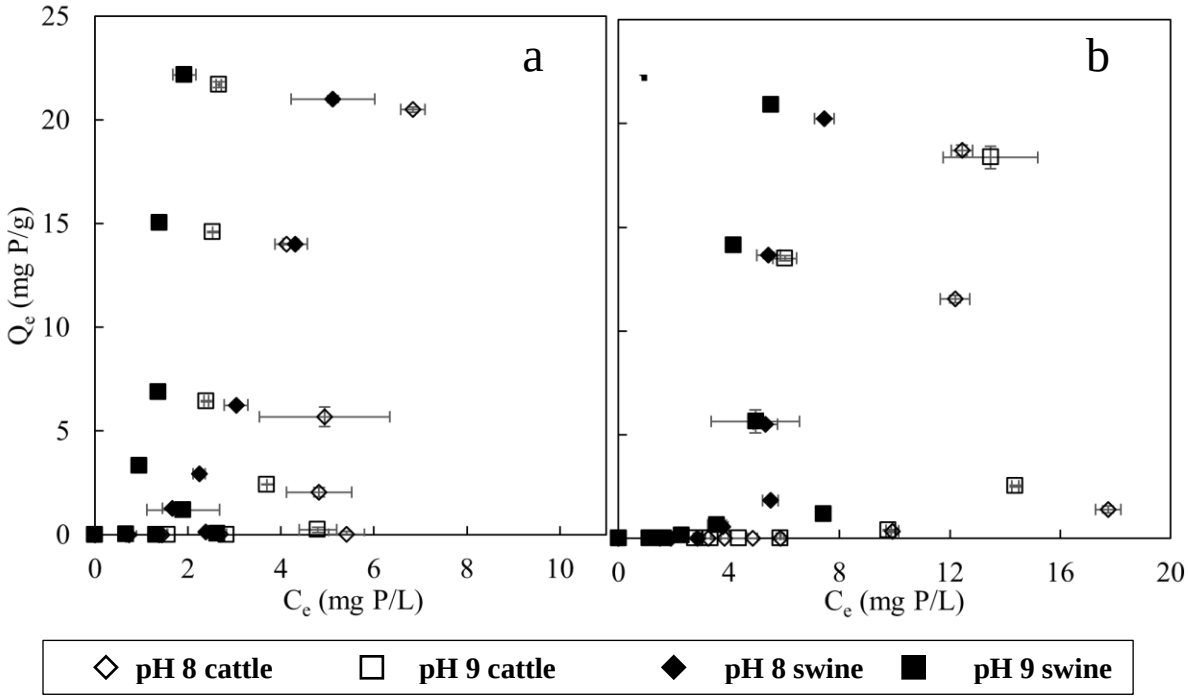

Figure 2.5 Phosphorus removal by 3 g/L of (a) Mg-char (pH 13, pre-pyrolysis) and (b) magnesium silicate synthesized from rice straw in model wastewaters. C_e is the equilibrium concentration in solution and Q_e is the equilibrium adsorbed concentration. The error bars show standard deviations of duplicate measurements

Second, lower equilibrium concentrations of phosphorus were generally achieved at pH 9 (Figure 2.5, squares) versus pH 8 (Figure 2.5, diamonds), which may be due to the greater deprotonation of orthophosphate (i.e., more HPO_4^{2-} versus $H_2PO_4^-$) at the higher pH value, which favors struvite formation (Darwish et al. 2016). Research has shown that pH values of 9 to 10 are most favorable for phosphorus recovery through struvite precipitation (Heraldy et al. 2017).

Finally, lower equilibrium concentrations were observed in the model swine wastewater compared to the model cattle wastewater. For example, for Mg-char (pH 13, pre-pyrolysis) at pH 9, lower C_e values were obtained for the swine wastewater ($C_{e,max}$<3 mg/L) versus the cattle wastewater ($C_{e,max}$<5 mg/L) (Figure 2.5a). The same trend was observed for phosphorus uptake

by magnesium silicate (Figure 2.5b). This can be explained by the significantly higher alkalinity in the model cattle wastewater (Table 2.2). Carbonate alkalinity likely competes with phosphate for dissolved Mg^{2+}, hindering phosphorus removal (Huchzermeier and Tao 2012). Evidence for this includes formation of the minerals magnesite ($MgCO_3$) and nesquehonite ($MgCO_3 \cdot 3H_2O$) on Mg-char (pH 13, pre-pyrolysis) that was equilibrated in model swine wastewater with no phosphorus (Figure 2.3d).

Despite the limitations discussed above, Mg-char (pH 13, pre-pyrolysis) and magnesium silicate made from rice straw removed a significant amount (97% and 92% of added 68.5 mg/L phosphorus, respectively) of the phosphorus present in pH 9 model wastewaters (Figure 2.5).

2.4.4 Release of phosphorus from spent materials

After exposure to phosphorus, Mg-char (pH 13, pre-pyrolysis) and magnesium silicate synthesized from rice straw were tested for phosphorus release using modified soil tests to mimic the spent material being applied as a fertilizer. Up to 55, 33, and 61 mg/g phosphorus was released using the Bray and Kurtz P1, modified Mehlich 3, and Olsen P procedures, respectively (Figure 2.6). The lowest phosphorus release in all cases was with the modified Mehlich 3 procedure, with significantly higher release being achieved with the Bray and Kurtz P1 and the Olsen P tests (Figure 2.6). In many cases, the Olsen-P test released more phosphorus than the Bray and Kurtz P-1. These trends suggest that a common process or processes are responsible for phosphorus release for both Mg-char (pH 13, pre-pyrolysis) and magnesium silicate-rice straw at both pH 8 and 9, consistent with the detection of struvite for both materials (Figure 2.3 b and c, Figure 2.4 c and d).

The Bray and Kurtz P1 and the modified Mehlich 3 methods both employ F^- (as NH_4F), which, like HCO_3^- serves to displace sorbed phosphate (Dickman and Bray 1941). Low pH

serves to release acid-soluble phosphorus, or phosphorus in mineral form. In this study, the Mehlich 3 extracting solution was adjusted to neutral pH, whereas the Bray and Kurtz P1 extractant had a considerably lower pH. Under these conditions, the modified Mehlich 3 test likely released the concentration of adsorbed phosphorus and the Bray and Kurtz P1 estimated the sum of mineral and adsorbed phosphorus. Poor phosphorus release by the modified Mehlich 3 method suggests that precipitation was the dominant mechanism for phosphorus removal from the animal wastewaters.

The Olsen P extractant consists of 0.5 M HCO_3^- (as $NaHCO_3$), which reacts with Mg^{2+}, driving dissolution of magnesium phosphorus minerals (Olsen 1954). Bicarbonate (HCO_3^-), like F^-, can also displace sorbed orthophosphate (Olsen 1954). Thus, the Olsen P test estimates concentrations of both solid (HCO_3^- soluble) and sorbed orthophosphate. Good phosphorus release with the Olsen P test for both Mg-char (pH 13, pre-pyrolysis) and magnesium silicate from rice straw is also consistent with precipitation as the dominant phosphorus removal mechanism.

In some cases, the phosphorus released (Figure 2.6), expressed as mg P per g solid, exceeded phosphorus uptake (Figure 2.5, points with the largest Q_e values (corresponding to C_0=68.5 mg P/L)). This can be explained by loss of significant sorbent mass during isotherm experiments (at least 50% in experiments with Mg-char (pH 13, pre-pyrolysis) and 6-13% in experiments with magnesium silicate-rice straw), most likely due to dissolution of soluble bishofite (Figure 2.3a) and halite (Figure 2.3a and 2.4a). Fine particles may also have been lost during solids retrieval after isotherm tests by centrifugation and filtration. Values of phosphorus uptake on the solids (i.e., Q_e values in Figure 2.5) were calculated using the mass of solids added

to the experiments, while values of released phosphorus (Figure 2.6) were calculated using the lower mass of solids retrieved from the isotherm experiments.

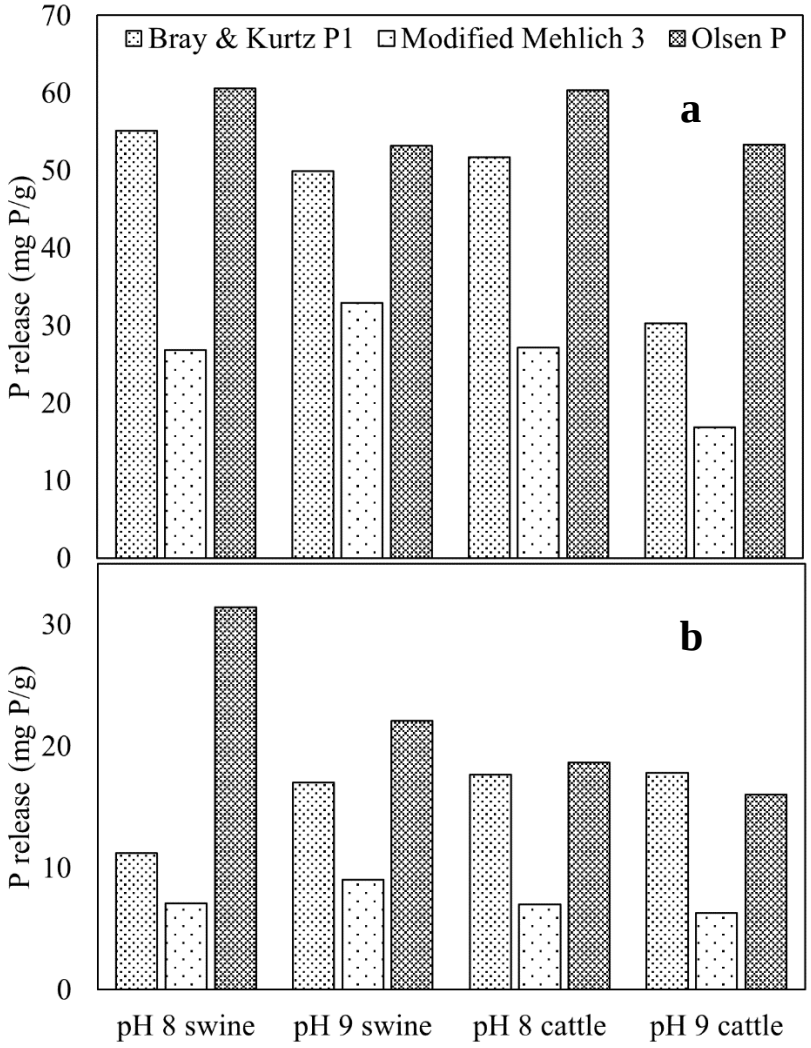

Figure 2.6 Phosphorus release by spent materials: (a) Mg-char (pH 13, pre-pyrolysis) and (b) magnesium silicate synthesized from rice straw. The final pH values of each extractant/solid mixture were 3.8-4.2 (Bray and Kurtz P1), 7.2-7.4 (Modified Mehlich 3), and 8.6 (Olsen P). The relative standard deviation ranged from 1-4% for measurements made in standard solutions of NaH_2PO_4

2.5 Conclusions

Magnesium modified biochars prepared from corn cobs and magnesium silicate prepared from rice straw were tested for phosphorus recovery from simple model animal wastewaters containing ammonia and alkalinity. Char from corn cobs that was equilibrated with dissolved Mg^{+2} at pH 13 prior to pyrolysis (Mg-char (pH 13, pre-pyrolysis)) showed the best phosphorus uptake. Precipitation of struvite was responsible for phosphorus uptake in the model wastewaters, and the best phosphorus removal was observed at pH 9 which was attributed to favorable phosphate speciation. Alkalinity in the model wastewaters significantly decreased phosphorus uptake through competition of bicarbonate and carbonate with phosphate for dissolved magnesium. After phosphorus uptake, spent materials were tested for phosphorus release using modified soil tests. Favorable levels of phosphorus release occurred from spent materials in the presence of bicarbonate (Olsen-P test), indicating the potential promise of these materials as fertilizers in calcareous soils.

The phosphorus uptake capacities measured in the model animal wastewaters (up to 22 mg/g, Figure 2.5) compare favorably to other studies of Mg amended biochars (30 mg/g (Chen et al. 2018) and 31 mg/g (Jiang et al. 2019)), considering the presence of significant alkalinity in the model wastewaters studied here. Furthermore, lowering the alkalinity prior to treatment for phosphorus uptake has the potential to significantly increase phosphorus removal efficiency (compare swine and cattle wastewaters (Figures 2.5a and b), which differ significantly in alkalinity (Table 2.2)). And although final C_e concentrations in the treated animal wastewaters were higher than desirable for discharge to surface waters (8-14 mg/L, Figure 2.5), the sorbent materials produced in this study removed a significant fraction of the total added mass of phosphorus (up to 88%) for subsequent use as fertilizer. Since phosphorus concentrations

significantly higher than the highest value studied here (68.5 mg/L as P) are common (e.g., Huchzermeier and Tao 2012), an even greater proportion of phosphorus could conceivably be recovered. In addition, treatment of animal wastewaters with the materials synthesized here could be the first step in phosphorus removal that is aimed at phosphorus recovery for reuse, with subsequent treatment by e.g., advanced biological processes or precipitation with iron or aluminum salts, intended to achieve concentrations acceptable for discharge to surface waters.

Important parameters to investigate in future research include the potential for formation of harmful byproducts in char, such as polynuclear aromatic hydrocarbons (Hale et al. 2012), as well as accumulation of metals, antibiotics, and antibiotic resistance genes in solids precipitated from animal waste (Cai et al. 2020). Furthermore, since sustainable phosphorus use requires consideration of both economic and environmental impacts (Bornø et al. 2018), the cost and environmental impacts, including water use, should be evaluated for phosphorus removal and recycling using waste-derived magnesium amended char and magnesium silicate.

2.6 Acknowledgements

The authors thank Andrew Elwood Madden for help with XRD analysis and Preston Larson for guidance with SEM-EDS analyses. Anna McClung and Laduska Sells at the USDA Dale Bumpers National Rice Research Center in Stuttgart, Arkansas kindly provided the rice straw used in this study. This work was supported by Agriculture and Food Research Initiative (AFRI) grant number 2018-67020-27805 from the USDA National Institute of Food and Agriculture.

2.7 References

Adam, F. and Thankappan, R. (2010) Oxidation of benzene over bimetallic Cu-Ce incorporated rice husk silica catalysts. Chemical Engineering Journal 160(1), 249-258.

Ali, I.M., Kotp, Y.H. and El-Naggar, I.M. (2010) Thermal stability, structural modifications and ion exchange properties of magnesium silicate. Desalination 259(1-3), 228-234.

American Public Health Association, A.W.W.A., Water Environment Federation (1992) Phosphorus (4500-P)/Ascorbic Method, p. 2, American Public Health Association, Washington, DC.

ASTM (2015) Standard Test Method for Sieve Analysis of Fine and Coarse Aggregates, West Conshohocken, PA. USA.

Bacelo, H., Pintor, A.M., Santos, S.C., Boaventura, R.A. and Botelho, C.M. (2020) Performance and prospects of different adsorbents for phosphorus uptake and recovery from water. Chemical Engineering Journal 381, 122566.

Berber-Villamar, N.K., Netzahuatl-Muñoz, A.R., Morales-Barrera, L., Chávez-Camarillo, G.M., Flores-Ortiz, C.M. and Cristiani-Urbina, E. (2018) Corncob as an effective, eco-friendly, and economic biosorbent for removing the azo dye Direct Yellow 27 from aqueous solutions. Plos One 13(4), e0196428.

Bornø, M.L., Müller-Stöver, D.S. and Liu, F. (2018) Contrasting effects of biochar on phosphorus dynamics and bioavailability in different soil types. Science of the Total Environment 627, 963-974.

Bray, R.H. and Kurtz, L. (1945) Determination of total, organic, and available forms of phosphorus in soils. Soil science 59(1), 39-46.

Brunson, L.R. and Sabatini, D.A. (2016) Methods for optimizing activated materials for removing fluoride from drinking water sources. Journal of Environmental Engineering 142(2), 04015078.

Cai, J., Ye, Z.-L., Ye, C., Ye, X. and Chen, S. (2020) Struvite crystallization induced the discrepant transports of antibiotics and antibiotic resistance genes in phosphorus recovery from swine wastewater. Environmental Pollution 266, 115361.

Chalmers, R.A. and Sinclair, A.G. (1966) Analytical applications of β-heteropoly acids: This influlsnce of complexing agents on selective formation. Analytica Chimica Acta 34, 412-418.

Chen, Q.C., Qin, J.L., Cheng, Z.W., Huang, L., Sun, P., Chen, L. and Shen, G.Q. (2018) Synthesis of a stable magnesium-impregnated biochar and its reduction of phosphorus leaching from soil. Chemosphere 199, 402-408.

Choudhary, V.R., Pataskar, S.G., Pandit, M.Y. and Gunjikar, V.G. (1992) Influence of Precipitation Conditions of Magnesium-hydroxide on Its Thermal-decomposition in the Preparation of Active MgO. Thermochimica Acta 194, 361-373.

Darwish, M., Aris, A., Puteh, M.H., Abideen, M.Z. and Othman, M.N. (2016) Ammonium-Nitrogen Recovery from Wastewater by Struvite Crystallization Technology. Separation and Purification Reviews 45(4), 261-274.

Ellis-Petersen, H. (2019) Delhi's smog blamed on crop fires – but farmers say they have little choice, The Guardian.

Fang, C., Zhang, T., Li, P., Jiang, R.F. and Wang, Y.C. (2014) Application of Magnesium Modified Corn Biochar for Phosphorus Removal and Recovery from Swine Wastewater. International Journal of Environmental Research and Public Health 11(9), 9217-9237.

Galhardo, C.X. and Masini, J.C. (2000) Spectrophotometric determination of phosphate and silicate by sequential injection using molybdenum blue chemistry. Analytica Chimica Acta 417(2), 191-200.

Hale, S.E., Lehmann, J., Rutherford, D., Zimmerman, A.R., Bachmann, R.T., Shitumbanuma, V., O'Toole, A., Sundqvist, K.L., Arp, H.P.H. and Cornelissen, G. (2012) Quantifying the total and bioavailable polycyclic aromatic hydrocarbons and dioxins in biochars. Environmental Science & Technology 46(5), 2830-2838.

Hanhoun, M., Montastruc, L., Azzaro-Pantel, C., Biscans, B., Frèche, M. and Pibouleau, L. (2011) Temperature impact assessment on struvite solubility product: A thermodynamic modeling approach. Chemical Engineering Journal 167(1), 50-58.

Heraldy, E., Rahmawati, F., Heriyanto and Putra, D.P. (2017) Preparation of struvite from desalination waste. Journal of Environmental Chemical Engineering 5(2), 1666-1675.

Huang, X.H., Wu, T., Li, Y.J., Sun, D.J., Zhang, G.C., Wang, Y., Wang, G.P. and Zhang, M.L. (2012) Removal of petroleum sulfonate from aqueous solutions using freshly generated magnesium hydroxide. Journal of Hazardous Materials 219, 82-88.

Huchzermeier, M.P. and Tao, W.D. (2012) Overcoming Challenges to Struvite Recovery from Anaerobically Digested Dairy Manure. Water Environment Research 84(1), 34-41.

Ippolito, J.A., Spokas, K.A., Novak, J.M., Lentz, R.D. and Cantrell, K.B. (2015) Biochar for environmental management: Science, technology and implementation, pp. 139-163.

Jiang, Y.H., Li, A.Y., Deng, H., Ye, C.H., Wu, Y.Q., Linmu, Y.D. and Hang, H.L. (2019) Characteristics of nitrogen and phosphorus adsorption by Mg-loaded biochar from different feedstocks. Bioresource Technology 276, 183-189.

Khan, M.A., Sarwar, M., Nisa, M.-u. and Khan, M.S. (2004) Feeding value of urea treated corncobs ensiled with or without enzose (corn dextrose) for lactating crossbred cows. Asian-Australasian Journal of Animal Sciences 17(8), 1093-1097.

Kok, D.J.D., Pande, S., van Lier, J.B., Ortigara, A.R.C., Savenije, H. and Uhlenbrook, S. (2018) Global phosphorus recovery from wastewater for agricultural reuse. Hydrology and Earth System Sciences 22(11), 5781-5799.

Mehlich, A. (1984) Mehlich 3 soil test extractant: A modification of Mehlich 2 extractant. Communications in Soil Science and Plant Analysis 15(12), 1409-1416.

Mitrogiannis, D., Psychoyou, M., Baziotis, I., Inglezakis, V.J., Koukouzas, N., Tsoukalas, N., Palles, D., Kamitsos, E., Oikonomou, G. and Markou, G. (2017) Removal of phosphate from aqueous solutions by adsorption onto Ca(OH)(2) treated natural clinoptilolite. Chemical Engineering Journal 320, 510-522.

Moraes, C.A., Fernandes, I.J., Calheiro, D., Kieling, A.G., Brehm, F.A., Rigon, M.R., Berwanger Filho, J.A., Schneider, I.A. and Osorio, E. (2014) Review of the rice production cycle: By-products and the main applications focusing on rice husk combustion and ash recycling. Waste Management & Research 32(11), 1034-1048.

Mukherjee, D., Ray, R. and Biswas, N. (2020) Sustaining Resources for Tomorrow. Stagner, J.A. and Ting, D.S.K. (eds), pp. 67-81, Springer International Publishing, Cham.

Nakhshiniev, B., Biddinika, M.K., Gonzales, H.B., Sumida, H. and Yoshikawa, K. (2014) Evaluation of hydrothermal treatment in enhancing rice straw compost stability and maturity. Bioresource Technology 151, 306-313.

Nixon, S.W. (1995) Coastal marine eutrophication: A definition, social causes, and future concerns. Ophelia 41(1), 199-219.

Olsen, S.R. (1954) Estimation of available phosphorus in soils by extraction with sodium bicarbonate, US Department of Agriculture.

Pierzynski, G.M. (2000) Methods of phosphorus analysis for soils, sediments, residuals, and waters, North Carolina State University Raleigh.

Pinzi, S. and Dorado, M.P. (2011) Handbook of Biofuels Production. Luque, R., Campelo, J. and Clark, J. (eds), pp. 61-94, Woodhead Publishing.

Rittmann, B.E., Mayer, B., Westerhoff, P. and Edwards, M. (2011) Capturing the lost phosphorus. Chemosphere 84(6), 846-853.

Roy, E.D. (2017) Phosphorus recovery and recycling with ecological engineering: A review. Ecological Engineering 98, 213-227.

Seida, Y. and Nakano, Y. (2002) Removal of phosphate by layered double hydroxides containing iron. Water research 36(5), 1306-1312.

Smith, R.W. and Hwang, M.-Y. (1978) Phosphate adsorption of magnesium silicates. Journal (Water Pollution Control Federation), 2189-2197.

Streets, D., Yarber, K., Woo, J.H. and Carmichael, G. (2003) Biomass burning in Asia: Annual and seasonal estimates and atmospheric emissions. Global Biogeochemical Cycles 17(4).

Szogi, A.A., Vanotti, M.B. and Ro, K.S. (2015) Methods for treatment of animal manures to reduce nutrient pollution prior to soil application. Current Pollution Reports 1(1), 47-56.

Terzioglu, P. and Yucel, S. (2012) Synthesis of magnesium silicate from wheat husk ash: effect of parameters on structural and surface properties. Bioresources 7(4), 5435-5447.

Valisko, M., Boda, D. and Gillespie, D. (2007) Selective adsorption of ions with different diameter and valence at highly charged interfaces. The Journal of Physical Chemistry C 111(43), 15575-15585.

Vanotti, M.B., Szogi, A.A. and Hunt, P.G. (2003) Extraction of soluble phosphorus from swine wastewater. Transactions of the Asae 46(6), 1665-1674.

Withers, P.J.A., Forber, K.G., Lyon, C., Rothwell, S., Doody, D.G., Jarvie, H.P., Martin-Ortega, J., Jacobs, B., Cordell, D., Patton, M., Camargo-Valero, M.A. and Cassidy, R. (2020) Towards resolving the phosphorus chaos created by food systems. Ambio 49(5), 1076-1089.

Yao, Y., Gao, B., Inyang, M., Zimmerman, A.R., Cao, X., Pullammanappallil, P. and Yang, L., 2011. Biochar derived from anaerobically digested sugar beet tailings: characterization and phosphate removal potential. Bioresource technology 102(10), 6273-6278.

Zhang, M., Gao, B., Yao, Y., Xue, Y.W. and Inyang, M. (2012) Synthesis of porous MgO-biochar nanocomposites for removal of phosphate and nitrate from aqueous solutions. Chemical Engineering Journal 210, 26-32.

Zhang, T., He, X., Deng, Y., Tsang, D.C., Yuan, H., Shen, J. and Zhang, S. (2020) Swine manure valorization for phosphorus and nitrogen recovery by catalytic–thermal hydrolysis and struvite crystallization. Science of the Total Environment 729, 138999.

Zhu, D.C., Chen, Y.Q., Yang, H.P., Wang, S.H., Wang, X.H., Zhang, S.H. and Chen, H.P., 2020. Synthesis and characterization of magnesium oxide nanoparticle-containing biochar composites for efficient phosphorus removal from aqueous solution. Chemosphere 247, 125847,

2.8 Supplementary Material

2.8.1 SEM images

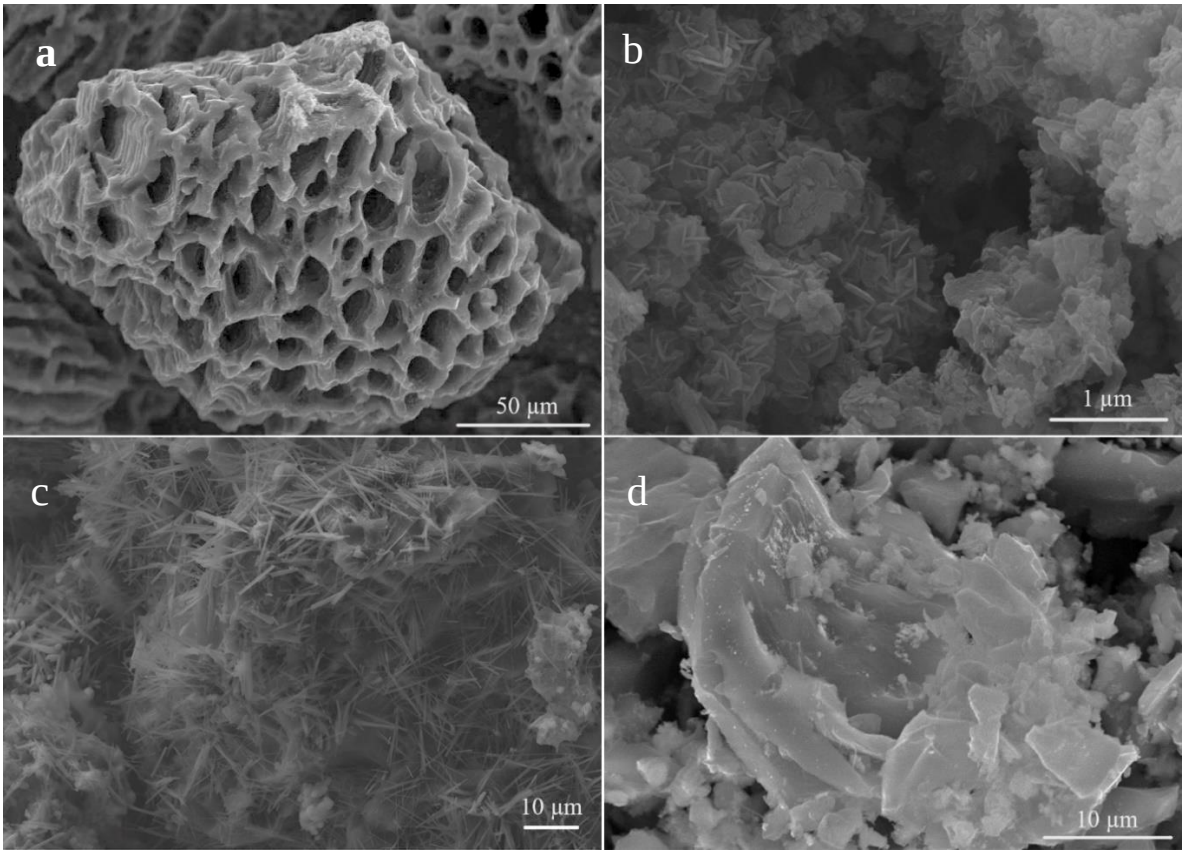

Figure 2S.1 Scanning electron microscope (SEM) images of (a) unamended char; (b) Mg-char (pH 13, post-pyrolysis); (c) Mg-char (pH 13, pre-pyrolysis); and (d) Mg-char

2.8.2 Preparation of biochar from corn cobs

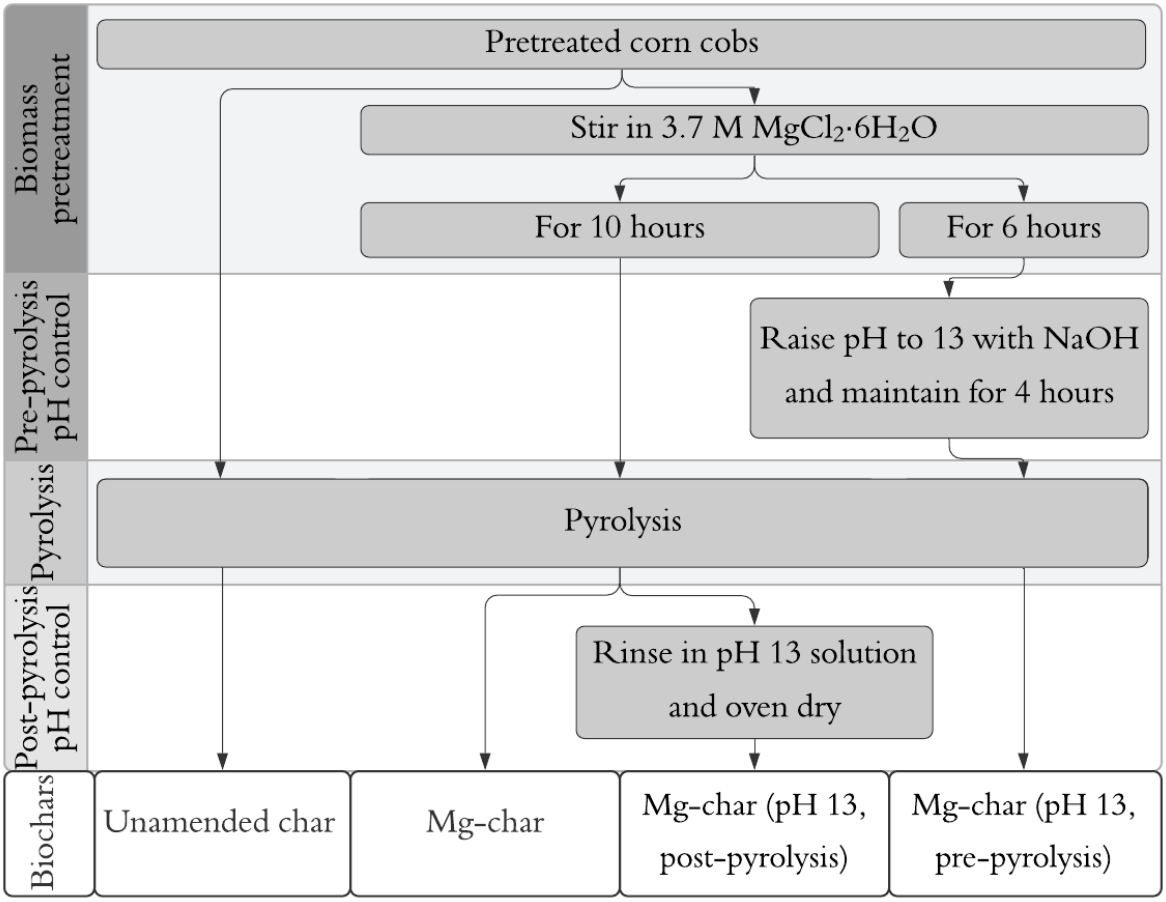

Figure 2S.2 Synthesis of unamended char, Mg-char, Mg-char (pH 13, post-pyrolysis), and Mg-char (pH 13, pre-pyrolysis)

2.8.3 Kinetics of phosphorus uptake

A kinetic study was conducted with 2 g/L of Mg-char (pH 13, pre-pyrolysis) and magnesium silicate synthesized from rice straw in 0.1 M HEPES buffer at pH 8 (Figure 2S.1). The buffer solution was made using 2-[4-(2-hydroxyethyl)piperazin-1-yl]ethanesulfonic (HEPES) acid crystal (≥ 99%, Fisher Bioreagents, Ottawa, Ontario) and pH was adjusted using 10 M NaOH solution. Experiments were done by equilibrating 0.05 g of each material with 24 mL buffer solution for 24 hours, then adding 1 mL of 548 mg P/L Na_2HPO_4 (ACS, Fisher Chemical, Fair Lawn, New Jersey) to obtain a mid-range initial concentration of 21.9 mg P/L.

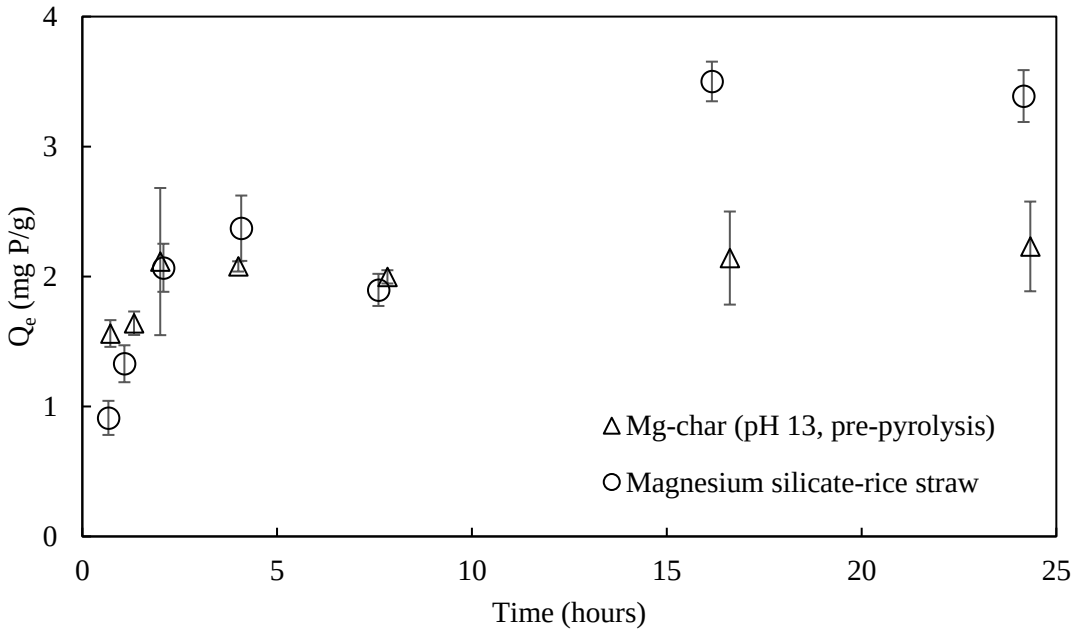

Figure 2S.3 Phosphorus uptake by 2 g/L of Mg-char (pH 13, pre-pyrolysis) and magnesium silicate synthesized from rice straw versus time in 0.1 M HEPES pH 8 buffer solution with an initial phosphorus concentration of 21.9 mg /L. Q_e is the equilibrium adsorbed concentration. The error bars show standard deviations of the mean of duplicate measurements

Chapter 3 Effects of pH and Soil Minerals on Phosphorus Release from Agricultural Waste-Based Sorbents: A Continuous Flow Column Study[†]

3.1 Abstract

Effective methods for recovery and reuse of phosphorus are needed for sustainable agriculture. In this study, magnesium amended corn cob chars prepared with brucite and sea bittern, and calcium silicate hydrate (CSH) synthesized with hydrated lime and rice husk ash, were tested for phosphorus recovery from a model animal wastewater at pH 8.0. After phosphorus uptake from the model wastewater, the two Mg-chars had a phosphorus concentration of 182-198 mg P/g, and CSH had a phosphorus concentration of 46 mg P/g. In continuous flow column release studies, in which these materials were mixed with sand after phosphorus uptake, Mg-chars released over 80% of the recovered phosphorus within five pore volumes at pH 5.5, 7.0, and 8.5. Post-P-exposure CSH, on the other hand, required 335 pore volumes to release 90% of the recovered phosphorus at pH 8.5. The more rapid release at pH 5.5 and 7.0 compared to pH 8.5 for the spent Mg-chars is attributed to the greater solubility of magnesium phosphate minerals at lower pH values. When goethite or kaolinite was added to the sand columns containing spent Mg char, the rate and extent of phosphorus release slowed significantly, especially for goethite versus kaolinite, and especially at pH 5.5. and 7.0 versus pH 8.5 for both minerals. This trend is attributed to the greater electrostatic driving force for adsorption of phosphate to the mineral surface below the mineral point of zero charge (pH_{pzc}).

[†] Ding, Y., Sabatini, D.A. and Butler, E.C. (2023) Effects of pH and Soil Minerals on Phosphorus Release from Agricultural Waste-Based Sorbents: A Continuous-Flow Column Study. Journal of Environmental Engineering 149(4), 04023010.

3.2 Introduction

Effective methods for phosphorus recovery from wastewaters and reuse as fertilizer are needed to close the phosphorus cycle (Nagarajan et al. 2020) and mitigate eutrophication (Li et al. 2020). Among the technologies being developed, magnesium and calcium-based sorbents derived from agricultural wastes, such as biochars, have shown promise for phosphorus recovery and potential for subsequent reuse (Rittmann et al. 2011). Numerous studies have used magnesium or calcium chloride salts to prepare sorbents for phosphorus recovery (e.g., Finn et al. 2022 and Sharmin et al. 2021), but many naturally occurring materials can also be used for this purpose.

Minerals such as brucite ($Mg(OH)_2(s)$), periclase (MgO(s)), and dolomite ($CaMg(CO_3)_2(s)$) (Jarosinski et al. 2020, Li et al. 2013, Li et al. 2019) can serve as sources of magnesium for biochar amendment, where MgO(s) on the biochar surface after pyrolysis is responsible for phosphorus recovery (Zhang et al. 2012, Ghodszad et al. 2021). In the case of dolomite, pyrolysis yields both MgO(s) and calcium oxide (CaO(s)) (Meldau and Robertson 1953). CaO(s) is also effective for phosphate recovery through adsorption (Khan et al. 2020) and precipitation with dissolved Ca^{2+} (Li et al. 2019).

In addition to these minerals, seawater and bittern are also rich sources of magnesium and calcium. Seawater contains over 0.05 M Mg^{2+} and over 0.01 M Ca^{2+} (Liu et al. 2013), and when used to treat biochar, it leads to formation of magnesium and calcium oxides that contribute to phosphate removal (Bradford-Hartke et al. 2021, Shirazinezhad et al. 2021). Similarly, bittern, a mixture of salts produced during evaporation of sea water, is another magnesium rich material suitable for biochar amendment (Lee et al. 2003, Ye et al. 2011, Sanghavi et al. 2020, Zangarini et al. 2020, Bradford-Hartke et al. 2021). In addition to its high magnesium content (1.33 M (Lee

et al. 2003)), bittern is a very cheap, and in some cases free, by-product from sea salt production (Zangarini et al. 2020). Bittern is effective in phosphorus immobilization to form struvite (Bradford-Hartke et al. 2021).

Calcium silicate hydrate (CSH) is another effective phosphorus recovery agent that can be derived from agricultural wastes and natural occurring minerals. Silicon-rich wastes such as rice straw or rice husks can be used to prepare dissolved silica that can form CSH under alkaline conditions in the presence of a calcium salt (Sharmin et al. 2021) or hydrated lime ($Ca(OH)_2$ (s)) (Okano et al. 2013).

Reuse of recovered phosphorus as fertilizer is needed to make progress toward the goal of a closed phosphorus cycle. Such phosphorus recovery and reuse, however, faces challenges. For example, constituents in realistic wastewater matrices, such as bicarbonate alkalinity (Huchzermeier et al. 2012, Okano et al. 2013, Ding et al. 2021, Sharmin et al. 2021) can significantly reduce the efficiency of phosphorus uptake by exerting a calcium or magnesium demand (Crutchik et al. 2018). In addition, interaction between phosphate and iron (hydr)oxide soil minerals such as goethite, hematite, and ferrihydrite yields strong inner-sphere complexes (Li et al. 2016, Nobaharan et al. 2021), retaining phosphorus in the soil. Soil clay minerals such as kaolinite can also immobilize phosphate through ligand exchange with hydroxyl functional groups (Ioannou and Dimirkou 1997, Kamiyango et al. 2009b). Aluminum-phosphate precipitation (Penn and Warren 2009) and electrostatic adsorption (Xiong et al. 2022) can also contribute to phosphate immobilization in the presence of clay minerals such as kaolinite at low soil pH.

Solution pH strongly affects phosphate interactions with soil minerals such as kaolinite and goethite. The pH_{pzc} values of goethite and kaolinite have been reported to be 8.6±0.8

(Kosmulski 2009) and 3.6 (Au et al. 2015), respectively, although Al-OH edge sites on clay minerals can have higher pH_{pzc} values than the bulk mineral (Schroth and Sposito 1996, Kamiyango et al. 2009). Solution pH values below these pH_{pzc} values would favor adsorption of anionic phosphate species through electrostatic attraction, while pH values above the pH_{pzc} would be less favorable for adsorption. Even above the pH_{pzc}, however, the strong driving force for inner sphere adsorption of phosphate species to iron oxides such as goethite could result in significant adsorption (e.g., Sigg and Stumm 1981) and sequestration in the soil.

In this study, two Mg-chars and CSH were used to remove phosphorus from a model animal wastewater, then the spent Mg-chars and CSH were tested for phosphorus release under flow through conditions in columns containing sand, and in some cases goethite or kaolinite. The effect of pH on phosphorus release was studied at pH 5.5, 7.0, and 8.5. The objectives were to (1) compare several waste-derived phosphorus sorbents in terms of phosphorus uptake, and (2) add the spent sorbents to soil columns to model their application to agricultural soils as fertilizers, and monitor phosphorus release upon water infiltration. The uniqueness of this study lies in the testing of our novel agricultural waste-based sorbents on model animal wastewaters containing components (such as carbonate alkalinity) that make phosphorus recovery more challenging, as well as testing the fertilizer potential of the phosphorous-loaded sorbent by measuring phosphorus release in model soils containing clay minerals and iron oxides known to sequester phosphorus.

3.3 Materials and Methods

3.3.1 Biomass and chemicals used in this study

Biomass samples used in this study were: corn cobs (Kaytee, Chilton, Wisconsin) and rice husks (Home Brew Ohio, Sandusky, OH). Chemicals used were: magnesium hydroxide

($Mg(OH)_2$, 95-100.5%, Alfa Aesar, Haverhill, MA), magnesium chloride hexahydrate ($MgCl_2 \cdot 6H_2O$, 98%, Thermo Fisher Scientific, Waltham, MA), calcium chloride dihydrate ($CaCl_2 \cdot 2H_2O$, ACS grade, EMD Millipore, Burlington, MA), sodium hydroxide (NaOH, purity ⩾97%, Thermo Fisher Scientific, Waltham, MA), nitric acid (HNO_3, 65%–70%, Thermo Fisher Scientific, Waltham, MA), calcium hydroxide ($Ca(OH)_2$, 95% min, Alfa Aesar, Thermo Fisher Scientific, Waltham, MA), ammonium carbonate ($(NH_4)_2CO_3$, ACS grade, Sigma-Aldrich, St. Louis, MO), sodium bicarbonate ($NaHCO_3$, ACS grade, Sigma-Aldrich, St. Louis, MO), sodium phosphate monobasic (NaH_2PO_4, 99%, Sigma-Aldrich, St. Louis, MO), ammonium chloride (NH_4Cl, ACS grade, Mallinckrodt Chemicals, Phillipsburg, NJ), 2-(N-morpholino)ethanesulfonic acid (MES hydrate, ≥99.5%, Sigma Aldrich, St. Louis, MO), (4-(2-hydroxyethyl)-1-piperazineethanesulfonic acid and sodium salt (HEPES and HEPES sodium salt, ≥99%, Fisher Bioreagents, Fair Lawn, NJ), Tris(hydroxymethyl)aminomethane (Trizma hydrochloride and Trizma base, ≥99%, Sigma Aldrich, St. Louis, MO), silica sand (F-75 whole grain silica, 94% within 70-140 mesh, US Silica, Ottawa, IL), goethite (75-105 μm, synthesized according to (Atkinson et al. 1967)), and kaolinite (KGa-1b, source clay, Clay Minerals Society, Aurora, CO). KGa-1b kaolinite was used for two reasons. First, as a non-swelling clay, it is suitable for continuous flow studies in which a swelling clay could break glass columns. And second, its low iron content (0.13% Fe_2O_3 and 0.08 % FeO% by mass, (Clay Minerals Society. 2021)) largely excluded interference from iron oxides, allowing us to separately study the effects of iron oxides and clay minerals.

3.3.2 Preparation of Mg-amended biochars from corn cobs

In a preliminary test, corn cob biochars prepared by amendment with several different magnesium (and in some cases calcium) sources were tested for phosphorus uptake

(Supplementary Materials, Table 3S.1, Table 3S.2, and Figure 3S.1). Magnesium amended biochars (Mg-chars) prepared from $Mg(OH)_2$ and bittern (hereafter called Mg-char ($Mg(OH)_2$) and Mg-char (bittern)) were best at phosphorus uptake from solution (Figure 3S.1), so these Mg-chars were used in all subsequent experiments. In preparing both Mg-chars, the corn cob to magnesium mass ratio was equal to 3.7:1 (Ding et al. 2021), i.e., 3.7 g corn cobs were treated with the mass of $Mg(OH)_2$ or bittern that contained 1 g of Mg. To prepare Mg-char ($Mg(OH)_2$), 30 g of corn cobs were mixed with 19.3 g $Mg(OH)_2$ in 120 mL deionized water. To prepare Mg-char (bittern), 30 g of corn cobs were mixed with 0.25 L of a model bittern containing 1.33 M Mg^{2+} and 0.20 M Ca^{2+} (Lee et al. 2003; Shirazinezhad et al. 2021) that was prepared with $MgCl_2$ and $CaCl_2$. The aqueous mixture of ground corn cobs and $Mg(OH)_2$ had a pH of approximately 9.7 due to the basic nature of $Mg(OH)_2$, and no pH adjustment was made. For the mixture of ground corn cobs and bittern, NaOH was added to raise the pH to 12.3 to promote $Mg(OH)_2$ precipitation on the cobs. The mixtures were stirred for 10 hours, oven dried at 100 ℃, then pyrolyzed in capped crucibles in an electric kiln as follows: heat for two hours to 600 ℃; hold for two hours: then cool naturally. The Mg-chars were then ground and sieved to retain the 38-125 μm (400-120 mesh) fraction for use in subsequent experiments (Ding et al. 2021).

3.3.3 Preparation of calcium silicate hydrate from rice husk ash

Calcium silicate hydrate (CSH) was prepared using rice husk ash and calcium hydroxide. Rice husks were first washed with deionized water, then with 1 M HNO_3. Then, the rice husks were rinsed with deionized water until the pH reached 6.3, oven-dried at 100 ℃, and pyrolyzed as described in the previous section, except in uncapped crucibles (Sharmin et al. 2021) to promote oxidation of carbon and release as CO_2. To prepare calcium silicate hydrate, 1 L of 0.017 M $Ca(OH)_2$ was prepared and stirred for 1 hour, then 1.08 g rice husk ash (which

contained 83 wt % silica, (Sharmin et al. 2021)) was added (James and Rao 1986). A mass of 0.14 g NaOH was added to raise the pH to 12.3 (Kuwahara et al. 2013), then the mixture was stirred for 24 hours in capped plastic bottles and filtered using Whatman Grade 1 qualitative filter paper. The solid was oven-dried at 100 ℃ for 24 hours then gently ground (Sharmin et al. 2021). Particles with diameters between 38 and 125 μm (400-120 mesh) were sieved and saved for subsequent tests.

3.3.4 Phosphorus recovery from model animal wastewater

Phosphorus recovery (uptake) from model animal wastewater by Mg-char ($Mg(OH)_2$)), Mg-char (bittern), and CSH was first studied in batch isotherm tests. The model wastewater in these experiments contained 0.0118 M $(NH_4)_2CO_3$, 0.2124 M NH_4Cl, 0.0236 M $NaHCO_3$, and NaH_2PO_4 ranging from 0.00221 to 0.0221 M. This composition was taken from (Ding et al. 2021), except that the concentrations of ammonia and phosphorus were increased by a factor of up to ten to simulate concentrated wastewaters. (Untreated animal wastewaters can have phosphate concentrations over 650 mg P/L (0.02 M) (Capdevielle et al. 2013).) The total ammonia concentration was 0.236 M, the alkalinity was 0.0472 eq/L (2360 mg/L as $CaCO_3$), and total phosphorus ranged from 0.00221 to 0.0221 M (0.69 to 685 mg P/L). The solution pH was adjusted to pH 8.0 before adding the Mg-chars or CSH, and once more during the equilibration process. The solid loading was 3 g/L. All samples were prepared in duplicate and equilibrated for 24 hours on a Cole-Parmer Ping-Pong TM #51504–00 shaker (Cole-Parmer, Vernon Hills, Illinois) at 60 excursions per minute. Samples were then centrifuged at a relative centrifugal force of 3661×G for 30 minutes and filtered using 0.22 μm PVDF syringe filters (Simsii Inc., Irvine, California). The filtered supernatant was used for phosphate analysis using the Ascorbic Acid Method (Standard methods for the examination of water and wastewater. 2005). Oxalic

acid was added to the molybdate reagent to reduce interference from silicate by preventing the formation of silicomolybdate, which could form molybdenum blue in addition to phosphate (Chalmers and Sinclair 1966). Details are in (Ding et al. 2021).

3.3.5 Phosphorus release column studies

The column setup consisted of a 1 cm diameter glass column (Ace glass, Vineland, NJ), a peristaltic pump (MasterFlex model 7523-30, Cole Parmer, Barrington, IL), and a fraction sample collector (Waters, Milford, MA). The mixture of sand, post-P-exposure Mg-char or CSH, and, in some cases goethite or kaolinite, was positioned between two layers of glass wool and glass beads. Post-P-exposure solids, sand, and, in some cases goethite or kaolinite, were thoroughly mixed with a spatula, then dry packed into the column with a funnel. The column was packed without water to prevent loss of phosphorus from the post-P-exposure solids prior to exposure to the column influent. Columns without goethite or kaolinite contained 19.53 g sand. Columns with sand and goethite contained 1% goethite by mass, with 0.195 g goethite and 19.33 g sand, providing a depth of 15 cm and a bed volume equal to 11.8 mL. Columns with sand and kaolinite contained 7.8% kaolinite by mass, with 1.35 g kaolinite and 15.97 g sand, providing a depth of 14 cm and a bed volume equal to 11.0 mL. The porosities were approximately 0.32, 0.32, and 0.30 for columns containing only sand, sand plus goethite, and sand plus kaolinite, respectively, giving pore volumes of 3.78 mL, 3.78 mL, and 3.3 mL for the three test conditions.

The flow rate through the columns was 0.4 mL/min. This flow rate would displace one pore volume in 9.5 and 8.3 minutes for columns containing sand with and without goethite, and sand with kaolinite, respectively. The empty bed contact time was 29.5 minutes for columns with sand only and sand plus goethite, and 27.5 minutes for columns with sand and kaolinite. These empty bed contact times were close to those in published studies in which columns were used to

test struvite as a fertilizer (Ryu and Lee 2016). Influent was pumped upward into the column. The effluent sampling interval was initially one minute, then gradually increased to 30 minutes. When flowing unbuffered atmosphere-equilibrated influent that had been previously adjusted to pH 5.5 or 8.5 through the columns, reactions with the sand either raised the effluent pH or lowered it, both to approximately 6.5. Consequently, experiments were done with pH buffers to maintain a constant pH at the target values of 5.5, 7.0, and 8.5. The buffer solutions were 0.05 M MES with pH adjusted to 5.5 using NaOH, 0.05 M HEPES at pH 7.0 (a mixture of 0.038 M HEPES acid and 0.012 M HEPES Na salt), and 0.05 M Tris at pH 8.5 (a mixture of 0.017 M Trizma HCl and 0.033 M Trizma base). These buffer solutions were chosen because of their low metal chelating tendency (Good et al. 1966), and because they were not expected to interact with Mg^{2+} or Ca^{2+}, nor with goethite or kaolinite. Sand used in the column studies was equilibrated in the pH 5.5, 7.0 or 8.5 buffer solutions for at least two days and air dried before mixing with the other constituents and adding to the column. Using pH buffers, effluent pH showed a variation of no more than one pH unit, typically within the first five pore volumes (Figure 3S.2). Dissolved phosphorus at the column outlet was quantified as described previously.

A separate batch of solids exposed to the highest concentration of added phosphorus used in batch experiments (0.0221 M) was collected by gravity filtration (GE Healthcare Whatman Grade 5 qualitative filter paper), oven dried at 60 °C, then used for phosphorus release column studies. The mass of solid remaining after equilibration was measured, and the solid phosphorus concentration was calculated by dividing the decrease in total mass of added phosphorus by the remaining mass of solid. The resulting phosphorus concentrations in post-phosphorus-exposure Mg-char ($Mg(OH)_2$), Mg-char (bittern), and CSH were 182, 198, and 46 mg P/g, respectively.

The quantity of spent Mg-char or CSH that contained a total phosphorus mass of 0.9 mg

was added to each column. This was 5.0 mg of spent Mg-char ($Mg(OH)_2$), 4.5 mg of spent Mg-char (bittern), or 19.7 mg spent CSH. The phosphorus mass loading was 0.046 mg P/g for columns containing sand or sand plus goethite, and 0.052 mg P/g for columns containing sand and kaolinite. A loading of 0.9 mg phosphorus over the cross sectional area of a column with a one cm diameter is equivalent to 115 kg P/ha, which is similar to recommended levels of 99-107 kg P/ha assuming the highest crop yields with the most critical phosphorus needs (Culman 2020).

3.4 Results and Discussion

3.4.1 Phosphorus recovery from model animal wastewater

Mg-char ($Mg(OH)_2$) yielded the best phosphorus recovery from the model animal wastewater (Figure 3.1), with more than 99% of the phosphorus removed from the sample with the highest initial phosphorus concentration (C_0=685 mg P/L), resulting in a C_e value of 0.85 mg P/L. The sigmoidal isotherm shape of Mg-char ($Mg(OH)_2$) (Figure 3.1) is similar to previous studies (Ding et al. 2021) in which Q_e increased almost vertically above a threshold C_0 value that in theory corresponded to the maximum soluble concentration of phosphorus minerals such as struvite. In other words, in this region of the isotherm, the concentration of dissolved phosphorus remained at a constant value due to its equilibrium with a mineral such as struvite. Evidence from X-ray diffraction analysis of magnesium amended biochar after exposure to a similar model wastewater confirmed the presence of the mineral struvite ($MgNH_4PO_4 \cdot 6H_2O(s)$) (Ding et al. 2021), which forms through the following reaction (e.g., Zangarini et al. 2020).

$$Mg^{2+} + HPO_4^{2-} + NH_4^+ = MgNH_4PO_4(s)\ (struvite) + H^+$$

For waters that do not contain ammonium, phosphorus uptake by magnesium amended biochars is mainly by adsorption, and Q_e values range from <1 to >800 mg/g, depending on

solids and phosphorus concentrations, pH, and other experimental variables (Finn et al. 2022, Jiang et al. 2021, Li et al. 2019, Nardis et al. 2021, Shirazinezhad et al. 2021, Zhang et al. 2012). On the other hand, in wastewaters that contain both orthophosphate and ammonium (like the model wastewaters used in this study) phosphorus removal by adsorption is dominant only when orthophosphate is significantly higher in concentration than ammonium (Fang et al. 2014). That was not the case in this study, for which the total added ammonium (0.236 M) was well in excess of orthophosphate (which ranged from 0.00221 to 0.0221 M). Under these conditions, phosphorus removal by precipitation as struvite is expected to be dominant, consistent with our results (Figure 3.1).

In comparison, Q_e values for phosphorus removal by CSH plateaued as C_0 increased, reaching a significantly lower maximum Q_e value in a manner consistent with Langmuir adsorption of phosphorus to the CSH surface (Figure 3.1). The characteristic isotherm shape for phosphate uptake by CSH (Figure 3.1) is comparable with prior results (Okano et al. 2013).

Estimates of the Langmuir parameters Q_{max} and K for phosphorus adsorption to CSH (Figure 3.1, dashed line) were 55±3 mg/g and 0.008±0.001 L/mg, respectively. These parameters were calculated with SigmaPlot version 13.0 using nonlinear least squares regression. SigmaPlot estimates unknown parameters by minimizing the sum of the squares of the residuals (i.e., the differences between measured Q_e values and those predicted by the model (the Langmuir isotherm)) using an iterative solution that employs the Marquardt-Levenberg algorithm.

Mg-char (bittern) showed characteristics of both materials, i.e., a sigmoidal shape at lower concentrations that seemed to approach a plateau at higher concentrations (Figure 3.1), possibly due to the presence of both magnesium and calcium in the bittern used to prepare the Mg-char.

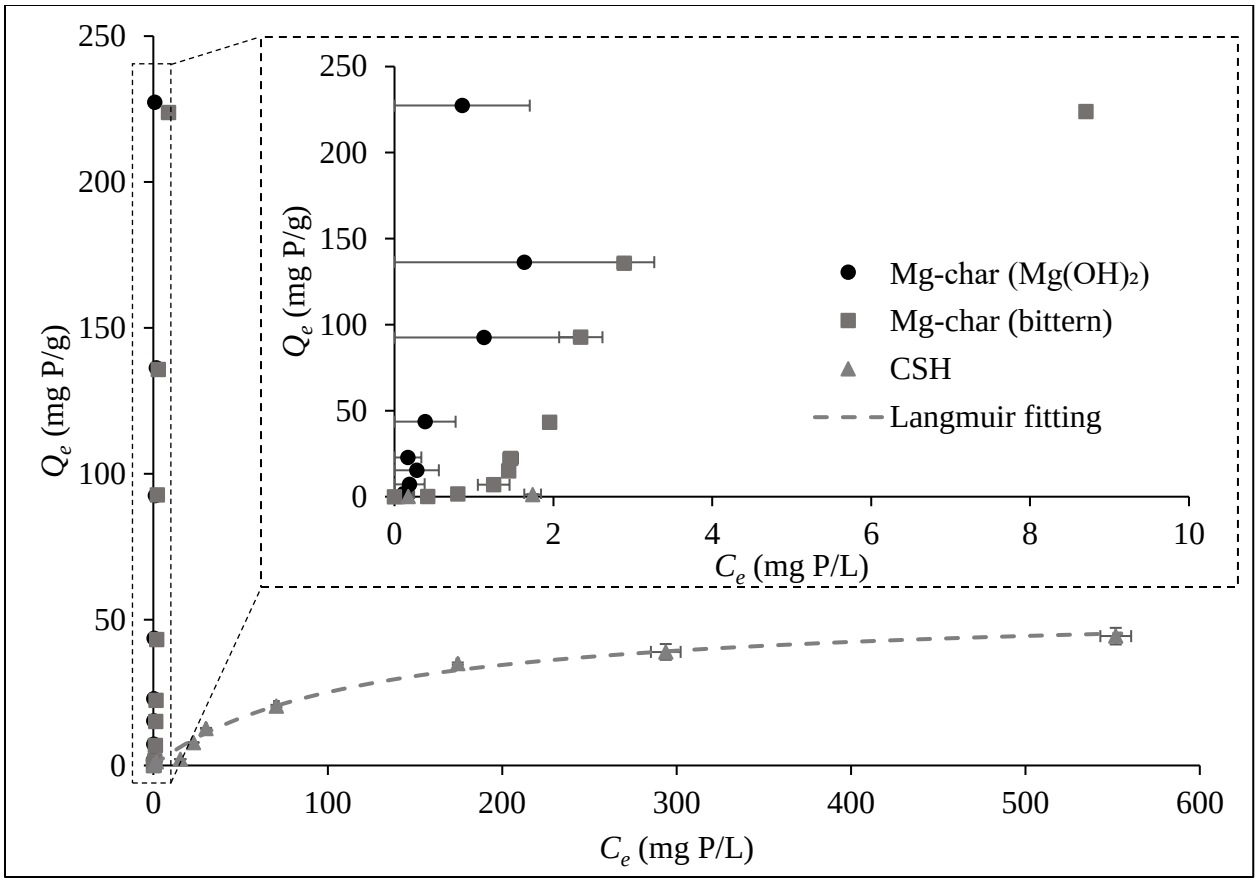

Figure 3.1 Isotherms of Mg-chars and calcium silicate hydrate (CSH) in model animal wastewater at pH 8.0. C_e is the equilibrium concentration in solution and Q_e is the equilibrium adsorbed concentration. Mean values are plotted and error bars are standard deviations of the means; at times error bars are not visible as they are smaller than the data symbol. Langmuir fitting parameters are Q_{max}=55±3 mg/g, K=0.008±0.001 L/mg, R^2=0.99; uncertainties are standard errors. Langmuir parameters were calculated by nonlinear regression with SigmaPlot 13.0 (Systat Software Inc., Palo Alto, CA).

3.4.2 Phosphorus release from post-P-exposure materials

Post-phosphorus-exposure Mg-char ($Mg(OH)_2$), Mg-char (bittern), and CSH were tested for phosphorus release in sand columns under continuous flow conditions, and the effects of pH and the addition of goethite or kaolinite were evaluated.

3.4.2.1 Effect of pH

For columns containing only sand and Mg-chars, pH 5.5 and 7.0 were more favorable for phosphorus release than pH 8.5 (Figure 3.2 a and 3.2 b), most likely due to the higher solubility of struvite at lower pH values (Bhuiyan et al. 2007). This resulted in slower release of phosphorus at pH 8.5 versus pH 5.5 and 7.0, and thus a smaller slope in the breakthrough curve (Figure 3.2 a and 3.2 b). Also, since there was a higher initial release of phosphorus at pH 5.5 and 7.0 due to the higher solubility of struvite at these pH values, the breakthrough curves for phosphorus release at pH 5.5 and 7.0 cross the curve for pH 8.5 between one and two pore volumes (Figure 3.2 a and 3.2 b).

The column study containing Mg-char ($Mg(OH)_2$) at pH 5.5 was run in duplicate, and the results showed that the relative standard deviation of replicate samples was typically less than 5% within first two pore volumes. The standard deviations of measurements from independent column studies are illustrated with error bars in Figure 3.2a.

At pH 5.5 and 7.0, both Mg-chars released over 60% of the total phosphorus within the first pore volume (Figure 3.3), which is equivalent to 48 mm of rainfall or irrigation on the column cross sectional area of 0.785 cm^2. At pH 7.0, 100% of the total phosphorus was released from both spent Mg-chars after five pore volumes, or 240 mm of rainfall or irrigation (Figure 3.3). Even at pH 8.5, nearly all (86-100%) of the phosphorus was released from columns containing both Mg-chars after 55 pore volumes (Figure 3.3). Furthermore, even though the concentrations of dissolved phosphorus released from the columns containing the Mg-chars were initially lower at pH 8.5 than at pH 7.0 and 5.5, they were higher at pH 8.5 compared to the lower pH values after two pore volumes or less (Figure 3.2 a and 3.2 b).

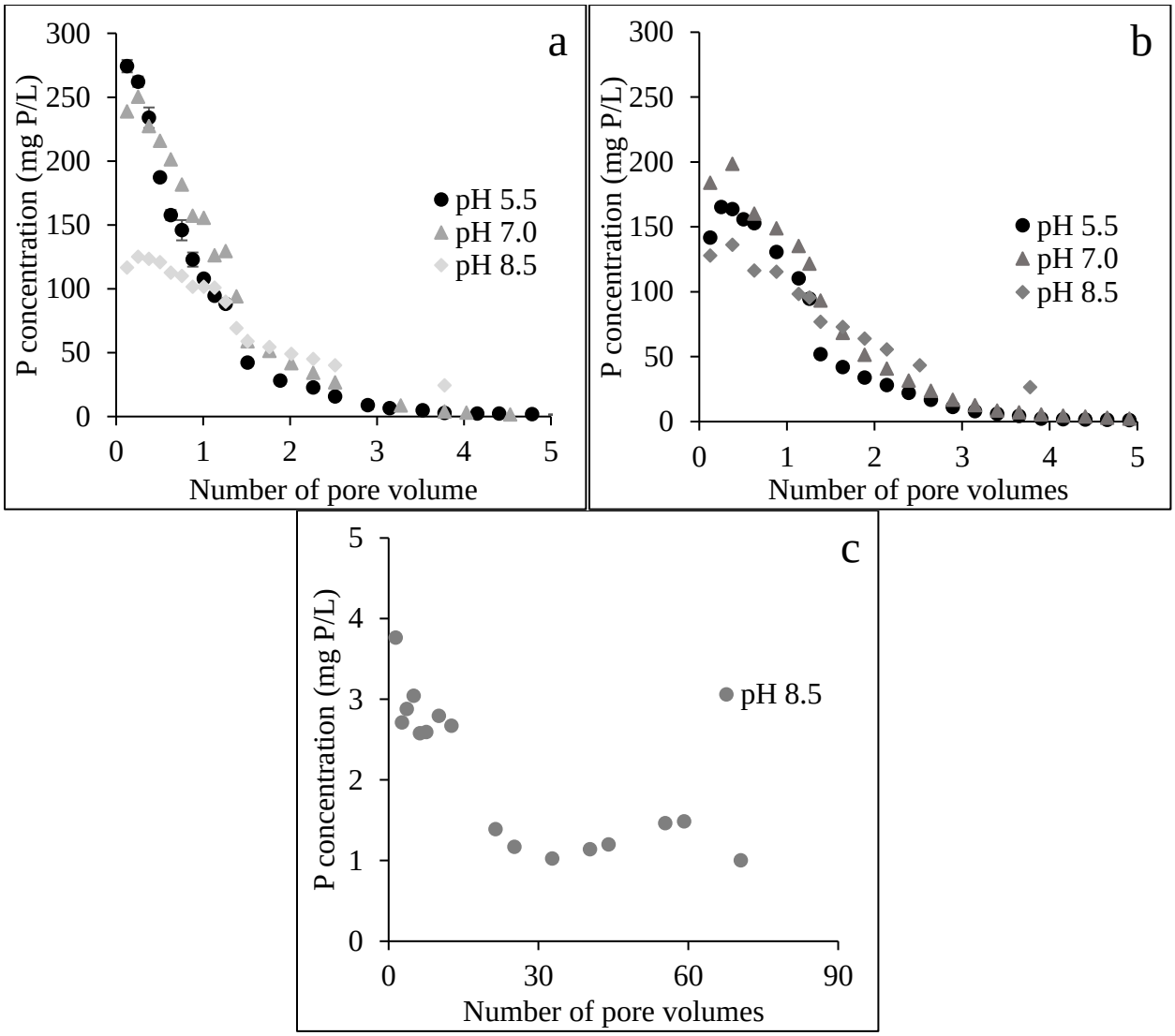

Figure 3.2 Phosphorus release from post-phosphorus-exposure solids: a. Mg-char ($Mg(OH)_2$), b. Mg-char (bittern), and c. calcium silicate hydrate (CSH), in buffered sand columns. Samples for Mg-char ($Mg(OH)_2$) at pH 5.5 were measured in duplicate, and mean values are plotted. Error bars are standard deviations of mean values; at times error bars are not visible as they are smaller than the data symbols.

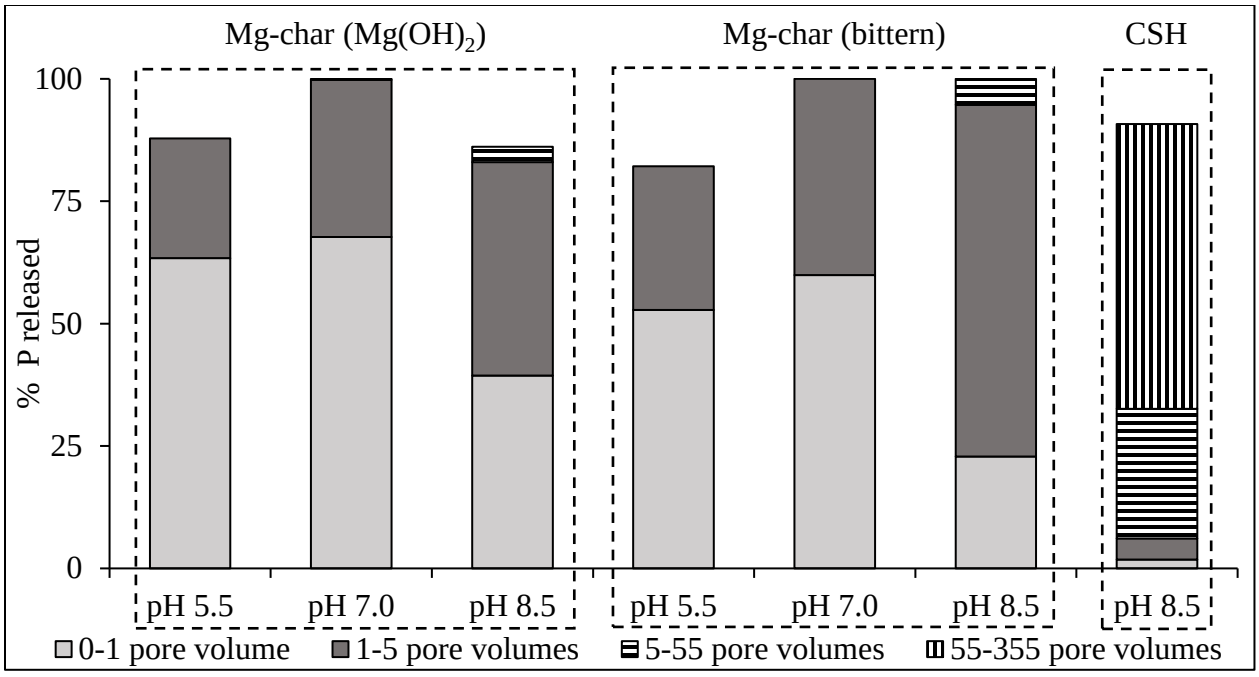

Figure 3.3 Phosphorus release percentages from the post-phosphorus-exposure solids in buffered sand columns. CSH stands for calcium silicate hydrate.

CSH released phosphorus at a significantly slower rate at pH 8.5 compared to the Mg-chars, and at significantly lower concentrations (Figure 3.2c). Approximately 335 pore volumes were required for 90% of the phosphorus to be released from the column with spent CSH at pH 8.5 (Figure 3.3), indicating a very slow phosphorus release, which has both advantages and drawbacks. The main advantage is a smaller potential for uncontrolled phosphorus release to the environment with runoff, as well as a long-term supply of phosphorus. The main drawback, on the other hand, is less plant-available phosphorus. Column experiments with CSH could not be completed at pH 5.5 and 7.0 due to significant interference from dissolved silica from the CSH in measuring dissolved phosphorus.

3.4.2.2 Effect of goethite

Column experiments were conducted in sand columns containing post-phosphorus-

exposure Mg-chars with added goethite to investigate its effect on phosphorus release as a function of pH. For Mg-char ($Mg(OH)_2$), columns were run at pH 5.5, 7.0, and 8.5. Columns containing spent Mg-char (bittern) were run at pH 5.5 and 8.5 only, since both Mg-chars had similar results at these pH values (Figure 3.4 a and 3.4 b). Columns containing spent CSH that were amended with goethite were not studied due to the inability to quantify phosphorus at low pH levels in the presence of CSH. The amount of goethite added to the columns (0.195 g, or 1% by mass) was chosen by trial and error to allow measurable phosphorus elution from the columns, but also to show a significant decrease in phosphorus breakthrough compared to columns with no added goethite.

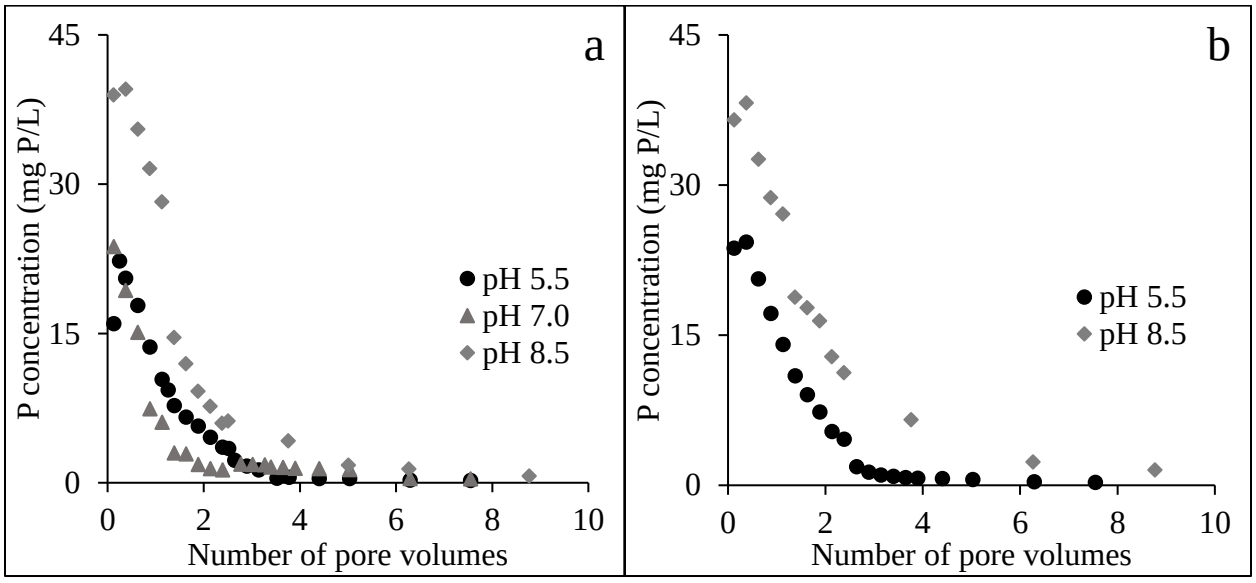

Figure 3.4 Phosphorus release from the post- phosphorus-exposure solids: a. Mg-char ($Mg(OH)_2$) and b. Mg-char (bittern), in buffered sand columns containing 1% by mass goethite.

Phosphorus release from sand columns containing Mg-char was significantly slower when goethite was present. Specifically, after one pore volume, only 5-7% of the total added

phosphorus was released from columns with added goethite containing both Mg-chars at pH 5.5 and from the column containing Mg-char ($Mg(OH)_2$) at pH 7.0 (Figure 3.5), compared to 53-68 % for Mg-char columns without goethite at these pH values (Figure 3.3). Phosphorus release from all columns amended with goethite ceased to change considerably after approximately five pore volumes for pH 5.5 and 7.0, and after approximately nine pore volumes for pH 8.5 (Figure 3.4 a and 3.4 b). When the column containing Mg-char (bittern) at pH 5.5 was run for 188 pore volumes, only another 3% of added phosphorus was released (Figure 3.5). At pH 8.5, however, there was greater phosphorus release from both Mg-chars over time in columns containing goethite. After 55 pore volumes, 29-36% of the total added phosphorus was released from the Mg-char columns at pH 8.5, compared to no more than 15% at pH 5.5 and 7.0 (Figure 3.5). However, this was still considerably less phosphorus release than columns containing no goethite (Figure 3.3).

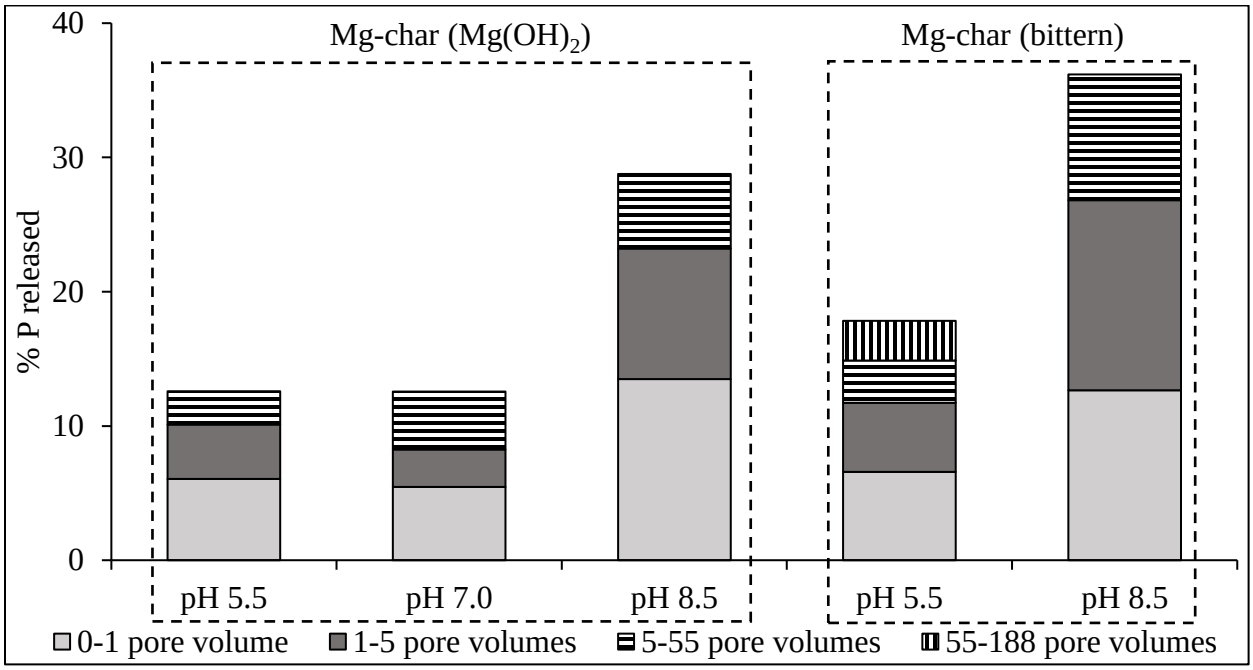

Figure 3.5 Phosphorus release percentages from the post- phosphorus-exposure solids in buffered sand columns containing 1% by mass goethite.

Chemical equilibrium modeling with MINEQL+ v. 5.0 indicates that only iron oxides, and no iron phosphate minerals such as strengite ($FePO_4 \cdot 2H_2O(s)$), would tend to precipitate in the pore water of columns containing goethite at pH 5.5, 7.0, or 8.5. (These calculations were done assuming that all the phosphate and iron added to the column (0.9 mg phosphorus and 0.195 g goethite containing 0.122 g Fe) were available for mineral formation in one pore volume of water (3.78 mL)). This indicates that the phosphorus retained in columns containing sand and goethite was most likely due to adsorption by goethite, and not precipitation. The greater retention of phosphorus in columns containing sand plus goethite versus sand alone might be explained by slow desorption of phosphate from bidentate versus monodentate surface complexes, and kinetically limited diffusion of phosphate through goethite pores (Ganta et al. 2021). Additionally, the greater release of phosphorus from the Mg-char columns at pH 8.5 versus pH 5.5 and 7.0 can be explained by the decrease in goethite surface charge with increasing pH, consistent with previous studies (Liao et al. 2021). The pH_{pzc} of goethite synthesized by the method used in this study (Atkinson et al. 1967) has been reported to be 8.6±0.8 (Kosmulski 2009). Thus, as the pH increases from 5.5 to 8.5, the net surface charge on the goethite becomes less positive, decreasing electrostatic attraction between the goethite surface and negatively charged $H_2PO_4^-$ and HPO_4^{2-}. At the same time, the driving force for phosphate adsorption to goethite increases above the pK_{a2} for phosphoric acid (pH 7.21) due to greater abundance of divalent HPO_4^{2-} versus monovalent $H_2PO_4^-$. Thus, even as the pH approached the pH_{pzc}, phosphate adsorption remained favorable due to the greater abundance of the divalent anion. Phosphate adsorption to the goethite surface has even been observed above the mineral pH_{pzc} due to the strong driving force for inner-sphere complex formation, although the overall trend of decreasing adsorption with increasing pH remains (e.g., Sigg and Stumm

1981).

3.4.2.3 Effect of kaolinite

Next, selected column experiments were conducted with post-phosphorus-exposure Mg-chars with added kaolinite to investigate its effect on phosphorus release. Columns with Mg-char ($Mg(OH)_2$) and added kaolinite were run at pH 5.5, 7.0, and 8.5 and a column with Mg-char (bittern) and added kaolinite was run at pH 5.5. Both Mg chars behaved similarly at pH 5.5, and, for Mg-char ($Mg(OH)_2$), there was greater initial retention of phosphorus in the column amended with kaolinite at pH 5.5 versus the higher pH values (Figure 3.6). Initially, at all pH values, less phosphorus was released in columns containing Mg-char that were amended with kaolinite versus those with sand alone (Figure 3.2 and 3.6). For columns containing Mg-char that were amended with kaolinite at pH 5.5, 59-83% of the added phosphorus was released after five pore volumes, compared to 82-87% released after five pore volumes in the absence of kaolinite (Figure 3.3 and 3.7). At pH 7 and 8.5, however, the percent of total added phosphorus released from the Mg-char columns amended with kaolinite after five pore volumes (73-87%) approached that in columns with no added kaolinite at the same pH values (83-100%) (Figure 3.3 and 3.7).

The greater retention of phosphorus in columns amended with kaolinite at pH 5.5 versus the higher pH values can be explained by pH-dependent mineral surface charge. While KGa-1b kaolinite has an overall pH_{pzc} of approximately 3.6 (Au et al. 2015), the Al-OH groups that tend to bind phosphorus are located on the edges of the crystal structure (Wei et al. 2014). These edge sites have a higher pH_{pzc}, with reported values of 5.01 for KGa-1 (Schroth and Sposito 1996, Kamiyango et al. 2009) and 5.34 for KGa-2 (Schroth and Sposito 1996). Edge site pH_{pzc} values for other clay minerals are even higher (e.g., 7.5 for Cornish China clay and 7.8 for hydrite PD-10 (Michaels and Bolger 1964, Wieland and Stumm 1992)). Therefore, even at pH

5.5 or possibly higher, the positive charge associated with kaolinite edge sites may have promoted phosphorus adsorption to the kaolinite surface.

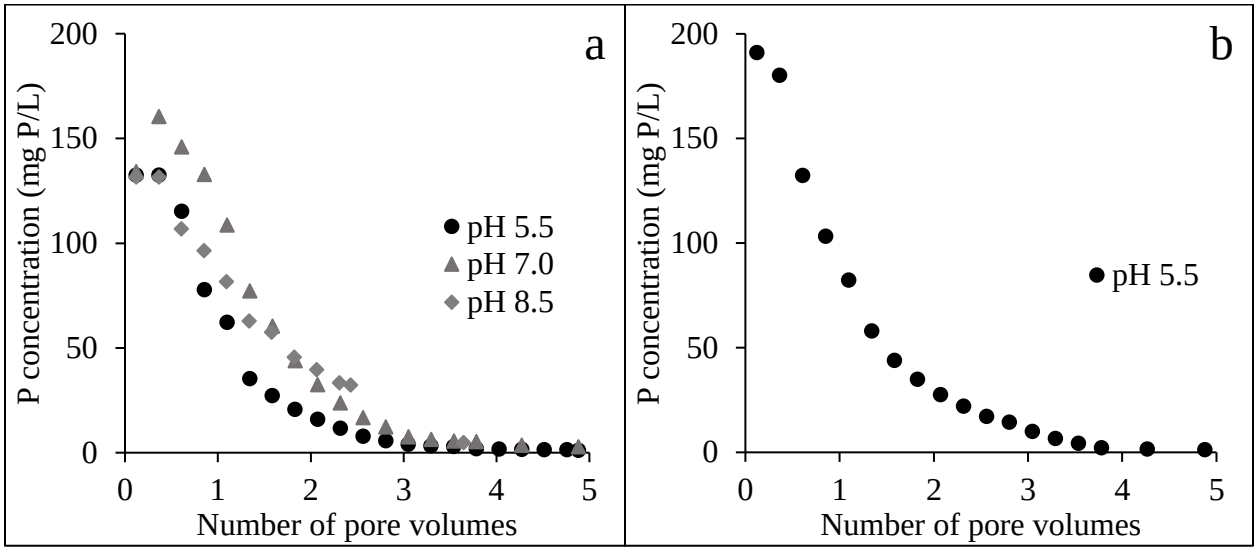

Figure 3.6 Phosphorus release from the post- phosphorus-exposure solids: a. Mg-char ($Mg(OH)_2$) and b. Mg-char (bittern), in buffered sand columns containing 7.8% by mass kaolinite.

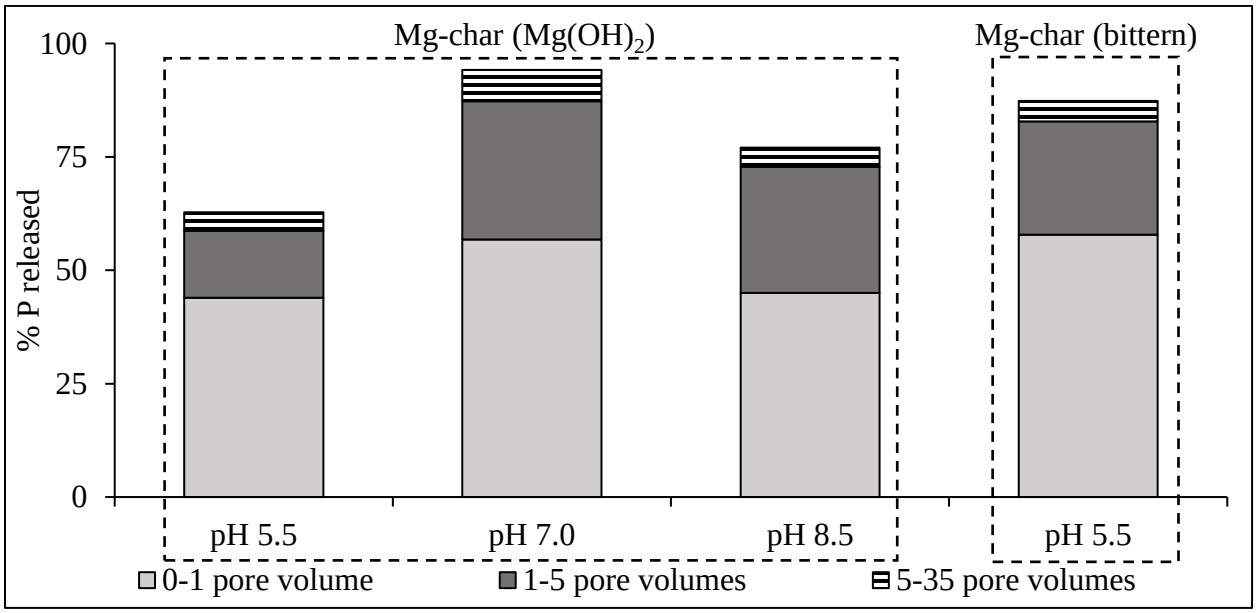

Figure 3.7 Phosphorus release percentages from the post- phosphorus-exposure solids in buffered sand columns containing 7.8% by mass kaolinite.

Kaolinite affected phosphorus retention in the sand columns containing Mg-chars significantly less than did goethite, even with a larger mass loading of 7.8% (kaolinite) versus 1% (goethite) (Figure 3.4 and 3.6). Specifically, in columns with Mg-char ($Mg(OH)_2$), the amount of total added phosphorus released after five pore volumes was approximately 6, 11, and 3 times greater in columns amended with kaolinite versus goethite at pH 5.5, 7.0, and 8.5, respectively (Figure 3.5 and 3.7). The greater impact of goethite versus kaolinite on phosphorus uptake has been reported elsewhere (Gérard 2016) and could be due to a lower phosphorus binding capacity in kaolinite versus goethite as well as the higher pH_{pzc} of goethite versus kaolinite.

3.5 Conclusions

Two low-cost magnesium sources, $Mg(OH)_2$ and bittern, were used to prepare Mg-amended biochars from corn cobs, and a low-cost calcium source, hydrated lime, was used to prepare calcium silicate hydrate (CSH) from rice husk ash. Mg-char ($Mg(OH)_2$), Mg-char (bittern), and CSH were then tested for phosphorus uptake in a model animal wastewater containing significant ammonium, phosphorus, and alkalinity. After exposure to the model wastewater, the recovered Mg-chars had phosphorus concentrations of 182 mg P/g (for Mg-char ($Mg(OH)_2$) and 198 mg P/g (for Mg-char (bittern)), and the CSH had a phosphorus concentration of 46 mg P/g. These concentrations are equal to 76, 82, and 19% of the phosphorus content in commercial monoammonium phosphate (MAP) fertilizer containing 55% P_2O_5 equivalents by mass, meaning they could readily be substituted for nitrogen and phosphorus fertilizers, particularly the Mg-chars.

There was excellent release of phosphorus from sand columns containing the two spent Mg-chars at all pH values, with 39-68% released after one pore volume (which is equivalent to

48 mm of rainfall or irrigation water), and 83-100% released after five pore volumes (equivalent to 240 mm of rainfall or irrigation water). Early release of phosphorus from sand columns containing Mg-chars was best at pH 5.5 and 7.0, compared to pH 8.5, due to the greater solubility of magnesium-phosphorus minerals such as struvite that likely formed when the Mg-chars reacted with the model wastewater. Release of phosphorus from columns containing spent CSH at pH 8.5 was much slower than from columns containing Mg-chars, and required 355 pore volumes for 90% of added phosphorus to be released. Spent CSH does not appear to be an effective fertilizer in alkaline soils, but may show promise in acid or neutral soils.

When sand columns containing Mg-char were amended with goethite, significant phosphorus was retained in the columns, particularly at pH 5.5 and 7.0. A similar effect, although to a lesser extent, was observed for kaolinite. Soils rich in these minerals would require a greater mass application of Mg-char fertilizer, at least initially, similar to what would be required for commercial fertilizers.

3.6 Acknowledgements

This work was supported by Agriculture and Food Research Initiative (AFRI) grant number 2018-6702027805 from the USDA National Institute of Food and Agriculture. The authors thank Hongbo Shao for preparing the goethite.

3.7 References

Atkinson, R.J., Posner, A.M. and Quirk, J.P. (1967) Adsorption of potential-determining ions at the ferric oxide-aqueous electrolyte interface. The Journal of Physical Chemistry 71(3), 550-558.

Au, P.-I., Clode, P., Smart, R.S.C. and Leong, Y.-K. (2015) Surface chemistry–microstructure–rheology of high and low crystallinity KGa-1b and KGa-2 kaolinite suspensions. Colloids and Surfaces A: Physicochemical and Engineering Aspects 484, 354-364.

Bhuiyan, M.I., Mavinic, D.S. and Beckie, R.D. (2007) A solubility and thermodynamic study of struvite. Environ Technol 28(9), 1015-1026.

Bradford-Hartke, Z., Razmjou, A. and Gregory, L. (2021) Factors affecting phosphorus recovery as struvite: Effects of alternative magnesium sources. Desalination 504, 114949.

Capdevielle, A., Sýkorová, E., Biscans, B., Béline, F. and Daumer, M.-L. (2013) Optimization of struvite precipitation in synthetic biologically treated swine wastewater—Determination of the optimal process parameters. Journal of Hazardous Materials 244, 357-369.

Chalmers, R.A. and Sinclair, A.G. (1966) Analytical applications of β-heteropoly acids: This influlsnce of complexing agents on selective formation. Analytica Chimica Acta 34 (Jan), 412-418.

Clay Minerals Society. (2021) Physical and chemical data of source clays. Accessed on October 22, 2021. https://www.clays.org/sourceclays_data/.

Culman, S.F., Anthony; Camberato, James; Steinke, Kurt (2020) Tri-State Fertilizer Recommendations for Corn, Soybean, Wheat, and Alfalfa, The Ohio State University.

Ding, Y., Sabatini, D.A. and Butler, E.C. (2021) Phosphorus recovery and recycling from model animal wastewaters using materials prepared from rice straw and corn cobs. Water Science and Technology 83(8), 1893-1906.

Finn, M., Rodriguez, R., Contrino, D., Swenson, J., Mazyck, D.W. and Suau, S. (2022) Impact of Inherent Magnesium in Biochar for Phosphate Removal from Reclaimed Water Streams. Journal of Environmental Engineering 148(2), 04021085.

Ganta, P.B., Morshedizad, M., Kuhn, O., Leinweber, P. and Ahmed, A.A. (2021) The Binding of Phosphorus Species at Goethite: A Joint Experimental and Theoretical Study. Minerals 11(3): 323.

Gérard, F. (2016) Clay minerals, iron/aluminum oxides, and their contribution to phosphate sorption in soils—A myth revisited. Geoderma 262, 213-226.

Good, N.E., Winget, G.D., Winter, W., Connolly, T.N., Izawa, S. and Singh, R.M.M. (1966) Hydrogen Ion Buffers for Biological Research*. Biochemistry 5(2), 467-477.

Ioannou, A. and Dimirkou, A. (1997) Phosphate adsorption an hematite, kaolinite, and kaolinite-hematite (k-h) systems as described by a constant capacitance model. Journal of Colloid and Interface Science 192(1), 119-128.

James, J., & Rao, M. S. (1986) Reaction product of lime and silica from rice husk ash. Cement and Concrete Research, 16(1), 67-73.

Jarosinski, A., Radomski, P., Lelek, L. and Kulczycka, J. (2020) New Production Route of Magnesium Hydroxide and Related Environmental Impact. Sustainability 12(21), 8822.

Jiang, S., Wang, J., Qiao, S. and Zhou, J. (2021) Phosphate recovery from aqueous solution through adsorption by magnesium modified multi-walled carbon nanotubes. Science of the Total Environment 796, 148907.

Kamiyango, M.W., Masamba, W.R.L., Sajidu, S.M.I. and Fabiano, E. (2009a) Phosphate removal from aqueous solutions using kaolinite obtained from Linthipe, Malawi. Physics and Chemistry of the Earth, Parts A/B/C 34(13), 850-856.

Kamiyango, M.W., Masamba, W.R.L., Sajidu, S.M.I. and Fabiano, E. (2009b) Phosphate removal from aqueous solutions using kaolinite obtained from Linthipe, Malawi. Physics and Chemistry of the Earth 34(13-16), 850-856.

Khan, M.D., Chottitisupawong, T., Vu, H.H.T., Ahn, J.W. and Kim, G.M. (2020) Removal of Phosphorus from an Aqueous Solution by Nanocalcium Hydroxide Derived from Waste Bivalve Seashells: Mechanism and Kinetics. ACS Omega 5(21), 12290-12301.

Kosmulski, M. (2009) Compilation of PZC and IEP of sparingly soluble metal oxides and hydroxides from literature. Advances in colloid and interface science 152(1-2), 14-25.

Kuwahara, Y., Tamagawa, S., Fujitani, T. and Yamashita, H. (2013) A novel conversion process for waste slag: synthesis of calcium silicate hydrate from blast furnace slag and its application as a versatile adsorbent for water purification. Journal of Materials Chemistry A 1(24), 7199-7210.

Lee, S.I., Weon, S.Y., Lee, C.W. and Koopman, B. (2003) Removal of nitrogen and phosphate from wastewater by addition of bittern. Chemosphere 51(4), 265-271.

Li, B., Li, P., Zeng, X.C., Yu, W., Huang, Y.F., Wang, G.Q. and Young, B.R. (2020) Assessing the sustainability of phosphorus use in China: Flow patterns from 1980 to 2015. Science of the Total Environment 704, 12.

Li, G., Li, Z.H., Ma, H.W., Jiang, X.Q. and Yao, W.G. (2013) Preparation of Magnesia Nanoballs from Dolomite. Integrated Ferroelectrics 145(1), 170-177.

Li, J., Li, B., Huang, H., Lv, X., Zhao, N., Guo, G. and Zhang, D. (2019) Removal of phosphate from aqueous solution by dolomite-modified biochar derived from urban dewatered sewage sludge. Science of the Total Environment 687, 460-469.

Li, R.H., Wang, J.J., Zhou, B.Y., Awasthi, M.K., Ali, A., Zhang, Z.Q., Lahori, A.H. and Mahar, A. (2016) Recovery of phosphate from aqueous solution by magnesium oxide decorated magnetic biochar and its potential as phosphate-based fertilizer substitute. Bioresource Technology 215, 209-214.

Liu, B., Giannis, A., Zhang, J., Chang, V.W.C. and Wang, J.-Y. (2013) Characterization of induced struvite formation from source-separated urine using seawater and brine as magnesium sources. Chemosphere 93(11), 2738-2747.

Meldau, R. and Robertson, R.H.S. (1953) Thermal Decomposition of Dolomite. Nature 172(4387), 998-999.

Michaels, A.S. and Bolger, J.C. (1964) Particle Interactions in Aqueous Kaolinite Dispersions. Industrial & Engineering Chemistry Fundamentals 3(1), 14-20.

Nagarajan, D., Lee, D.J., Chen, C.Y. and Chang, J.S. (2020) Resource recovery from wastewaters using microalgae-based approaches: A circular bioeconomy perspective. Bioresource Technology 302, 15.

Nardis, B.O., Santana Da Silva Carneiro, J., Souza, I.M.G.D., Barros, R.G.D. and Azevedo Melo, L.C. (2021) Phosphorus recovery using magnesium-enriched biochar and its potential use as fertilizer. Archives of Agronomy and Soil Science 67(8), 1017-1033.

Okano, K., Uemoto, M., Kagami, J., Miura, K., Aketo, T., Toda, M., Honda, K. and Ohtake, H. (2013) Novel technique for phosphorus recovery from aqueous solutions using amorphous calcium silicate hydrates (A-CSHs). Water research 47(7), 2251-2259.

Penn, C.J. and Warren, J.G. (2009) Investigating Phosphorus Sorption onto Kaolinite Using Isothermal Titration Calorimetry. Soil Science Society of America Journal 73(2), 560-568.

Rittmann, B.E., Mayer, B., Westerhoff, P. and Edwards, M. (2011) Capturing the lost phosphorus. Chemosphere 84(6), 846-853.

Ryu, H.D. and Lee, S.I. (2016) Struvite recovery from swine wastewater and its assessment as a fertilizer. Environmental Engineering Research 21(1), 29-35.

Sanghavi, R.J., Dobariya, R., Bhatti, S. and Kumar, A. (2020) Preparation of high-purity magnesium-ammonium-phosphate fertilizer using sea bittern and industrial waste streams. Environmental Science and Pollution Research 27(7), 7720-7728.

Schroth, B.K. and Sposito, G. (1996) Surface Charge Properties Of Kaolinite. MRS Proceedings 432 (1): 87-92.

Sharmin, N., Sabatini, D.A. and Butler, E.C. (2021) Phosphorus Recovery and Reuse Using Calcium-Silicate Hydrate Made from Rice Husk. Journal of Environmental Engineering 147(6), 04021015.

Shirazinezhad, M., Faghihinezhad, M., Baghdadi, M. and Ghanbari, M. (2021) Phosphate removal from municipal effluent by a porous MgO-expanded graphite composite as a novel adsorbent: Evaluation of seawater as a natural source of magnesium ions. Journal of Water Process Engineering 43, 102232.

Sigg, L. and Stumm, W. (1981) The interaction of anions and weak acids with the hydrous goethite (α-FeOOH) surface. Colloids and Surfaces 2(2), 101-117.

Wei, S., Tan, W., Liu, F., Zhao, W. and Weng, L. (2014) Surface properties and phosphate adsorption of binary systems containing goethite and kaolinite. Geoderma 213, 478-484.

Wieland, E. and Stumm, W. (1992) Dissolution kinetics of kaolinite in acidic aqueous solutions at 25°C. Geochimica Et Cosmochimica Acta 56, 3339-3355.

Xiong, J., Liu, Z., Yan, Y., Xu, J., Liu, D., Tan, W. and Feng, X. (2022) Role of clay minerals in controlling phosphorus availability in a subtropical Alfisol. Geoderma 409, 115592.

Ye, Z.-l., Chen, S., Lu, M., Shi, J.-W., Lin, L. and Wang, S. (2011) Recovering phosphorus as struvite from the digested swine wastewater with bittern as a magnesium source. Water science and technology : a journal of the International Association on Water Pollution Research 64 2, 334-340.

Zangarini, S., Sciarria, T.P., Tambone, F. and Adani, F. (2020) Phosphorus removal from livestock effluents: recent technologies and new perspectives on low-cost strategies. Environmental Science and Pollution Research 27(6), 5730-5743.

Zhang, M., Gao, B., Yao, Y., Xue, Y.W. and Inyang, M. (2012) Synthesis of porous MgO-biochar nanocomposites for removal of phosphate and nitrate from aqueous solutions. Chemical Engineering Journal 210, 26-32.

3.8 Supplementary Materials

Six magnesium sources were initially tested for preparation of Mg-amended biochar. These were: magnesium hydroxide ($Mg(OH)_2$, 95-100.5%, Alfa Aesar, Haverhill, MA), magnesium oxide (MgO, 98%, Acros Organics, NJ), dolomite (dolomite powder, Spectrum Chemical, New Brunswick, NJ), model bittern (Lee et al. 2003), model seawater (Liu et al. 2013), and model desalination brine (Gong et al. 2018). In all cases, the mass ratio of corn cobs to magnesium was 3.7, as in (Ding et al. 2021). For mineral sources of magnesium, the appropriate masses of $Mg(OH)_2$ or MgO were mixed in deionized water, and dolomite was completely dissolved in concentrated HCl (Fisher Scientific, Hampton, NH) then diluted with deionized water. Every 30 g of corn cobs were mixed with 120 mL of these suspended or dissolved magnesium minerals (Table 3S.1 and 3S2). For aqueous magnesium sources (model bittern, seawater, and desalination brine), specific volumes of the model solutions were prepared, and corn cobs were introduced accordingly (Table 3S.1 and 3S.2). No pH adjustment was made for $Mg(OH)_2$ and MgO since these materials naturally raised the pH, while NaOH (purity $\geqslant$ 97%, Thermo Fisher Scientific, Waltham, MA) was added to maintain pH above 12 for all the other materials. The mixtures containing corn cobs were mixed 10 hours, then oven dried, followed by pyrolysis, grinding, and sieving procedures described as in the section called "Preparation of Mg-amended biochars from corn cobs". The prepared Mg-amended biochars with diameters from 38 and 125 μm (400-120 mesh) were used in the phosphorus uptake experiments.

Phosphorus uptake by these Mg-amended biochars was studied in a model animal wastewater in batch isotherm studies. The total ammonia was 24 mM, the alkalinity was 1955

mg/L as $CaCO_3$, the pH was 9.0, and phosphate concentrations ranged from 0 to 68.5 mg/L as phosphorous. Results are shown in Fig. S1.

Table 3S.1 Composition and mass of mineral magnesium sources for treating corn cobs to prepare Mg-chars

Mineral Mg sources	Magnesium content (wt %)	Mass (g) used per 30 g corn cobs
$Mg(OH)_2$	41.17	19.3
MgO	59.55	13.3
Dolomite	12.90	61.5

Table 3S.2 Composition and volume of dissolved magnesium sources for treating corn cobs to prepare Mg-chars

Dissolved Mg sources	Ionic composition (M)							Volume (L) used per 30 g corn cobs
	Mg^{2+}	Ca^{2+}	Na^{+}	K^{+}	SO_4^{2-}	HCO_3^{-}	Cl^{-}	
Model bittern (Lee et al. 2003)	1.33	0.20	-	-	-	-	3.06	0.25
Model sea water (Liu et al. 2013)	0.05	0.01	0.39	0.02	0.01	-	0.51	6.4
Model desalination brine (Gong et al. 2018)	0.11	0.02	0.81	-	0.06	0.01	0.94	3.15

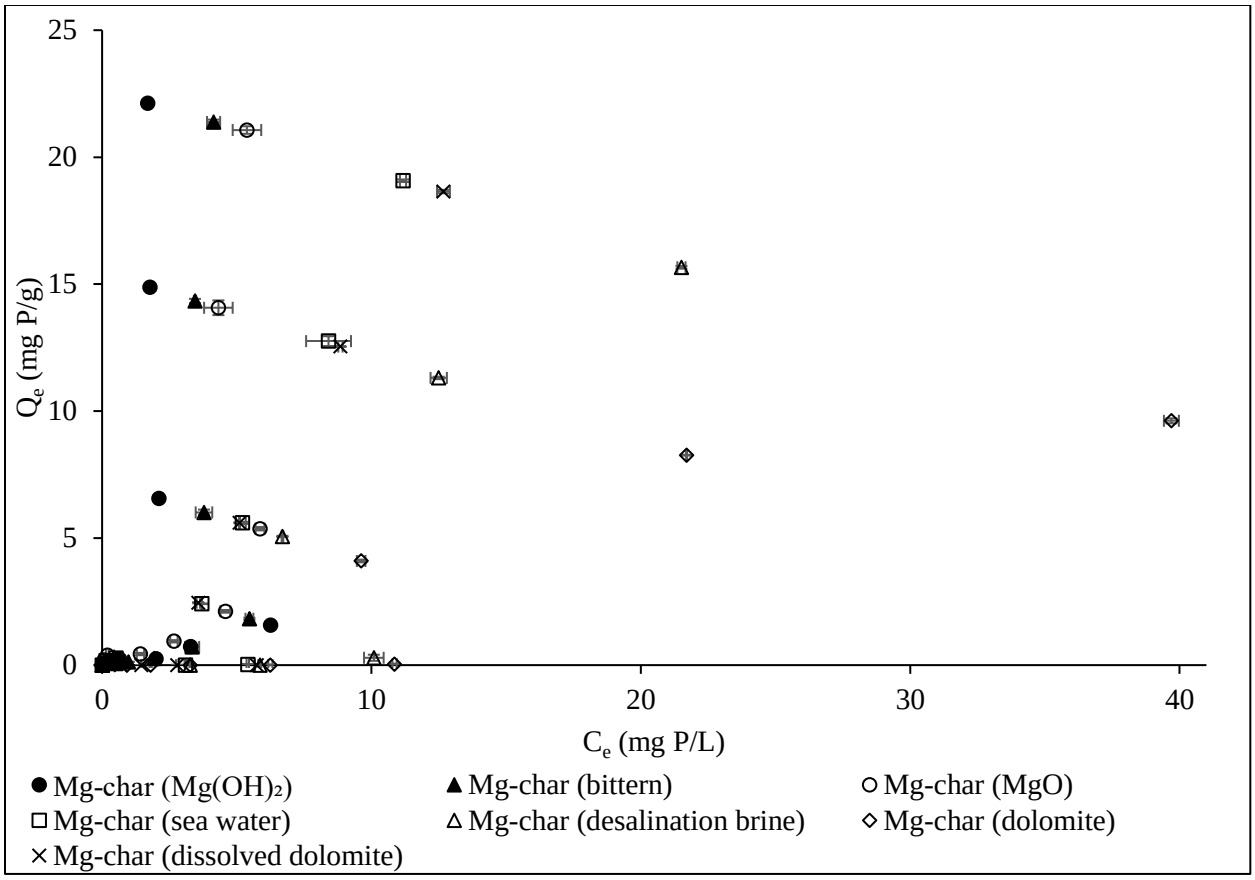

Figure 3S.1 Preliminary isotherm studies of magnesium amended biochars in a model animal wastewater at pH 9.0. C_e stands for final concentration and Q_e stands for sorption capacity indicating mg of phosphorus sorbed per g of sorbent. Data points are mean values, and error bars are standard deviations of the mean of duplicate measurements.

The pH of the effluent from pH-buffered columns was monitored using a pH electrode (9110DJWP, Thermo Fisher Scientific, Chelmsford, MA) and the results are shown in Fig. S2.

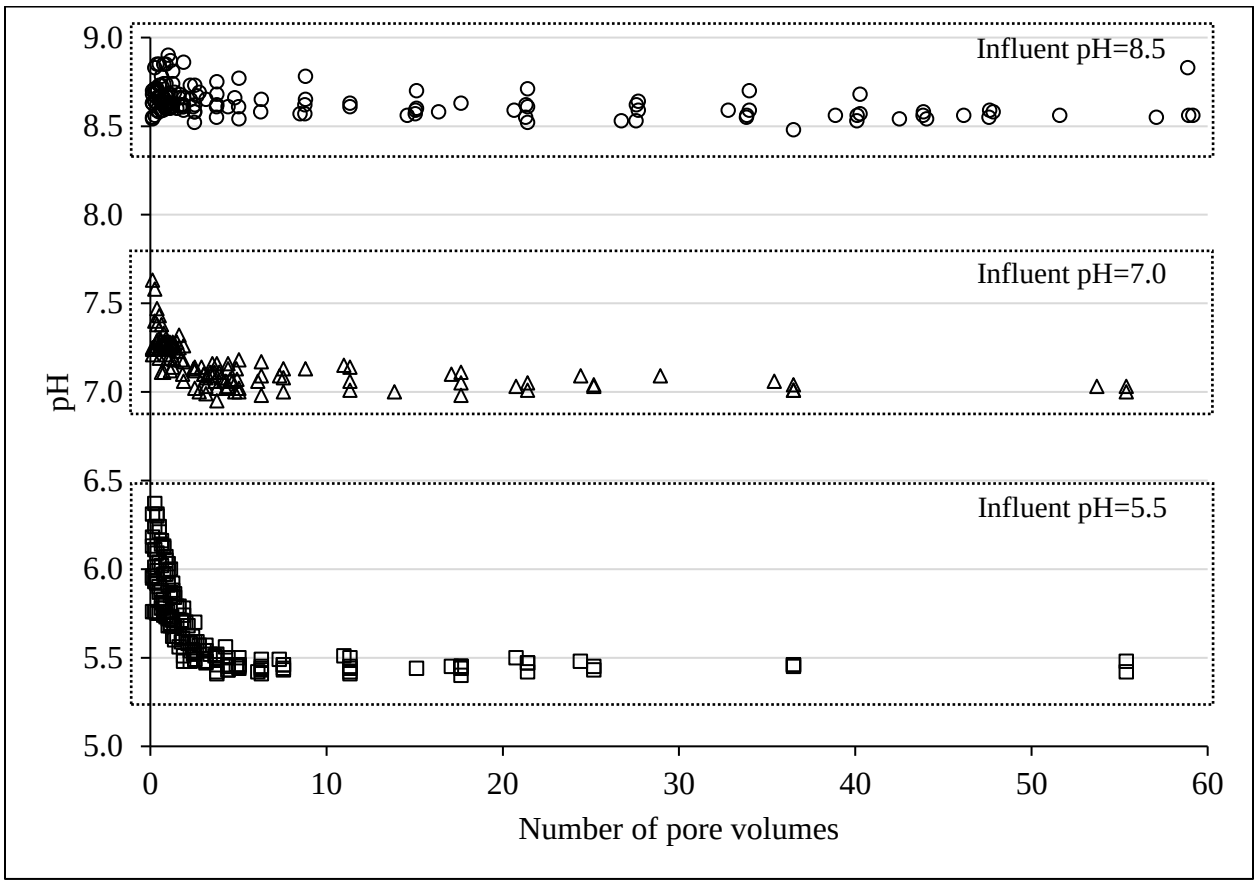

Figure 3S.2 Effluent pH from sand columns buffered at pH 5.5, 7.0, and 8.5.

3.9 References in Supplementary Materials

Ding, Y., Sabatini, D.A. and Butler, E.C. (2021) Phosphorus recovery and recycling from model animal wastewaters using materials prepared from rice straw and corn cobs. Water Science and Technology 83(8), 1893-1906.

Gong, M.H., Johns, M., Fridjonsson, E. and Heckley, P. (2018) Magnesium recovery from desalination brine. CEED Semin. Proc, 49-54.

Lee, S.I., Weon, S.Y., Lee, C.W. and Koopman, B. (2003) Removal of nitrogen and phosphate from wastewater by addition of bittern. Chemosphere 51(4), 265-271.

Liu, B., Giannis, A., Zhang, J., Chang, V.W.C. and Wang, J.-Y. (2013) Characterization of induced struvite formation from source-separated urine using seawater and brine as magnesium sources. Chemosphere 93(11), 2738-2747.

Chapter 4 Agricultural Waste-based Sorbents for Phosphorus Recovery and Reuse: A Life Cycle and Cost Assessment[‡]

4.1 Abstract

This study compared the environmental impact and cost of providing phosphorus fertilizer using the commercial fertilizer monoammonium phosphate (MAP) and three novel sorbents that had been exposed to phosphorus rich model animal wastewaters. The novel sorbents were corn cob chars amended with either $Mg(OH)_2$ or bittern, and calcium silicate hydrate (CSH) synthesized from $Ca(OH)_2$ and rice husk ash. Both Mg-chars had lower environmental impacts and cost than MAP. CSH had higher environmental impacts and costs than any other material due to its high biomass and material inputs, arising from its comparatively low solubility and poor release of phosphorus in simulated soil. Mg-char (bittern) had the lowest environmental impacts and cost since Mg was derived from a natural source (seawater bittern) rather than a commercial chemical Mg source. Using Mg-chars for phosphorus recovery and reuse could be beneficial environmentally and economically, thereby helping achieve a more sustainable phosphorus cycle.

[‡] Ding, Y., Sharmin, N., Sabatini, D.A. and Butler, E.C. (2023) Agricultural Waste-based Sorbents for Phosphorus Recovery and Reuse: A Life Cycle and Cost Assessment. In review (May 1, 2023).

4.2 Introduction

The concept of "second-generation phosphorus" (Hollas et al. 2021) illustrates the need to conserve limited phosphorus reserves (Ulrich and Frossard 2014) given growing fertilizer demand (Ludemann et al. 2022), and to alleviate the adverse environmental effects from nutrient rich wastes (van der Wiel et al. 2019). Turning waste into resource is aligned with the concept of sustainability (Ahmed et al. 2019) while forming a circular economy with minimum resource materials (Robles et al. 2020).

Magnesium (Mg) and calcium (Ca) based materials have shown promise for phosphorus recovery and reuse (Bradford-Hartke et al. 2021, Ghodszad et al. 2021, Rittmann et al. 2011, Sharmin et al. 2021). Our previous studies developed and tested several materials designed for phosphorus recovery from animal wastewater, followed by phosphorus release as a fertilizer (Ding et al. 2021, 2023). Two Mg amended biochars (Mg-chars) produced from corn cobs, and one calcium silicate hydrate (CSH) mineral synthesized from rice husk ash showed effective phosphorus recovery. Struvite formation was found to be the main mechanism for phosphorus uptake by the two Mg-chars, which exhibited rapid phosphorus release in simulated soils (Ding et al. 2023).

Along with testing the potential for phosphorus recovery and reuse using novel materials, evaluating their environmental impacts and costs is needed prior to adoption. Life cycle assessment (LCA) can be used for quantifying the environmental impacts of products or process (Lam et al. 2020), where the impacts arise from chemical emissions and resource extraction. Through LCA, steps that have the greatest impacts in the life cycle can be identified, and possible optimization strategies can be implemented. For instance, LCA indicated that biochar generated via pyrolysis had high greenhouse gas emissions from combustion of the fuels used for

pyrolysis; thus, a cleaner energy source would be a possible optimization (Gahane et al. 2022, Puettmann et al. 2020, Tadele et al. 2019).

Currently, LCAs have found that the environmental impacts associated with phosphorus recovery strategies mainly originate from chemical and energy usage (Amann et al. 2018, Niero et al. 2014, Ravi et al. 2022). These impacts are nonnegligible, even though the phosphorus recovery can offset some of the impacts from traditional fertilizer production and waste disposal (Bradford-Hartke et al. 2015). Several other studies have compared phosphorus recovery and reuse to traditional phosphorus fertilizer production and also concluded that impacts associated with chemical inputs and energy consumption limit adoption of non-traditional phosphorus fertilizer alternatives. For example, a comparison of phosphorus recovery from sludge with production of the commercial fertilizers triple super phosphate (TSP or $Ca(H_2PO_4)_2$) and diammonium phosphate (DAP or $(NH_4)_2HPO_4$) indicated that commercial fertilizers meet the fertilizer need with lower environmental impact (Goel et al. 2021, Pradel and Aissani 2019). In addition to the chemical and energy usage, infrastructural and operational changes required for phosphorus recovery implementation at wastewater treatment plants produced additional emissions (Bradford-Hartke et al. 2015).

Hence, research on evaluating additional low-impact strategies for phosphorus recovery and reuse is needed to support sustainable practices for agriculture and environmental protection, especially in emerging regions (Mavhungu et al. 2021). Possible optimization strategies, such as switching the energy source from fossil fuel to renewable energy (Goel et al. 2021), or identifying lower-impact chemical feedstocks, can improve the performance of alternatives to commercial fertilizers (Lam et al. 2020, Sena and Hicks 2018) with respect to environmental impacts.

The overall goal of this study was to compare the production and use of two Mg-chars and CSH with the commercial fertilizer monoammonium phosphate (MAP or $NH_4H_2PO_4$) in terms of cost and environmental impact. One Mg-char was synthesized with the commercial chemical $Mg(OH)_2$ (Mg-char $Mg(OH)_2$) and the second with a potentially lower impact Mg source: sea bittern (Mg-char (bittern)). MAP was selected for comparison due to the same 1:1 nitrogen to phosphorus molar ratio as in struvite, the product of phosphorus uptake by the Mg-chars in wastewaters containing ammonia (Ding et al. 2021), and because it is used widely. According to the phosphate products report from the International Fertilizer Association (IFA), MAP accounted for more than 43% of total phosphorus fertilizer production in 2018 (IFA 2021). The specific goals of this study were to: (1) evaluate whether use of bittern to produce Mg-char has lower environmental impacts and costs than use of commercial $Mg(OH)_2$; (2) identify the life cycle stages in production and use of the phosphorus sorbent materials with the greatest environmental impacts and costs; and (3) identify possible strategies to lower the impacts and costs of these novel fertilizers.

4.3 Methods

4.3.1 Overview

The LCA and cost analysis used data from a previous study in which agricultural waste-based materials were synthesized and tested for phosphorus recovery and release (Ding et al. 2023). The overall process is illustrated in Figure 4S.1. First, Mg-char ($Mg(OH)_2$), Mg-char (bittern), and CSH were synthesized using pyrolyzed corn cobs (for Mg-char) or rice husk (for CSH) and chemical amendments. Next, the three sorbent materials were equilibrated with a high concentration model animal wastewater containing phosphorus, ammonia, and alkalinity to promote phosphorus uptake, and, for the Mg-chars, struvite formation. Then, the phosphorus-

loaded sorbents (called “spent sorbents” below) were recovered, mixed with sand in a proportion similar to fertilizer application, and packed in glass columns. Fresh water buffered at pH 8.5, 7.0, or 5.5 was then flowed through the columns for at least five pore volumes in order to transfer (leach) the sorbent-associated phosphorus to the aqueous phase, modeling the behavior of solid fertilizers in soil under rainfall or irrigation. The phosphorus released over the course of five pore volumes was quantified by standard method (APHA 2005). The quantities of materials and chemicals used and/or recovered in all steps of this process are shown in Figure 4S.1. These quantities were used as inputs in modeling the life cycles of the sorbents.

4.3.2 System boundary, functional unit, and life cycle impact assessment method

The life cycles of the sorbents were divided into four stages (Figure 4.1) and Stages I and II were considered in this study. Stages III and IV were not considered since they were assumed to be similar for all materials. The functional unit was production of the quantity of fertilizer sufficient to release 2.81 kg of phosphorus (or 6.44 kg as P_2O_5) over the course of five rainfall/irrigation events, or five pore volumes (flushing cycles) in the column experiments (Figure 4S.1). The mass of 2.81 kg phosphorus is equal to the phosphorus fertilizer consumed worldwide divided by the world population, both for the year 2018, and represents the annual phosphorus consumption per capita (section 4.8.2.1). Five pore volumes of water, which corresponded to 240 mm of water from rainfall or irrigation (Figure 4S.1), was selected because most solid phosphorus was mobilized in five pore volumes in our prior studies (Figure 4S.1) (Ding et al. 2023).

The LCA followed ISO guidelines (ISO 2006a, b) and used SimaPro v.8.1 (PRé Sustainability, Amersfoort, Netherlands). The life cycle impact assessment (LCIA) method was ReCiPe version 1.12 with a Hierarchist perspective, impacts calculated at the midpoint level, and

with normalization based on the annual impact of one world citizen (Huijbregts et al. 2016, Huijbregts et al. 2017).

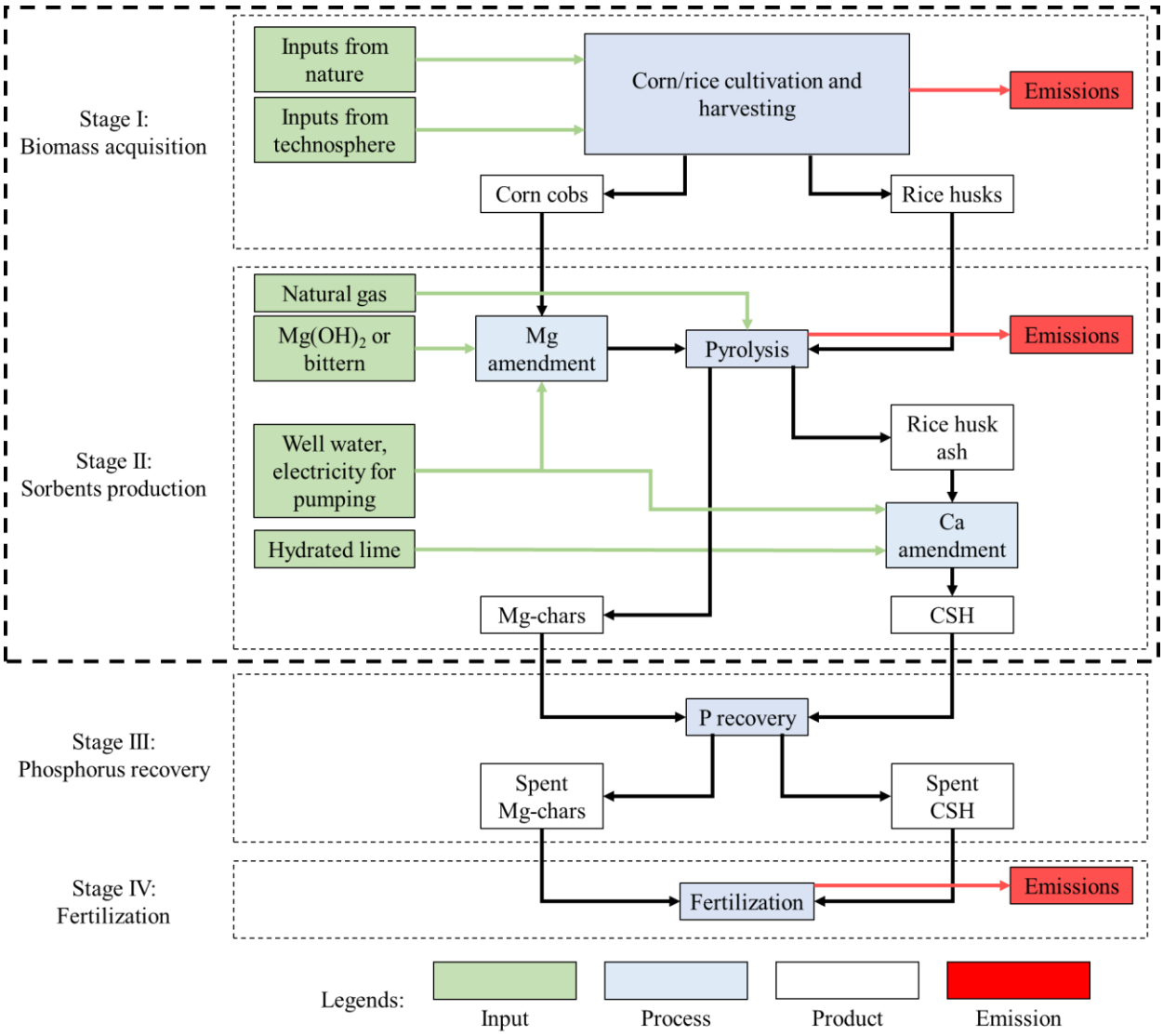

Figure 4.1 Life cycle stages of Mg-chars and CSH. Only stages inside the bold dashed box were considered in this LCA and cost analysis.

4.3.3 Life cycle inventory

The life cycle inventory of the sorbents was developed using datasets (Table 4.1) that were from the Ecoinvent database, or that were developed by combining or modifying other datasets. Details are provided in Supplementary Materials section 4.8.2.3.

Table 4.1 Life cycle inventory inputs used for modeling three sorbents and monoammonium phosphate (MAP) in different scenarios

Material	Life cycle stage	Dataset	Unit	Input quantities[1]					
				pH 8.5	pH 7.0	pH 5.5	pH 8.5 + 5 km	pH 8.5 + 50 km	pH 8.5 + 100 km
Mg-char ($Mg(OH)_2$)	I	Corn, at farm/US U[2]	kg	1.21×10^{0}	1.01×10^{0}	1.15×10^{0}	1.21×10^{0}	1.21×10^{0}	1.21×10^{0}
	II	Magnesium oxide, at plant/RER U[2]	kg	1.67×10^{1}	1.39×10^{1}	1.57×10^{1}	1.67×10^{1}	1.67×10^{1}	1.67×10^{1}
	II	Groundwater production[3]	kg	1.49×10^{2}	1.24×10^{2}	1.40×10^{2}	1.49×10^{2}	1.49×10^{2}	1.49×10^{2}
	II	Corn cobs pyrolysis[3]	kg	9.30×10^{0}	7.73×10^{0}	8.78×10^{0}	9.30×10^{0}	9.30×10^{0}	9.30×10^{0}
	I,II	Transport, lorry 3.5-7.5t, EURO5/RER U[2]	tkm	-	-	-	2.70×10^{-1}	2.70×10^{0}	5.40×10^{0}
Mg-char (bittern)	I	Corn, at farm/US U[2]	kg	1.35×10^{0}	1.28×10^{0}	1.55×10^{0}	1.35×10^{0}	1.35×10^{0}	1.35×10^{0}
	II	Bittern[3]	L	5.05×10^{1}	4.79×10^{1}	5.82×10^{1}	5.05×10^{1}	5.05×10^{1}	5.05×10^{1}
	II	Corn cobs pyrolysis[3]	kg	1.04×10^{1}	9.77×10^{0}	1.19×10^{1}	1.04×10^{1}	1.04×10^{1}	1.04×10^{1}
	I,II	Transport, lorry 3.5-7.5t, EURO5/RER U[2]	tkm	-	-	-	2.1×10^{-1}	2.1×10^{0}	4.1×10^{0}
CSH	I	Rice, at farm/US U[2]	kg	4.72×10^{1}	-	-	4.72×10^{1}	4.72×10^{1}	4.72×10^{1}
	II	Lime, hydrated, loose, at plant/CH U[2]	kg	3.36×10^{2}	-	-	3.36×10^{2}	3.36×10^{2}	3.36×10^{2}
	II	Sodium hydroxide, 50% in H_2O, membrane cell, at plant/RER U[2]	kg	3.76×10^{1}	-	-	3.76×10^{1}	3.76×10^{1}	3.76×10^{1}
	II	Groundwater production[3]	kg	2.69×10^{5}	-	-	2.69×10^{5}	2.69×10^{5}	2.69×10^{5}
	II	Rice husk pyrolysis[3]	kg	2.89×10^{2}	-	-	2.89×10^{2}	2.89×10^{2}	2.89×10^{2}
	I,II	Transport, lorry 3.5-7.5t, EURO5/RER U[2]	tkm	-	-	-	9.5×10^{0}	9.5×10^{1}	1.9×10^{2}
MAP	NA[4]	Monoammonium phosphate, as P_2O_5, at regional storehouse/RER U[2]	kg	6.44×10^{0}	6.44×10^{0}	6.44×10^{0}	6.44×10^{0}	6.44×10^{0}	6.44×10^{0}

[1] Calculations of input quantities are in the section 4.8.2.4; [2] Dataset was from the Ecoinvent version 2.2 database, abbreviations RER: Europe, US: United States, CH: Switzerland, U: unit process; [3] Dataset was created in this study (section 4.8.2.3); [4] Not applicable.

General assumptions made in the LCA were that: (1) processes, including mixing, grinding, phosphorus leaching / recovery, and fertilization were common for all the sorbents and were therefore not included; (2) raw groundwater pumped from the well co-located at the site of sorbent preparation was used to meet the water demand without further treatment; (3) no raw materials or sorbents were lost during any life stages; and (4) drying needed during raw material pretreatment and sorbent production used natural sunlight and air, thus no external energy input was required (Hamdani and Cheng 1992). In addition, all infrastructure needed for farming, chemical production facilities and vendors, water and natural gas pipelines, and fertilizer application was not considered. Allocation was based on the values of co-products (section 4.8.2.2).

4.3.4 Life cycle scenarios

Several scenarios were considered in the life cycle and cost assessment, including soil pH values ranging from 5.5-8.5 representing acidic to alkaline soil types, and transportation distances ranging from 0-100 km in the production of fertilizers from corn cobs and rice husks. In the baseline scenario, the soil pH was 8.5, and the farmland, animal husbandry operations, and chemical production facilities and vendors were assumed to be co-located. The sorbents were assumed to be synthesized at the point of use. A pH value of 8.5 was chosen as the baseline since phosphorus release data were available for all three sorbents at this pH value (Figure 4S.1). Scenarios at pH 7.0 and 5.5 had identical assumptions about the co-location of farmland, animal husbandry operations, and chemical production facilities and vendors. Due to the greater solubility of struvite at lower pH values, the extent of phosphorus release from Mg-chars pre-exposed to model animal wastewater was typically greater at pH 7.0 and 5.5 than at pH 8.5

(Figure 4S.1). Therefore, a smaller mass of sorbent and other inputs were typically needed to yield the functional unit of 2.81 kg phosphorus in five pore volumes of water (Table 4.1).

In addition, the effect of transportation on the environmental impacts of the sorbents were estimated at a soil pH value of 8.5 with the same assumptions and considerations as above, except that the chemical production facility and vendors were assumed to be 5, 50, or 100 km from the point of sorbent synthesis and use. Masses and transportation distances for these "Transportation scenarios" are summarized in Table 4.1.

Because of its high solubility [356 g/L at 20 ℃ (Xu et al. 2016)], MAP was assumed to fully dissolve at all pH values, hence, its mass input did not vary (Table 4.1). Additionally, since the Ecoinvent process for MAP production (Table 4.1) accounts for production-related transportation, no additional transportation was considered for MAP.

4.3.5 Cost analysis

All three sorbents and MAP were compared on this same basis as the functional group, i.e., the mass of material required to release 2.81 kg phosphorus after five pore volumes, or 240 mm of rainfall/irrigation. Cost categories considered included: (1) chemical inputs; (2) energy inputs; and (3) for the transportation scenario, transportation costs. When considering the transportation scenario, a single distance of 100 km was considered. Additional assumptions in the cost analysis included: (1) the cost of infrastructure for biomass cutting, grinding, sieving, and water consumption were identical for all the sorbents and thus not considered; (2) the pyrolysis furnace was run continuously with 1.67 m^3 natural gas per ton of feedstock for initial start-up, and later energy input provided by the exothermic pyrolysis reaction (Roberts et al. 2010, Saft 2007); and (3) bittern was assumed to be free, as it is a by-product left at the NaCl

production facility. Although this last assumption differs from the approach taken in the life cycle assessment, it was chosen since bittern is not currently regarded as a commercial resource.

4.4. Results and Discussion

Impact assessment was done with the LCIA method ReCiPe (version 1.12). However, the implementation of ReCiPe (version 1.12) in SimaPro (version 8.1) does not account for metal depletion, so impacts in this category are not reported. Furthermore, the normalization factor is zero for water depletion in ReCiPe (version 1.12), meaning it does not calculate impacts in this category relative to the annual impact of one world citizen, thus, normalized results for water depletion category are not reported.

4.4.1 Soil pH 8.5

The LCIA results indicate that the impacts of using CSH for phosphorus recovery and reuse were significantly greater in all impact categories than any other material (Figure 4.2a) due to the significantly greater quantities of CSH, and all associated upstream material and energy inputs, needed to release 2.81 kg phosphorus in five pore volumes or 240 mm of water at pH 8.5. These inputs included the considerably higher farming demand, greater energy input for pyrolysis, larger $Ca(OH)_2$ and NaOH requirements, as well as more than 1,800 times higher water consumption required for CSH compared to the two Mg-chars (Table 4.1). For this reason, and to focus on the more promising Mg-char alternatives, results for CSH are not shown in subsequent figures, although numerical LCIA results are shown in the Supplementary Materials (Tables 4S.1 and 4S.9).

The impacts of the two Mg-chars were similar in magnitude, although Mg-char ($Mg(OH)_2$) had more adverse environmental effects than Mg-char (bittern) in 14 impact categories (Figure 4.2, Table 4S.1). The inputs and life cycle stages that contributed the most to

the adverse impacts for each Mg-char differed due to the different synthesis processes for each material (Figure 4.3). For Mg-char ($Mg(OH)_2$), production of $Mg(OH)_2$ contributed significantly to nearly all impact categories (Figure 4.3), while use of a natural Mg source for Mg-char (bittern) made corn farming a major contributor in most impact categories (Figure 4.3). Production of bittern, which is a by-product of NaCl production, did not contribute significantly to the impacts for production of Mg-char (bittern) (Figure 4.3). Thus, using a less refined Mg source (seawater bittern) versus a refined industrial chemical ($Mg(OH)_2$) lowered the impacts of Mg-char.

Mg-char (bittern) had greater impacts than Mg-char ($Mg(OH)_2$) in three impact categories: photochemical oxidation formation, terrestrial ecotoxicity, and agricultural land occupation (Figure 4.2, Table 4S.1). This was because greater quantities of corn farming and pyrolysis were needed for Mg-char (bittern) (Table 4.1) due to its lower sorbent yield during production (Figure 4S.1).

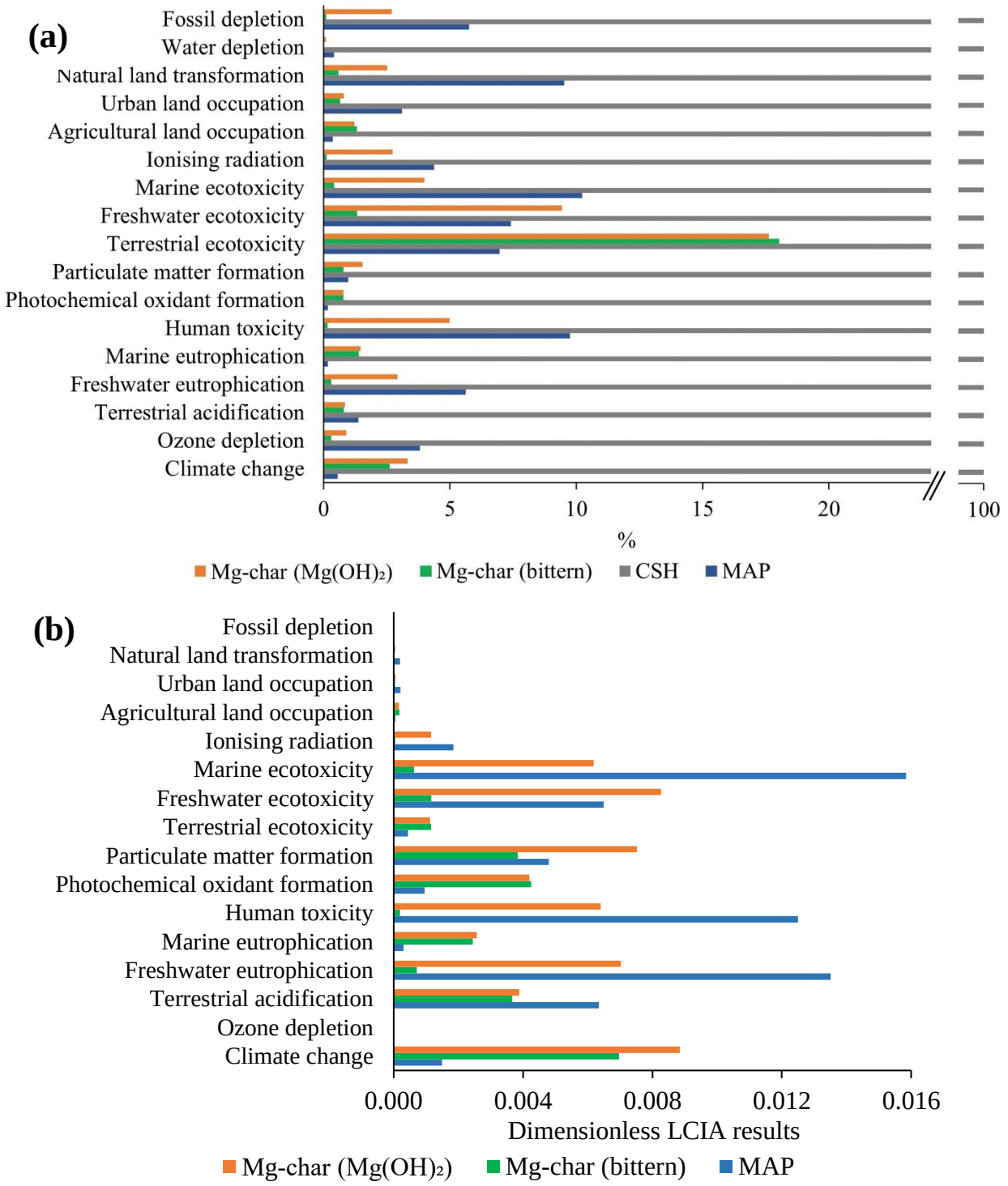

Figure 4.2 Life cycle impact assessment of Mg-char ($Mg(OH)_2$), Mg-char (bittern), calcium silicate hydrate (CSH), and monoammonium phosphate (MAP) in scenario 1. Original characterization data (shown in Table 4S.1) were normalized by: (a) the maximum impact in each category (which was set equal to 100%); (b) the annual impact of one world citizen, and thus is dimensionless. Normalized results in fossil depletion category for Mg-char ($Mg(OH)_2$), Mg-char (bittern), and MAP are 2.52×10^{-6}, 1.07×10^{-7}, 5.39×10^{-6}, respectively; and normalized results in ozone depletion category for Mg-char ($Mg(OH)_2$), Mg-char (bittern), and MAP are 5.92×10^{-6}, 1.97×10^{-6}, 2.52×10^{-5}, respectively.

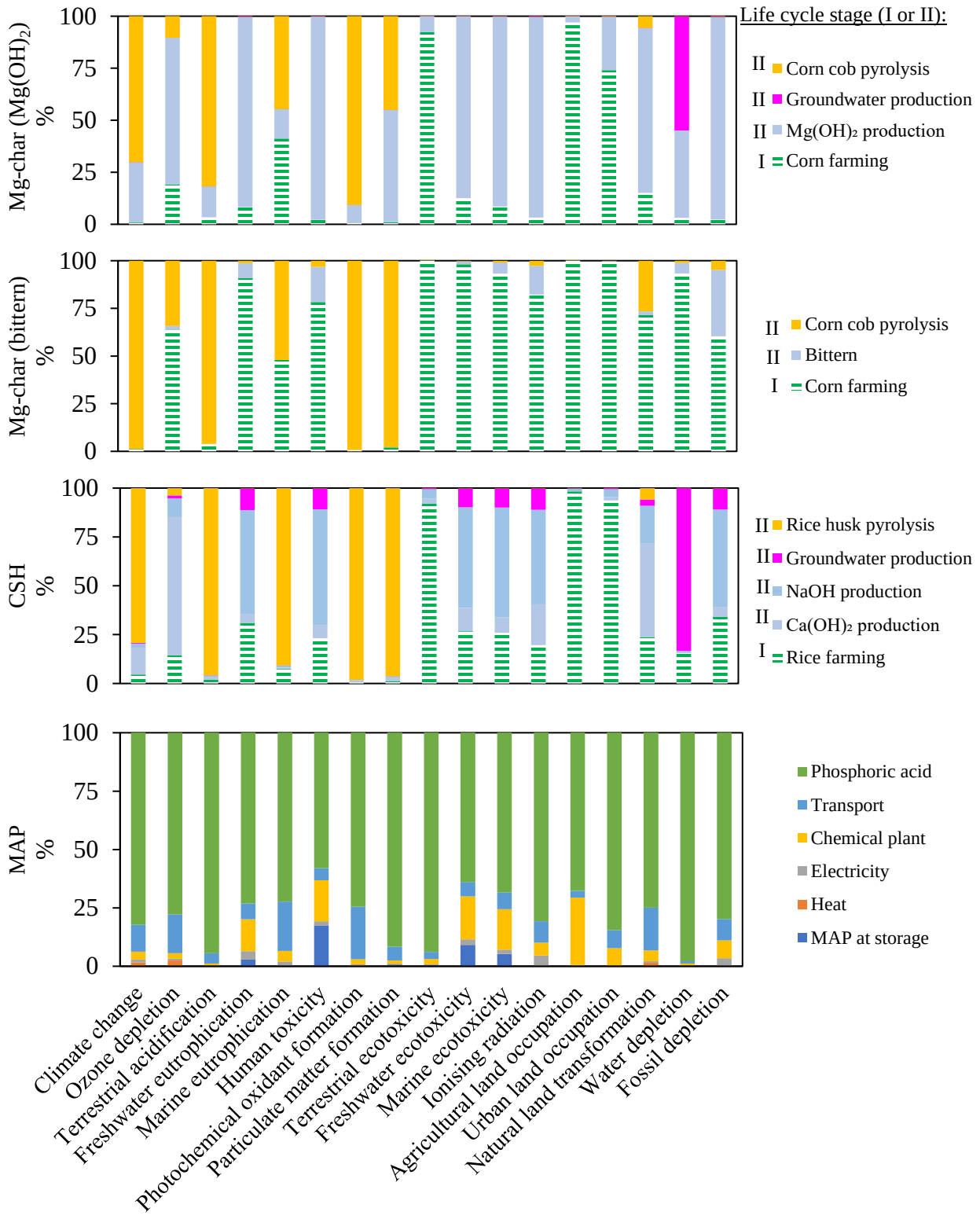

Figure 4.3 Percent total impact from different processes in the life cycles of Mg-char ($Mg(OH)_2$), Mg-char (bittern), and calcium silicate hydrate (CSH) at pH 8.5, and monoammonium phosphate (MAP). Impact assessment values are given in Tables 4S.2, 4S.3, and 4S.4.

Pyrolysis also contributed significantly to the impacts of the two Mg-chars, particularly in terms of climate change, photochemical oxidant formation, terrestrial acidification, particulate matter formation, and marine eutrophication (Figure 4.3). Climate change was the impact category for which both Mg-chars had the greatest impact, relative to the impact of one world citizen in one year (Figure 4.2b), and 70-98% of the impacts in this category for the two Mg-chars were due to pyrolysis (Table 4S.5). Pyrolysis of agricultural wastes would also lead to formation of NO_x and products of incomplete combustion such as CO and volatile organic compounds (VOCs) that are precursors to photochemical ozone formation (Huijbregts et al. 2016, Kley et al. 1999), explaining the significant contribution of pyrolysis to photochemical oxidant formation (Figure 4.3). NO_x from pyrolysis can also lead to terrestrial acidification and marine eutrophication (Huijbregts et al. 2016), also consistent with these results (Figure 4.3). Finally, in addition to soot and carbonaceous particulate matter (PM) from pyrolysis, when NH_3(g) from agriculture is present, NO_x emissions can also lead to formation of NH_4NO_3, which is a significant component of $PM_{2.5}$ in some instances (NASA 2016). These significant impacts from pyrolysis might be reduced through alternative biomass treatments such as chemical activation. Chemical activation in some cases could enhance biochar's sorption capacity by increasing specific surface area using a lower temperature than needed for pyrolysis (Tseng and Tseng 2005). Such treatments also have the potential to reduce the adverse impacts of biomass production (corn and rice farming (Table 4.1, Figure 4.3)), since they may result in a lower mass loss than pyrolysis (Yami et al. 2016).

Production of MAP led to greater impacts than the two Mg-chars in ten categories (Figure 4.2, Table 4S.1), and production of phosphoric acid contributed the most to all impact categories (Figure 4.3), in different ways. For instance, production of commercial fertilizers such

as MAP requires mining of phosphorus rock (Sena et al. 2021) for phosphoric acid production (Schorr and Valdez 2016, Zheng et al. 2021), leading to natural land transformation. In addition, sulfuric acid is a common reagent for acidifying the phosphorus ore (Schorr and Valdez 2016), and can lead to terrestrial acidification.

4.4.2 Soil pH 7.0 and 5.5

Based on the phosphorus release test (Figure 4S.1), at pH 7.0, 17% less Mg-char ($Mg(OH)_2$) and 5.4% less Mg-char (bittern) were required to yield the quantity of phosphorus defined in the functional unit (2.81 kg per five pore volumes or 240 mm of water) compared to pH 8.5, as well as all the other raw material inputs shown in Table 4.1. And at pH 5.5, 5.6% less Mg-char ($Mg(OH)_2$) was needed, but 15% more Mg-char (bittern) was needed compared to pH 8.5. Despite these differences in required material inputs to the life cycle assessment (Table 4.1), the overall impacts of the two Mg-chars, normalized to the annual impacts of one world citizen, did not change significantly with soil pH (Figure 4S.5). Furthermore, because the changes in material inputs for pH 5.5 and 7.0 compared to pH 8.5 led to proportional changes in each impact category, the specific contributions of different life cycle processes (Figure 4.3) did not change with pH value. Changing the soil pH also did not change the relative impacts of the two Mg-chars versus MAP (Figure 4S.5).

4.4.3 Addition of transportation

The addition of 5, 50, or 100 km of truck transportation to the LCA led to comparatively small increases in impacts across all impact categories, and generally, the impact of transportation was not significant compared to other steps in the life cycle (Figure 4.4). Even considering 100 km of transportation, the two Mg-chars still had lower impacts than MAP in nine impact categories, and Mg-char (bittern) was still the best of the two Mg-chars (Figure 4.4).

The relative impact of transportation was greater for the two Mg-chars in the impact categories for which the impacts relative to the annual impacts of one world citizen were lowest (Figure 4.2b). For example, when a distance of 100 km was included in the LCA, ozone depletion increased by 64% for Mg-char ($Mg(OH)_2$) and 80% for Mg-char (bittern) (Figure 4.4 insets). The impacts for Mg-char (bittern) upon addition of 100 km of transportation also increased significantly in several other impact categories: human toxicity, marine ecotoxicity, ionizing radiation, natural land transformation, and fossil depletion (Figure 4.4)—all impact categories for which the impacts were otherwise comparatively low. Thus, because the Mg-chars, particularly Mg-char (bittern), had low impacts in several impact categories compared to the annual impact of one world citizen (Figure 4.2b), the LCIA results for these materials were more sensitive to transportation. In practice, maintaining their comparatively low impacts would necessitate minimizing the use of transportation by co-location to the extent possible of crop, animal, and chemical production. For production of Mg-char (bittern), location near a source of salt water (e.g., coastal regions) is also needed to minimize the impacts of material production.

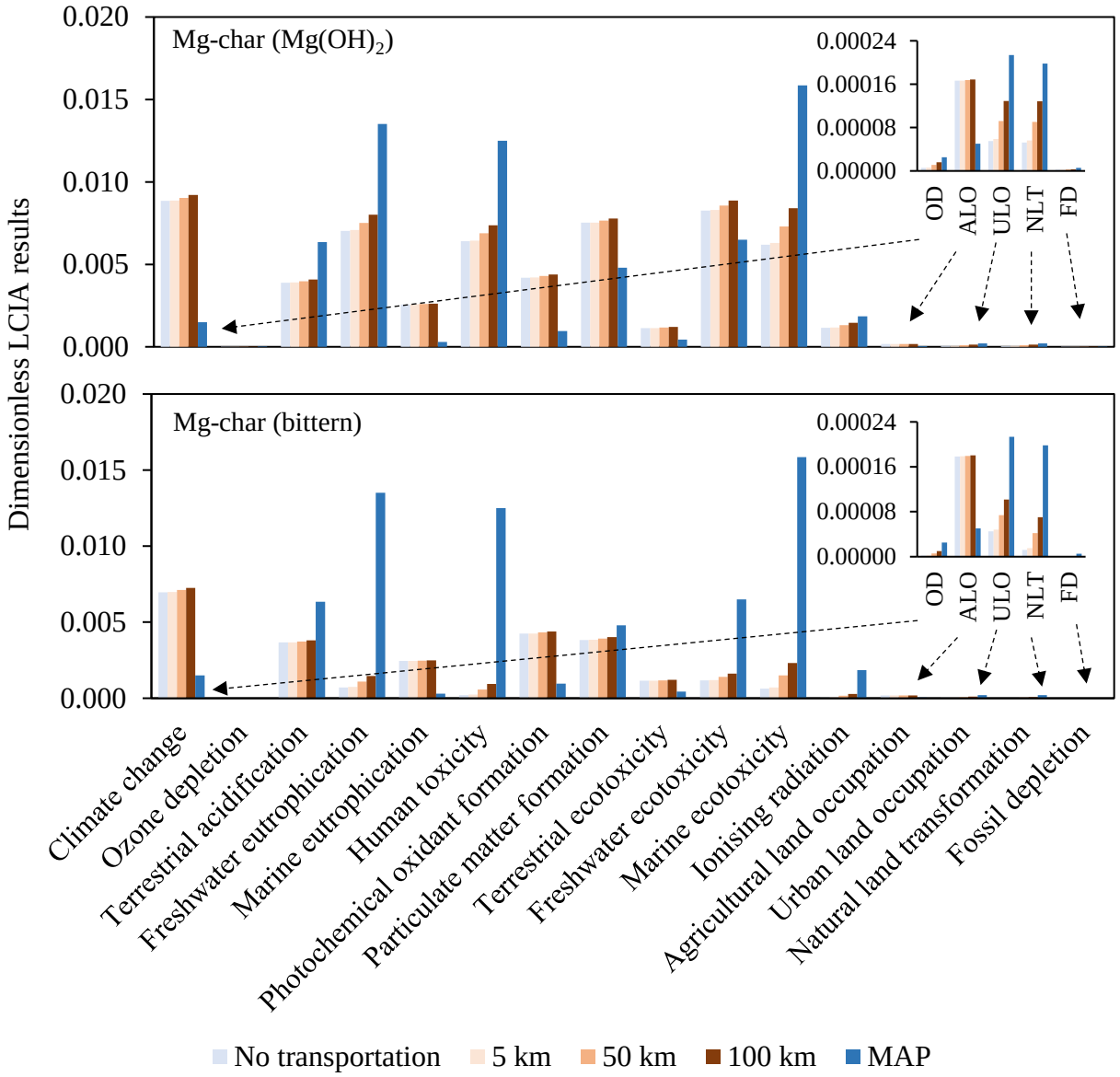

Figure 4.4 Impacts normalized by the annual impact of one word citizen of Mg-char ($Mg(OH)_2$), Mg-char (bittern), and calcium silicate hydrate (CSH) at pH 8.5 with varied transportation distances, and monoammonium phosphate (MAP). Abbreviations in the insets: OD, ozone depletion; ALO, agricultural land occupation; ULO, urban land occupation; NLT, natural land transformation; FD, fossil depletion. The y-axis is the impact assessment values divided by the impact of one world citizen in one year, and thus is dimensionless. Impact assessment values are given in Table 4S.8.

4.4.4 Cost analysis

Both Mg-chars were less expensive than MAP for all scenarios modeled, and Mg-char (bittern) had the lowest cost (Table 4S.10). For Mg-char ($Mg(OH)_2$), the biggest contributor to the total cost was $Mg(OH)_2$ production (Figure 4.5). Mg-char (bittern), on the other hand, cost considerably less (Figure 4.5) because it utilized an industrial by-product. Additionally, due to the low cost of other inputs (Table 4S.10), the total cost of producing Mg-char (bittern) was the most sensitive to the addition of transportation. Specifically, with 100 km of transportation added to the LCA, the cost of Mg-char (bittern) increased by nearly four times (Figure 4.5). Thus, as for environmental impacts, the comparatively low costs of this material depend on the co-location of crop residue, animal wastewater, and a source of seawater, making it most applicable to coastal regions.

CSH was the most expensive among the four materials, even without considering transportation (Table 4S.10). Similar to the LCIA results (Figure 4.2a), this was due to the large quantities of raw materials needed to synthesize the quantity of CSH sufficient to take up and release 2.81 kg phosphorus in five pore volumes or 240 mm (Table 4.1). This, in turn, is due to the relatively poor release of phosphorus from CSH under flow through conditions at pH 8.5 due to the lower solubility of calcium phosphates compared to the struvite formed when the Mg-chars were exposed to wastewater containing phosphorus and ammonia (Figure 4S.1). Additionally, adding 100 km transportation almost doubled the cost of producing CSH, due to transporting the large quantity of rice husk needed to produce silica (Figure 4.5).

The cost calculations for the three sorbents were repeated using European prices for natural gas and electricity, which were higher than U.S. Prices. The impact on overall costs were no more than 3% for Mg-char ($Mg(OH)_2$) and CSH, and 12% for Mg-char (bittern) (Table

4S.11), since natural gas and electricity prices did not contribute significantly to overall costs for the preparation of any sorbents (Table 4S.10).

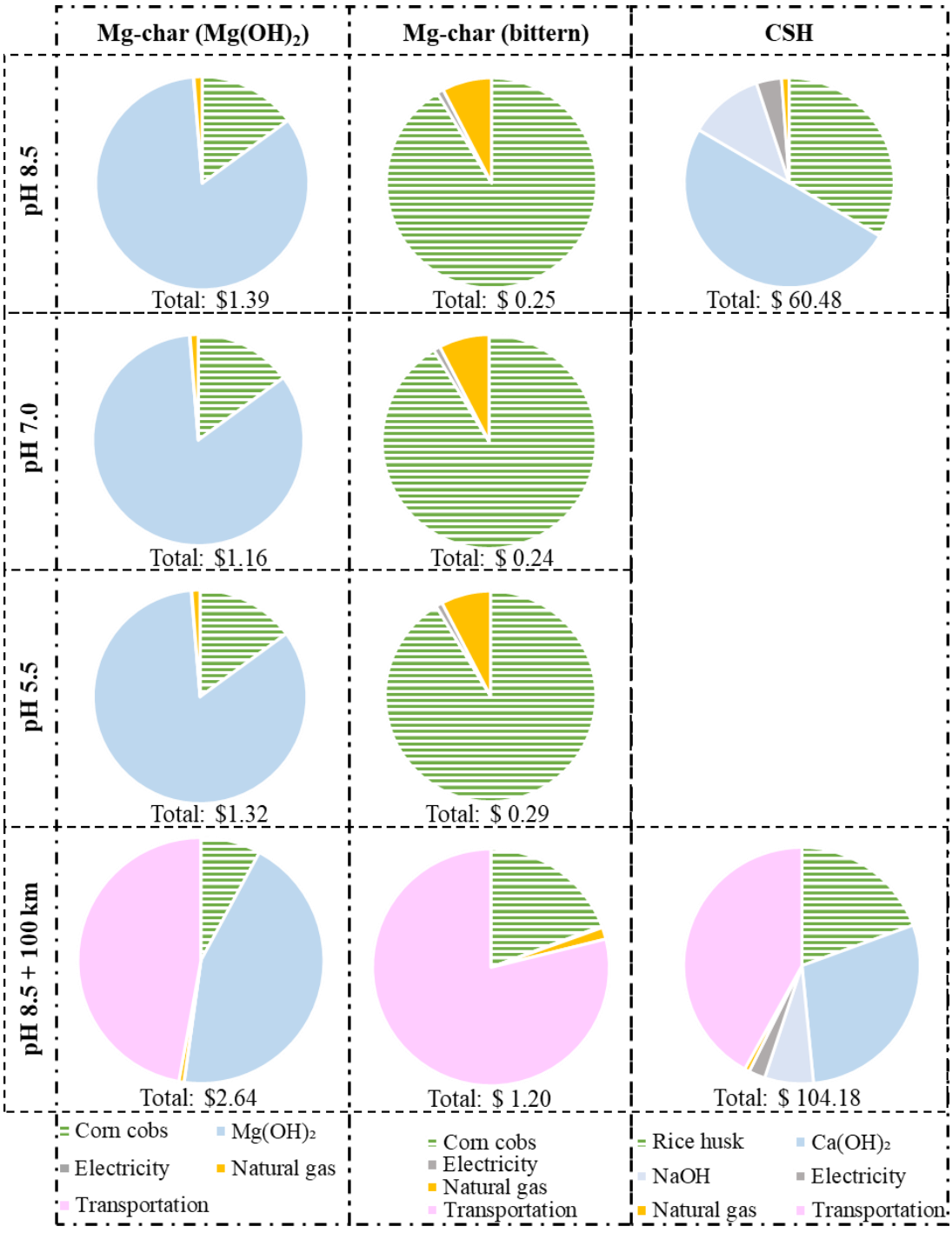

Figure 4.5 Cost analysis of producing sorbents for phosphorus recovery from wastewater and release 2.81 kg phosphorus after five rain/irrigation events. The cost of monoammonium phosphate (MAP) is $5.92. CSH stands for calcium silicate hydrate.

4.5 Conclusions

The two Mg-chars had significantly lower impacts in most impact categories and had considerably lower costs than MAP for all life cycle scenarios, even considering a transportation distance of 100 km. In neutral (pH 7.0) and acidic (pH 5.5) soils where phosphorus release from the Mg chars was more complete (Figure 4S.1), the advantages of using Mg-chars over MAP were greater in terms of both environmental impact and cost due to the lower material and energy inputs required. Because it used an industrial byproduct (bittern) that has minimal allocated emissions and currently no cost, Mg-char (bittern) was the best sorbent for phosphorus recovery and subsequent reuse in terms of environmental impacts and cost. This conclusion, however, assumes nearby (<100 km) location of a saltwater source, agricultural residues, and animal wastes, and thus is most applicable in coastal regions. In addition, the cost of Mg-char (bittern) should be reevaluated on a case-by-case basis if bittern becomes a valuable commodity in the future. Other natural sources of Mg should be investigated in future studies as alternatives to commercial $Mg(OH)_2$, which has significant costs and environmental impacts. CSH was considerably more impactful and costly than other materials analyzed in this study, due to its high demand for raw material and chemical inputs which arises from the need to apply significantly more of it to the soil to produce a phosphorus mass equal to the functional unit. This is simply due to the considerably lower solubility of calcium phosphate minerals compared to struvite, and points to the potentially lower environmental impacts and costs of magnesium phosphate minerals in phosphorus recovery and reuse. Thus, phosphorus recovery from concentrated wastewaters using Mg-amended biochars and subsequent reuse as a fertilizer can contribute to a more sustainable and economical closing of the phosphorus cycle in light of the limited availability of this valuable resource.

4.6 Acknowledgements

This work was supported by Agriculture and Food Research Initiative (AFRI) grant number 2018-6702027805 from the USDA National Institute of Food and Agriculture.

4.7 References

Ahmed, M., Ahmad, S., Hassan, F.Y., Qadir, G., Hayat, R., Shaheen, F.A. and Raza, M.A. (2019) Innovative Processes and Technologies for Nutrient Recovery from Wastes: A Comprehensive Review. Sustainability 11(18).

Amann, A., Zoboli, O., Krampe, J., Rechberger, H., Zessner, M. and Egle, L. (2018) Environmental impacts of phosphorus recovery from municipal wastewater. Resources Conservation and Recycling 130, 127-139.

APHA, A., WEF. (2005) Standard methods for the examination of water and wastewater. American Public Health Association (APHA): Washington, DC, USA.

Bradford-Hartke, Z., Lane, J., Lant, P. and Leslie, G. (2015) Environmental Benefits and Burdens of Phosphorus Recovery from Municipal Wastewater. Environmental Science & Technology 49(14), 8611-8622.

Bradford-Hartke, Z., Razmjou, A. and Gregory, L. (2021) Factors affecting phosphorus recovery as struvite: Effects of alternative magnesium sources. Desalination 504, 114949.

Ding, Y., Sabatini, D.A. and Butler, E.C. (2021) Phosphorus recovery and recycling from model animal wastewaters using materials prepared from rice straw and corn cobs. Water Science and Technology 83(8), 1893-1906.

Ding, Y., Sabatini, D.A. and Butler, E.C. (2023) Effects of pH and Soil Minerals on Phosphorus Release from Agricultural Waste-Based Sorbents: A Continuous-Flow Column Study. Journal of Environmental Engineering 149(4), 04023010.

Gahane, D., Biswal, D. and Mandavgane, S.A. (2022) Life Cycle Assessment of Biomass Pyrolysis. Bioenergy Research. 15(3), 1387–1406.

Ghodszad, L., Reyhanitabar, A., Maghsoodi, M.R., Asgari Lajayer, B. and Chang, S.X. (2021) Biochar affects the fate of phosphorus in soil and water: A critical review. Chemosphere 283, 131176.

Goel, S., Kansal, A. and Pfister, S. (2021) Sourcing phosphorus for agriculture: Life cycle assessment of three options for India. Resources Conservation and Recycling 174: 105750.

Hamdani, K. and Cheng, K.L. (1992) Adsorption of biochemically significant phosphates on silica. Colloids and Surfaces 63(1), 29-31.

Hollas, C.E., Bolsan, A.C., Venturin, B., Bonassa, G., Tapparo, D.C., Candido, D., Antes, F.G., Vanotti, M.B., Szogi, A.A. and Kunz, A. (2021) Second-Generation Phosphorus: Recovery from Wastes towards the Sustainability of Production Chains. Sustainability 13(11).

Huijbregts, M., Steinmann, Z., Elshout, P., Stam, G., Verones, F., Vieira, M., Hollander, A., Zijp, M. and van Zelm, R. (2016) ReCiPe 2016 : A harmonized life cycle impact assessment method at midpoint and endpoint level Report I: Characterization, Rijksinstituut voor Volksgezondheid en Milieu RIVM.

Huijbregts, M.A.J., Steinmann, Z.J.N., Elshout, P.M.F., Stam, G., Verones, F., Vieira, M., Zijp, M., Hollander, A. and van Zelm, R. (2017) ReCiPe2016: a harmonised life cycle impact assessment method at midpoint and endpoint level. The International Journal of Life Cycle Assessment 22(2), 138-147.

IFA (2021) Phosphate Products. Accessed on January 20. 2023. https://www.ifastat.org/supply/Phosphate%20Products/Processed%20Phosphates.

ISO (2006a) ISO 14040:2006 Environmental management — Life cycle assessment — Principles and framework, Geneva, Switzerland.

ISO (2006b) ISO 14044:2006 Environmental management — Life cycle assessment — Requirements and guidelines, Geneva, Switzerland.

Kley, D., Kleinmann, M., Sanderman, H. and Krupa, S. (1999) Photochemical oxidants: state of the science. Environmental Pollution 100(1), 19-42.

Lam, K.L., Zlatanovic, L. and van der Hoek, J.P. (2020) Life cycle assessment of nutrient recycling from wastewater: A critical review. Water research 173, 16.

Ludemann, C.I., Gruere, A., Heffer, P. and Dobermann, A. (2022) Global data on fertilizer use by crop and by country. Scientific Data 9(1), 501.

Mavhungu, A., Foteinis, S., Mbaya, R., Masindi, V., Kortidis, I., Mpenyana-Monyatsi, L. and Chatzisymeon, E. (2021) Environmental sustainability of municipal wastewater treatment through struvite precipitation: Influence of operational parameters. Journal of Cleaner Production 285.

NASA (2016) The Seasonal Rhythms of Ammonia. Accessed on March 9. 2023. https://earthobservatory.nasa.gov/images/144351/the-seasonal-rhythms-of-ammonia.

Niero, M., Pizzol, M., Bruun, H.G. and Thomsen, M. (2014) Comparative life cycle assessment of wastewater treatment in Denmark including sensitivity and uncertainty analysis. Journal of Cleaner Production 68, 25-35.

Pradel, M. and Aissani, L. (2019) Environmental impacts of phosphorus recovery from a "product" Life Cycle Assessment perspective: Allocating burdens of wastewater treatment in the production of sludge-based phosphate fertilizers. Science of the Total Environment 656, 55-69.

Puettmann, M., Sahoo, K., Wilson, K. and Oneil, E. (2020) Life cycle assessment of biochar produced from forest residues using portable systems. Journal of Cleaner Production 250, 119564.

Ravi, R., Beyers, M., Bruun, S. and Meers, E. (2022) Life cycle assessment of struvite recovery and wastewater sludge end-use: A Flemish illustration. Resources Conservation and Recycling 182, 106325.

Rittmann, B.E., Mayer, B., Westerhoff, P. and Edwards, M. (2011) Capturing the lost phosphorus. Chemosphere 84(6), 846-853.

Roberts, K.G., Gloy, B.A., Joseph, S., Scott, N.R. and Lehmann, J. (2010) Life cycle assessment of biochar systems: estimating the energetic, economic, and climate change potential. Environmental Science & Technology 44(2), 827-833.

Robles, A., Aguado, D., Barat, R., Borras, L., Bouzas, A., Gimenez, J.B., Marti, N., Ribes, J., Ruano, M.V., Serralta, J., Ferrer, J. and Seco, A. (2020) New frontiers from removal to recycling of nitrogen and phosphorus from wastewater in the Circular Economy. Bioresource Technology 300, 18.

Saft, R.J. (2007) Life cycle assessment of a pyrolysis/gasification plant for hazardous paint waste. The International Journal of Life Cycle Assessment 12(4), 230.

Schorr, M. and Valdez, B. (2016) The phosphoric acid industry: equipment, materials, and corrosion. Corrosion Reviews 34(1-2), 85-102.

Sena, M. and Hicks, A. (2018) Life cycle assessment review of struvite precipitation in wastewater treatment. Resources Conservation and Recycling 139, 194-204.

Sena, M., Seib, M., Noguera, D.R. and Hicks, A. (2021) Environmental impacts of phosphorus recovery through struvite precipitation in wastewater treatment. Journal of Cleaner Production 280, 124222.

Sharmin, N., Sabatini, D.A. and Butler, E.C. (2021) Phosphorus Recovery and Reuse Using Calcium-Silicate Hydrate Made from Rice Husk. Journal of Environmental Engineering 147(6), 04021015.

Tadele, D., Roy, P., Defersha, F., Misra, M. and Mohanty, A.K. (2019) Life Cycle Assessment of renewable filler material (biochar) produced from perennial grass (Miscanthus). Aims Energy 7(4), 430-440.

Tseng, R.-L. and Tseng, S.-K. (2005) Pore structure and adsorption performance of the KOH-activated carbons prepared from corncob. Journal of Colloid and Interface Science 287(2), 428-437.

Ulrich, A.E. and Frossard, E. (2014) On the history of a reoccurring concept: phosphorus scarcity. Sci Total Environ 490, 694-707.

van der Wiel, B.Z., Weijma, J., van Middelaar, C.E., Kleinke, M., Buisman, C.J.N. and Wichern, F. (2019) Restoring nutrient circularity: A review of nutrient stock and flow analyses of local agro-food-waste systems. Resources Conservation and Recycling: X 3, 100014.

Xu, D., Xiong, X., Yang, L., Zhang, Z. and Wang, X. (2016) Determination of the Solubility of Ammonium Dihydrogen Phosphate in Water–Ethanol System at Different Temperatures from 283.2 to 343.2 K. Journal of Chemical & Engineering Data 61(1), 78-82.

Yami, T.L., Butler, E.C. and Sabatini, D.A. (2016) Chemically activated cow bone for increased fluoride removal from drinking water. Journal of Water, Sanitation and Hygiene for Development 6(2), 215-223.

Zheng, G.Y., Xia, J.P. and Chen, Z.J. (2021) Overview of Current Phosphoric Acid Production Processes and a New Idea of Kiln Method. Mini-Reviews in Organic Chemistry 18(3), 328-338.

4.8 Supplementary Materials

4.8.1 Experimental details on sorbents production, phosphorus recovery and release

The processes of production, phosphorus recovery, and phosphorus release of three sorbents were based on (Ding et al. 2023) and illustrated in Figure 4S.1.

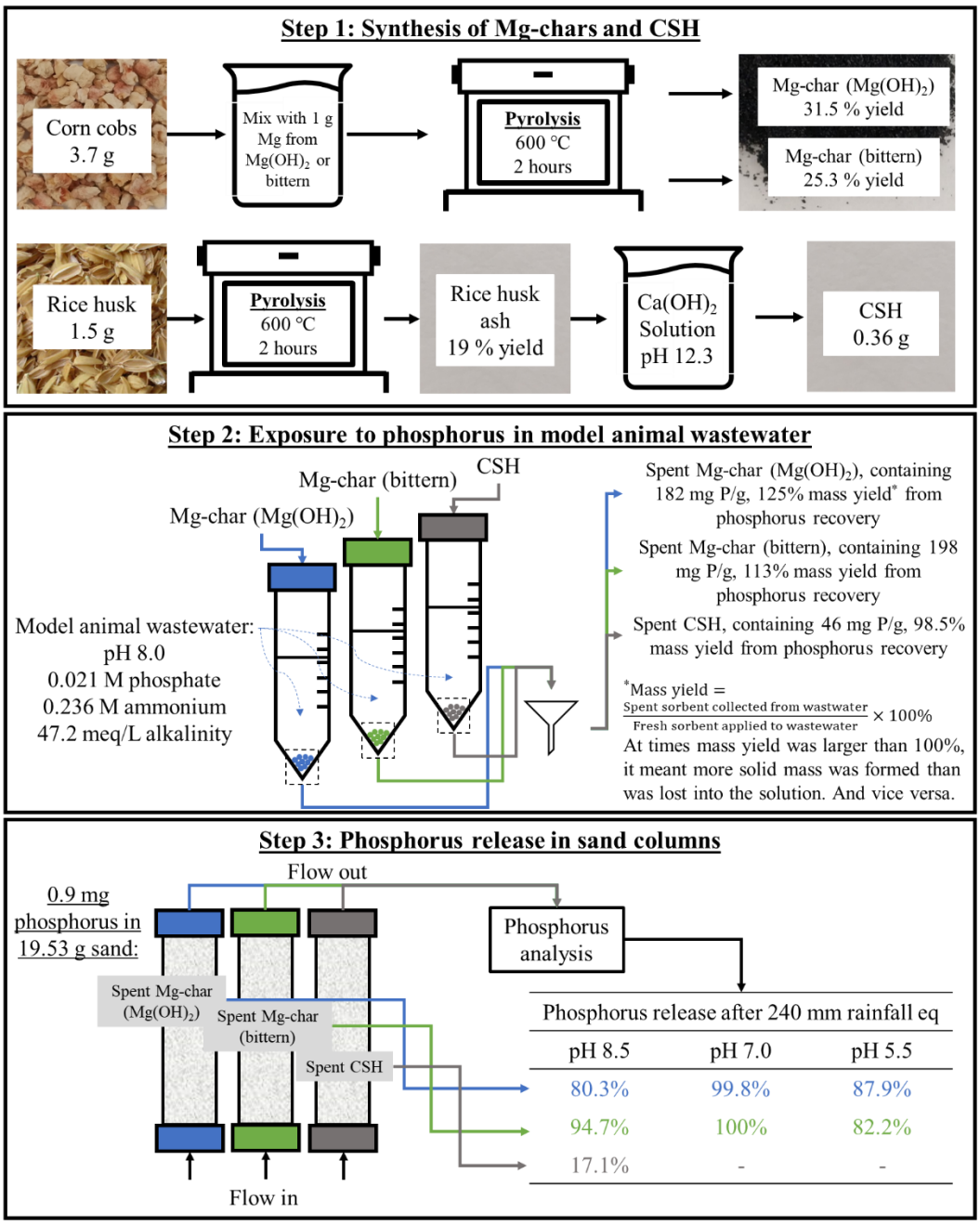

Figure 4S.1 The production, phosphorus recovery, and phosphorus release from the sorbents investigated in this study (Ding et al. 2023)

4.8.2 Functional unit, co-product allocation, and life cycle inventory

4.8.2.1 Functional unit

The global phosphorus fertilizer consumption of 49,310,442,360 kg as P_2O_5 in 2018 (IFA 2022) was divided by the 2018 world population of 7,661,776,338 (WorldBank 2022) to yield the annual phosphorus fertilizer use per capita:

$$\frac{49{,}310{,}442{,}360\ kg\ P_2O_5 \times \frac{2 \times \frac{30.97\ g}{mole}}{2 \times \frac{30.97\ g}{mole} + 5 \times \frac{16.00\ g}{mole}}}{7{,}661{,}776{,}338\ people} = \frac{2.81\ kg\ P}{Person}$$

4.8.2.2 Allocation factors

When using datasets with more than one co-product (e.g., corn and corn cobs), the impacts associated with the co-product of interest were estimated by value-based allocation (ISO 2006). Allocation factors were calculated by dividing the value of the product of interest by the total value of all products, as described in the following subsections.

4.8.2.2.1 Corn cobs

A total of 0.15 kg of corn cobs are produced for every kg of corn grain (Wojcieszak et al. 2022). Then the value-based allocation factor for corn cobs (F_{cobs}) is (Figure 4S.2):

$$F_{cobs} = \frac{Value\ of\ cobs}{Value\ of\ cobs\ and\ grain}$$

$$= \frac{\left[0.15\ kg\ cobs \times \frac{ton\ cobs}{1{,}000\ kg\ cobs} \times \frac{\$\ 5.6}{ton\ cobs}\right]}{\left[0.15\ kg\ cobs \times \frac{\text{ton cobs}}{1{,}000\ kg\ cobs} \times \frac{\$\ 5.6}{ton\ cobs}\right] + \left[1\ kg\ grain \times \frac{ton\ grain}{1{,}000\ kg\ grain} \times \frac{\$\ 171}{ton\ grain}\right]}$$

$= 0.0049.$

The quantity of corn that was needed to produce required amount of corn cobs was multiplied by F_{cobs} and the result was used as the input to the Ecoinvent dataset "Corn, at farm/US U" for analysis, providing the impacts allocated to corn cobs production.

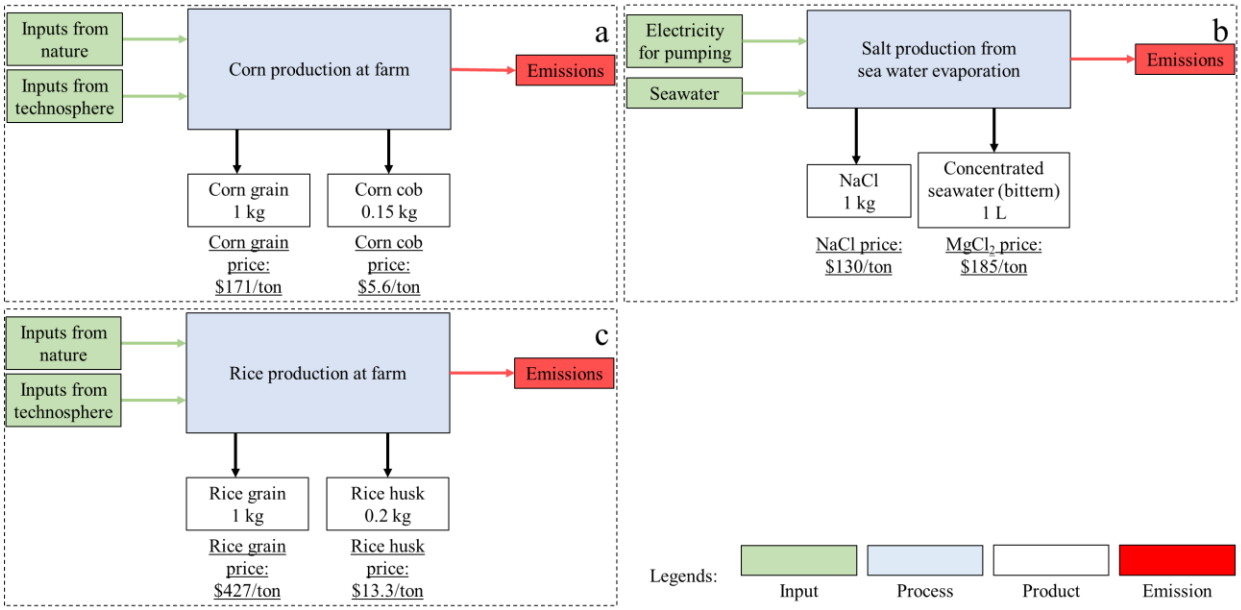

Figure 4S.2 Data used in value-based allocation for (a) corn cobs, (b) bittern, and (c) rice husks. The price of corn grain is the five-year median for 2017-2022 from (Indexmundi 2022a); the price of corn cobs is $5.6/ton from Alibaba.com; the mean prices of $MgCl_2$ and NaCl are from (Bagastyo et al. 2021); the price of rice grain is the 2017-2022 five-year median from (Indexmundi 2022b); and the price of rice husk is from (Thengane et al. 2020).

4.8.2.2.2 Rice husk

There are 0.20 kg rice husk generated as a by-product per one kg of rice grain produced (Moraes et al. 2014). Therefore, the value-based allocation factor for rice husk (F_{husk}) is (Figure 4S.2):

$$F_{husk} = \frac{Value\ of\ husk}{Value\ of\ husk\ and\ grain}$$

$$= \frac{0.2\ kg\ husk \times \frac{1\ ton\ husk}{1000\ kg\ husk} \times \frac{\$\ 13.3}{ton}}{\left(0.2\ kg\ husk \times \frac{1\ ton\ husk}{1000\ kg\ husk} \times \frac{\$\ 13.3}{ton}\right) + \left(1\ kg\ grain \times \frac{1\ ton\ grain}{1000\ kg\ grain} \times \frac{\$\ 427}{ton}\right)}$$

$$= 0.0062$$

The quantity of rice that was needed to produce required amount of rice husk was multiplied by F_{husk} and the result was used as the input to the Ecoinvent dataset "Rice, at farm/US U" for analysis, providing the impacts allocated to rice husk production.

4.8.2.2.3 Bittern

The Ecoinvent version 3.9 dataset "Salt production from seawater, evaporation pond, GLO" was modified to describe bittern production. This dataset assumed that one liter of seawater contains 35 g NaCl (USGS 2023), meaning that the production of one kg NaCl requires 28.57 L seawater. During evaporation of seawater for salt production, magnesium salts start to precipitate after evaporation of approximately 97% of the water (Sharkh et al. 2022). Therefore, to retain dissolved magnesium salts in the concentrated bittern brine, 96.5% water evaporation was assumed, leaving 3.5% water by volume. Therefore, 28.57 L × 0.035, or approximately 1 L of bittern is produced in the production of 1 kg NaCl (Figure 4S.2).

There are 1.28 g Mg per kg of seawater (Sharkh et al. 2022). Since the predominant anion in natural seawater is Cl^- (Millero 2002), then one kg of seawater contains 5.01 g $MgCl_2$. Considering the density of seawater, the $MgCl_2$ concentration in seawater can be calculated as:

$$\frac{5.01 g\ MgCl_2}{1\ kg\ seawater} \times \frac{1.026\ kg\ seawater}{1\ L\ seawater} = \frac{5.14\ g\ MgCl_2}{1\ L\ seawater}.$$

Considering 96.5% water evaporation, the $MgCl_2$ concentration in bittern is:

$$\frac{5.14\ g\ MgCl_2}{1\ L\ seawater} \times \frac{1\ L\ seawater}{(1-0.965)\ L\ bittern} = \frac{146.96\ g\ MgCl_2}{1\ L\ bittern}.$$

Considering the values (i.e., prices) of $MgCl_2$ and NaCl (Figure 4S.2), the allocation factor for bittern is:

$$F_{bittern} = \frac{Value\ of\ \ MgCl_2}{Value\ of\ MgCl_2\ and\ NaCl}$$

$$= \frac{\frac{146.96\ g\ MgCl_2}{L\ bittern} \times 1\ L\ bittern \times \frac{kg}{1000\ g} \times \frac{\$\ 185}{ton} \times \frac{1\ ton}{1000\ kg}}{(\frac{146.96\ g\ MgCl_2}{L\ bittern} \times 1\ L \times \frac{kg}{1000\ g} \times \frac{\$\ 185}{ton} \times \frac{1\ ton}{1000\ kg}) + (1\ kg\ NaCl \times \frac{\$\ 130}{ton} \times \frac{1\ ton}{1000\ kg})}$$

$$= 0.17$$

The use of $F_{bittern}$ can be seen in section 2.3 where the dataset "Bittern" is created. Essentially, the input of "Bittern" dataset was the needed bittern quantity multiplied with $F_{bittern}$ to quantify the impacts allocated to bittern production.

4.8.2.3 New datasets

Datasets for groundwater supply, corn cob pyrolysis, rice husk pyrolysis, and bittern were created to carry out the LCA (Figure 4S.3). Details are provided in the following subsections.

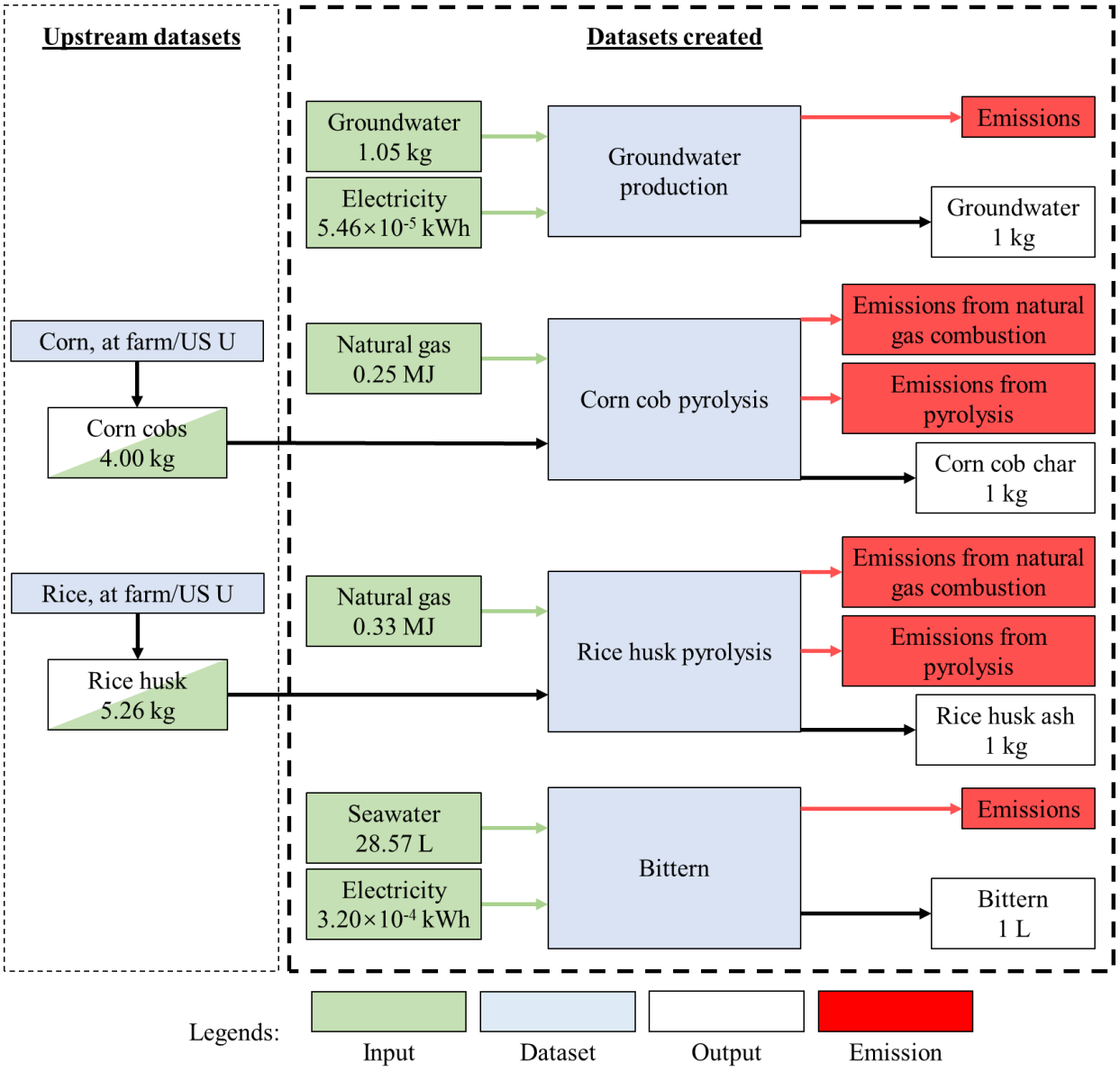

Figure 4S.3 Datasets created for this LCA and their inputs from upstream datasets. Abbreviations in dataset names: US, United States; U, unit process. Upstream inputs were not included in the model to avoid double-counting since they were as outputs of the farming datasets.

4.8.2.3.1 Groundwater production

The Ecoinvent dataset "Tap water, at use/RER U" (acronyms are defined in the footnotes to Table 4.1) was modified to include only well water. Other water sources, water treatment,

transportation, and infrastructure were omitted from the dataset, which was further modified to consider the electricity required for pumping. The electricity dataset used throughout this research was "Electricity, medium voltage, production UCTE, at grid/UCTE U", where UCTE stands for Union for the Co-ordination of Transmission of Electricity, now part of the European Network of Transmission System Operators for Electricity (ENTSO-E). The pumping efficiency was assumed to be 95%, meaning 5% water loss in the pumping process. The pump energy efficiency was assumed to be 52.5%, which is the mean value for a centrifugal pump (de Souza et al. 2021), meaning there was 52.5% conversion of electrical to mechanical energy. The groundwater table was assumed to be 10 m below the ground surface. Therefore, to obtain one kg of groundwater, the electrical energy required is:

$$[(1\ kg\ water\ needed \div 0.95\ pumping\ efficiency) \times 10\ m\ elevation\ gain] \div 0.525\ energy\ efficiency = 20.05\ kg \cdot m = 5.46 \times 10^{-5} kWh.$$

Therefore, the inputs for the dataset "Groundwater production" were 1.05 kg groundwater and 5.46×10^{-5} kWh electricity for pumping, and the output was 1 kg groundwater (Figure 4S.3).

4.8.2.3.2 Corn cob pyrolysis

The dataset "corn cob pyrolysis" was developed considering biomass production and pyrolysis. The corn cob char yield for slow pyrolysis was assumed to be 25% by mass (Singh et al. 2021), which is consistent with our observed range (Figure 4S.1). Corn cob contains 47% by mass carbon (C) and 0.47% by mass nitrogen (N) (Zhang et al. 2022), and, after pyrolysis under similar conditions as in this work, corn cob char contains 63% C and 1.17% N by mass (Ippolito et al. 2015).

The carbon emitted during charring one kg of corn cobs can be calculated from the difference in the mass of carbon in the corn cobs and in the resulting char. The mass of carbon in 1 kg cobs is: $1.00\ kg\ cobs\ x \frac{0.47\ kg\ C}{kg\ cobs} = 0.47\ kg\ C$. The mass of carbon in the char produced from 1 kg cobs is: $1.00\ kg\ cobs\ x \frac{0.25\ kg\ char}{kg\ cobs} x \frac{0.63\ kg\ C}{kg\ char} = 0.158\ kg\ C$. The carbon lost in charring 1 kg cobs is the difference between these two values, or 0.312 kg C. Expressing this in units of mass of C per kg char (not cobs) yields: $\frac{0.312\ kg\ C}{kg\ cobs} x \frac{kg\ cobs}{0.25\ kg\ char} = \frac{1.25\ kg\ C}{kg\ char}$. Expressing as kg CO_2 (44.01 g/mol) instead of kg C (12.01 g/mol) yields 4.6 kg CO_2 per kg char.

Emissions of NO_2 from nitrogen in the corn cobs can be calculated in a similar manner. First, the nitrogen emitted during charring one kg of corn cobs can be calculated from the difference in the mass of nitrogen in the corn cobs and in the resulting char. The mass of nitrogen in 1 kg cobs is $1.00\ kg\ cobs\ x \frac{0.0047\ kg\ N}{kg\ cobs} = 0.0047\ kg\ N$. The mass of nitrogen in the char produced from 1 kg cobs is $1.00\ kg\ cobs\ x \frac{0.25\ kg\ char}{kg\ cobs} x \frac{0.0117\ kg\ N}{kg\ char} = 0.00292\ kg\ N$. The nitrogen lost in charring 1 kg cobs is the difference between these two values, or 0.00178 kg N. Expressing this in units of mass of N per kg char (not cobs) yields $\frac{0.00178\ kg\ N}{kg\ cobs} x \frac{kg\ cobs}{0.25\ kg\ char} = \frac{0.00712\ kg\ C}{kg\ char}$. Expressing as kg NO_2 (46.01 g/mol) instead of kg N (14.01 g/mol) yields 0.023 kg NO_2 per kg char.

The natural gas needed for pyrolysis was assumed to be 1.67 m^3 per ton of biomass (Saft 2007). Emissions associated with combustion of this gas were estimated using the Ecoinvent version 2.2 dataset "Natural gas, burned in industrial furnace >100kW/RER U". The amount of natural gas needed to produce one kg char is:

$$\frac{1\ kg\ cobs}{0.25\ kg\ char} \times \frac{1.67\ m^3\ natural\ gas}{1{,}000\ kg\ cobs} = 6.68 \times 10^{-3}\ m^3\ natural\ gas.$$

Considering the heat content of natural gas (37.63 MJ/m^3) (EIA 2022), 6.68×10^{-3} m^3 natural gas produces 0.25 MJ of heat. Therefore, the input for the dataset "Corn cobs pyrolysis" for producing one kg of corn cob char was 0.25 MJ heat from natural gas (using the Ecoinvent dataset referenced above) (Figure 4S.3). In addition to the emissions from natural gas combustion, 4.58 kg CO_2 and 2.32×10^{-2} kg NO_2 were added to the emissions inventory for the "Corn cobs pyrolysis" dataset. Other emissions associated with natural gas combustion were unchanged.

4.8.2.3.3 Rice husk pyrolysis

Rice husk is reported to have 26% C and 0.60% N by mass (Hossain et al. 2020). Rice husk ash yield was 19% (Ding et al., 2023), and all the C and N were assumed to be lost to the atmosphere. The CO_2 and NO_2 emissions from rice husk pyrolysis were calculated in the same way as for corn cob char:

$$\frac{kg\ husk}{0.19\ kg\ ash} x \frac{0.26\ kg\ C}{kg\ husk} x \frac{44.01\ kg\ CO_2}{12.01\ kg\ C} = 5.0\ kg\ CO_2\ per\ kg\ ash$$

$$\frac{kg\ husk}{0.19\ kg\ ash} x \frac{0.0060\ kg\ N}{kg\ husk} x \frac{46.01\ kg\ NO_2}{12.01\ kg\ N} = 0.12\ kg\ NO_2\ per\ kg\ ash$$

Like for corn cob char, the Ecoinvent version 2.2 process "Natural gas, burned in industrial furnace >100kW/RER U" was used to quantify emissions from natural gas combustion. The natural gas demand was $\frac{1\ kg\ husk}{0.19\ kg\ ash} \times \frac{1.67\ m^3\ natural\ gas}{1{,}000\ kg\ husk} = 8.79 \times 10^{-3}\ m^3\ natural\ gas,$

which corresponds to 0.33 MJ of heat.

Therefore, the input for process “Rice husk pyrolysis” for producing one kg of rice husk ash was 0.33 MJ natural gas (Figure 4S.3); and the emissions were 5.0 kg CO_2 and 0.12 kg NO_2. Other emissions associated with natural gas combustion were not changed.

4.8.2.3.4 Bittern

The Ecoinvent version 3.9 dataset “Salt production from seawater, evaporation pond, GLO” based on research by (Akridge 2008) was modified to represent bittern production by modifying the electricity required to pump seawater to an evaporation pond at the coast, using the same electricity dataset used for pumping groundwater (section 2.3.1). The required elevation gain for seawater during pumping was assumed to be two meters. The calculations used the same pumping efficiency of 95% and pump energy efficiency of 52.5% as in section 2.3.1. To produce one liter of bittern as a by-product of one kg of NaCl, 28.57 L seawater is needed, and the corresponding electricity consumed for pumping the seawater for two meters of elevation gain was:

$$\left[\left((28.57\ L\ seawater \times \frac{1.026\ kg\ seawater}{1\ L\ seawater}) \div 0.95\ pumping\ efficiency\right) \times 2\ m\right] \div$$

$$0.525\ energy\ efficiency = 117.55\ kg \cdot m = 3.20 \times 10^{-4}\ kWh.$$

Therefore, the electricity input for “Salt production from seawater, evaporation pond, GLO” was changed to 3.2×10^{-4} kWh using “Electricity, medium voltage, production UCTE, at grid/UCTE U”, and the dataset was called “Bittern”. Quantity of bittern needed was multiplied with $F_{bittern}$ to be the input for the “Bittern” dataset quantifying the emissions assigned to bittern production by value-based allocation (section 2.2.3).

4.8.2.4 Inputs for the life cycle inventory

The overall flows of raw materials and the process outputs for the three sorbents are shown in Figure 4S.4. All the raw material inputs were back-calculated from the functional unit using the experimentally determined quantities in Figure 4S.1. The functional unit (i.e., the quantity of fertilizer sufficient to release 2.81 kg phosphorus in five pore volumes) was used in conjunction with the phosphorus release data from the column studies (Figure 4S.1) to determine how much spent sorbent was needed for each scenario. The fresh sorbent needed was estimated from the spent sorbent yield (Figure 4S.1). Finally, the biomass, chemicals, and water required to prepare the fresh sorbent were estimated based on results from previous experiments (Figure 4S.1).

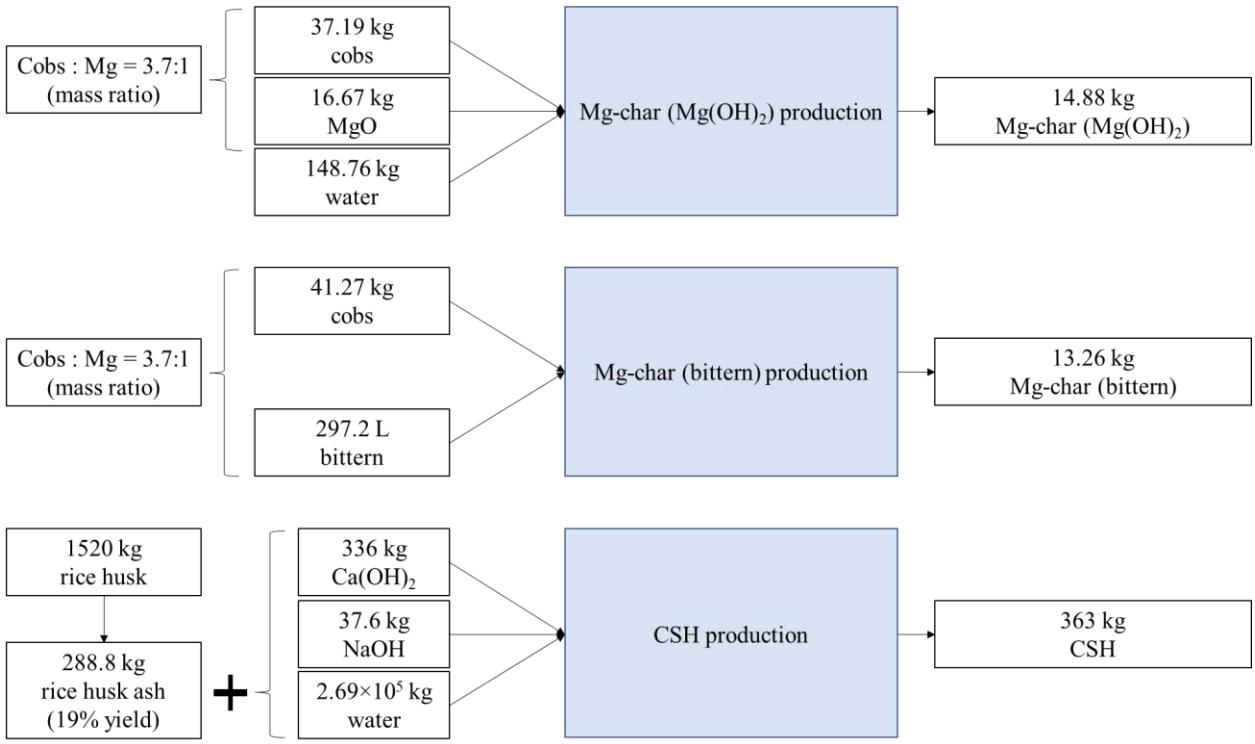

Figure 4S.4 Quantities of raw materials needed for producing Mg-char ($Mg(OH)_2$), Mg-char (bittern), and calcium silicate hydrate (CSH)

The following is an example calculation of LCA input quantities (summarized in Table 4.1) for Mg-char ($Mg(OH)_2$). The pH 8.5 scenario is used in the example calculation. Other pH values had the same approach, except that the percentage of phosphorus released in five pore volumes differed as a function of pH (Figure 4S.1).

For preparing Mg-char ($Mg(OH)_2$), the mass ratios of corn cobs to Mg and corn cobs to water are in Figure 4S.4. These quantities resulted in a 31.5% yield of fresh Mg-char ($Mg(OH)_2$) after pyrolysis (Figure 4S.1). After exposure to the model animal wastewater, the spent Mg-char ($Mg(OH)_2$) contained 182 mg phosphorus /g (Figure 4S.1). The spent sorbent yield was approximately 125%, i.e., 100 g fresh Mg-char ($Mg(OH)_2$) formed approximately 125 g spent Mg-char ($Mg(OH)_2$) containing recovered phosphorus (Figure 4S.1). In the column experiment conducted at pH 8.5, 83% of the total sorbent-associated phosphorus was released in five pore volumes.

Based on these values, to produce spent char that would release 2.81 kg phosphorus in five pore volumes (the functional unit), the fresh Mg-char ($Mg(OH)_2$) needed was:

$$2{,}810\ g\ P\ needed \times \frac{g\ P\ recovered}{0.83\ g\ P\ released\ from\ recovered} \times \frac{g\ spent\ sorbent}{0.182\ g\ P} \times \frac{100\ g\ fresh\ \text{sorbent}}{125\ g\ spent\ sorbent} \times \frac{1\ kg}{1000\ g} = 14.88\ kg\ fresh\ sorbent.$$

To calculate the corresponding corn cob needed to prepare 14.88 kg fresh Mg-char ($Mg(OH)_2$), a mass balance was used. Specifically, the mass of fresh Mg-char ($Mg(OH)_2$) was equal to (mass of cobs + mass of Mg) × sorbent yield after pyrolysis, or:

$14.88\ kg\ fresh\ Mg\ char\ (Mg(OH)_2) = \left(mass\ of\ cobs + \frac{mass\ of\ cobs}{\frac{3.7\ kg\ cobs}{1\ kg\ Mg}}\right) \times 31.5\%$. Solving for the mass of cobs yields 37.19 kg.

Then, the MgO needed was calculated to be: $37.19\ kg\ cobs \times \frac{1\ kg\ Mg}{3.7\ kg\ cobs} \times \frac{40.31\ kg\ MgO}{24.31\ kg\ Mg} = 16.67\ kg$ (MgO was used as a proxy for $Mg(OH)_2$ in SimaPro). The water needed was: $37.19\ kg\ cobs \times \frac{0.12\ L\ water}{0.03\ kg\ cob} \times \frac{1\ L\ water}{1\ kg\ water} = 148.76\ kg$.

The corn farming demand was back-calculated from the required mass of corn cobs. Based on the Figure 4S.2, the corn farming demand in terms of corn grain was: $37.19\ kg\ cobs \times \frac{1\ kg\ corn\ grain}{0.15\ kg\ cobs} = 247.9\ kg\ corn\ grain$. The total corn farming needed was multiplied by the allocation factor F_{cobs} to yield the corn farming impacts allocated to obtaining 37.19 kg corn cobs: $247.9\ kg \times 0.0049 = 1.21\ kg$ of corn farming.

The required output from the dataset "corn cob pyrolysis" was calculated considering the char yield of 25% (section 2.3.2), or $37.19\ kg\ cobs \times 25\% = 9.30\ kg$.

Additionally, for scenario with the addition of transportation, the inputs other than transportation need were all identical to Scenario-pH 8.5. And the transportation need (tkm) was calculated by multiplying total mass to transport (t) with distance (km). For example, Mg-char ($Mg(OH)_2$) needed to transport 0.037 t cobs and 0.017 t MgO, then the total mass to transport was 0.054 t. Considering transportation distances 5, 50, and 100 km, the transportation needs were 2.70×10^{-1}, 2.70×10^{0}, and 5.40×10^{0} tkm. These inputs are also shown in main text Table 4.1.

4.8.3 LCIA and cost analysis results

4.8.3.1 LCIA results for pH 8.5

Table 4S.1 Life cycle impact assessment (LCIA) results for three sorbents and monoammonium phosphate (MAP) at pH 8.5 (illustrated Figure 4.2a)

Impact category	Unit[1]	Mg-char ($Mg(OH)_2$)	Mg-char (bittern)	CSH	MAP
Climate change	kg CO_2 eq	6.10×10^{1}	4.81×10^{1}	1.83×10^{3}	1.03×10^{1}
Ozone depletion	kg CFC-11 eq	2.23×10^{-7}	7.42×10^{-8}	2.49×10^{-5}	9.47×10^{-7}
Terrestrial acidification	kg SO_2 eq	1.48×10^{-1}	1.40×10^{-1}	1.76×10^{1}	2.42×10^{-1}
Freshwater eutrophication	kg P eq	2.04×10^{-3}	2.07×10^{-4}	6.95×10^{-2}	3.92×10^{-3}
Marine eutrophication	kg N eq	1.89×10^{-2}	1.80×10^{-2}	1.29×10^{0}	2.23×10^{-3}
Human toxicity	kg 1,4-DB eq	2.08×10^{0}	6.42×10^{-2}	4.18×10^{1}	4.07×10^{0}
Photochemical oxidant formation	kg NMVOC	2.38×10^{-1}	2.42×10^{-1}	3.06×10^{1}	5.42×10^{-2}
Particulate matter formation	kg PM_{10} eq	1.06×10^{-1}	5.39×10^{-2}	6.86×10^{0}	6.74×10^{-2}
Terrestrial ecotoxicity	kg 1,4-DB eq	6.71×10^{-3}	6.86×10^{-3}	3.81×10^{-2}	2.65×10^{-3}
Freshwater ecotoxicity	kg 1,4-DB eq	3.56×10^{-2}	5.02×10^{-3}	3.78×10^{-1}	2.80×10^{-2}
Marine ecotoxicity	kg 1,4-DB eq	1.52×10^{-2}	1.55×10^{-3}	3.81×10^{-1}	3.90×10^{-2}
Ionizing radiation	kBq ^{235}U eq	1.53×10^{0}	6.74×10^{-2}	5.58×10^{1}	2.44×10^{0}
Agricultural land occupation	m^2a	9.03×10^{-1}	9.71×10^{-1}	7.38×10^{1}	2.74×10^{-1}
Urban land occupation	m^2a	4.26×10^{-2}	3.51×10^{-2}	5.34×10^{0}	1.66×10^{-1}
Natural land transformation	m^2	6.31×10^{-4}	1.47×10^{-4}	2.50×10^{-2}	2.38×10^{-3}
Water depletion	m^3	2.86×10^{-1}	1.07×10^{-2}	3.40×10^{2}	1.43×10^{0}
Metal depletion	kg Fe eq	0.00×10^{0}	0.00×10^{0}	0.00×10^{0}	0.00×10^{0}
Fossil depletion	kg oil eq	3.25×10^{-3}	1.38×10^{-4}	1.21×10^{-1}	6.95×10^{-3}

[1] Abbreviations are: CFC-11: trichlorofluoromethane; 1,4-DB: 1,4-dichlorobenzene; NMVOC: non-methane volatile organic compounds.

Table 4S.2 Life cycle impact assessment (LCIA) results by life cycle stage for Mg-char ($Mg(OH)_2$) and Mg-char (bittern) at pH 8.5 (illustrated in Figure 4.3)

Impact category	Unit[1]	Mg-char ($Mg(OH)_2$)				Mg-char (bittern)		
		$Mg(OH)_2$ production	Groundwater	Corn farming	Corn cobs pyrolysis	Bittern	Corn farming	Corn cobs pyrolysis
Climate change	kg CO_2 eq	1.76×10^{1}	4.32×10^{-3}	5.28×10^{-1}	4.28×10^{1}	2.28×10^{-2}	5.84×10^{-1}	4.75×10^{1}
Ozone depletion	kg CFC-11 eq	1.57×10^{-7}	2.12×10^{-10}	4.28×10^{-8}	2.29×10^{-8}	1.41×10^{-9}	4.73×10^{-8}	2.54×10^{-8}
Terrestrial acidification	kg SO_2 eq	2.22×10^{-2}	1.80×10^{-5}	4.92×10^{-3}	1.21×10^{-1}	7.69×10^{-5}	5.44×10^{-3}	1.34×10^{-1}
Freshwater eutrophication	kg P eq	1.86×10^{-3}	4.27×10^{-6}	1.70×10^{-4}	2.38×10^{-6}	1.60×10^{-5}	1.88×10^{-4}	2.64×10^{-6}
Marine eutrophication	kg N eq	2.68×10^{-3}	1.22×10^{-6}	7.78×10^{-3}	8.44×10^{-3}	4.83×10^{-6}	8.61×10^{-3}	9.35×10^{-3}
Human toxicity	kg 1,4-DB eq	2.03×10^{0}	2.47×10^{-3}	4.54×10^{-2}	1.86×10^{-3}	1.19×10^{-2}	5.03×10^{-2}	2.06×10^{-3}
Photochemical oxidant formation	kg NMVOC	2.05×10^{-2}	9.02×10^{-6}	1.50×10^{-3}	2.16×10^{-1}	5.52×10^{-5}	1.66×10^{-3}	2.40×10^{-1}
Particulate matter formation	kg PM10 eq	5.72×10^{-2}	5.67×10^{-6}	1.01×10^{-3}	4.76×10^{-2}	4.21×10^{-5}	1.12×10^{-3}	5.28×10^{-2}
Terrestrial ecotoxicity	kg 1,4-DB eq	5.12×10^{-4}	1.08×10^{-7}	6.20×10^{-3}	4.12×10^{-7}	1.16×10^{-6}	6.86×10^{-3}	4.56×10^{-7}
Freshwater ecotoxicity	kg 1,4-DB eq	3.12×10^{-2}	2.02×10^{-5}	4.45×10^{-3}	1.24×10^{-5}	7.88×10^{-5}	4.93×10^{-3}	1.37×10^{-5}
Marine ecotoxicity	kg 1,4-DB eq	1.39×10^{-2}	2.08×10^{-5}	1.31×10^{-3}	1.39×10^{-5}	8.92×10^{-5}	1.45×10^{-3}	1.54×10^{-5}
Ionizing radiation	kBq ^{235}U eq	1.47×10^{0}	3.40×10^{-3}	5.01×10^{-2}	1.61×10^{-3}	1.02×10^{-2}	5.55×10^{-2}	1.78×10^{-3}
Agricultural land occupation	m^2a	2.65×10^{-2}	5.58×10^{-5}	8.77×10^{-1}	5.56×10^{-5}	3.44×10^{-4}	9.70×10^{-1}	6.17×10^{-5}
Urban land occupation	m^2a	1.10×10^{-2}	1.34×10^{-5}	3.16×10^{-2}	6.16×10^{-5}	1.07×10^{-4}	3.49×10^{-2}	6.83×10^{-5}
Natural land transformation	m^2	5.01×10^{-4}	4.60×10^{-7}	9.51×10^{-5}	3.53×10^{-5}	3.06×10^{-6}	1.05×10^{-4}	3.91×10^{-5}
Water depletion	m^3	1.20×10^{-1}	1.57×10^{-1}	9.05×10^{-3}	1.10×10^{-4}	5.88×10^{-4}	1.00×10^{-2}	1.21×10^{-4}
Metal depletion	kg Fe eq	0.00×10^{0}	0.00×10^{0}	0.00×10^{0}	0.00×10^{0}	0.00×10^{0}	0.00×10^{0}	0.00×10^{0}
Fossil depletion	kg oil eq	3.16×10^{-3}	7.16×10^{-6}	7.55×10^{-5}	5.94×10^{-6}	4.81×10^{-5}	8.36×10^{-5}	6.58×10^{-6}

[1] Abbreviations are: CFC-11: trichlorofluoromethane; 1,4-DB: 1,4-dichlorobenzene; NMVOC: non-methane volatile organic compounds.

Table 4S.3 Life cycle impact assessment (LCIA) results by life cycle stage for calcium silicate hydrate (CSH) at pH 8.5 (illustrated in Figure 4.3)

Impact category	Unit[1]	$Ca(OH)_2$ production	NaOH production	Groundwater	Rice farming	Rice husk pyrolysis	Rice farming	Rice husk pyrolysis
Climate change	kg CO_2 eq	2.52×10^{2}	3.76×10^{1}	7.80×10^{0}	8.43×10^{1}	1.45×10^{3}	2.52×10^{2}	3.76×10^{1}
Ozone depletion	kg CFC-11 eq	1.76×10^{-5}	2.36×10^{-6}	3.83×10^{-7}	3.60×10^{-6}	9.38×10^{-7}	1.76×10^{-5}	2.36×10^{-6}
Terrestrial acidification	kg SO_2 eq	2.11×10^{-1}	1.62×10^{-1}	3.25×10^{-2}	3.42×10^{-1}	1.68×10^{1}	2.11×10^{-1}	1.62×10^{-1}
Freshwater eutrophication	kg P eq	3.25×10^{-3}	3.70×10^{-2}	7.71×10^{-3}	2.15×10^{-2}	9.76×10^{-5}	3.25×10^{-3}	3.70×10^{-2}
Marine eutrophication	kg N eq	7.62×10^{-3}	1.38×10^{-2}	2.20×10^{-3}	9.62×10^{-2}	1.17×10^{0}	7.62×10^{-3}	1.38×10^{-2}
Human toxicity	kg 1,4-DB eq	2.87×10^{0}	2.47×10^{1}	4.46×10^{0}	9.65×10^{0}	7.62×10^{-2}	2.87×10^{0}	2.47×10^{1}
Photochemical oxidant formation	kg NMVOC	3.23×10^{-1}	8.66×10^{-2}	1.63×10^{-2}	1.64×10^{-1}	3.00×10^{1}	3.23×10^{-1}	8.66×10^{-2}
Particulate matter formation	kg PM10 eq	1.01×10^{-1}	5.36×10^{-2}	1.02×10^{-2}	8.57×10^{-2}	6.61×10^{0}	1.01×10^{-1}	5.36×10^{-2}
Terrestrial ecotoxicity	kg 1,4-DB eq	9.78×10^{-4}	1.86×10^{-3}	1.95×10^{-4}	3.50×10^{-2}	1.69×10^{-5}	9.78×10^{-4}	1.86×10^{-3}
Freshwater ecotoxicity	kg 1,4-DB eq	4.51×10^{-2}	1.95×10^{-1}	3.65×10^{-2}	1.01×10^{-1}	5.07×10^{-4}	4.51×10^{-2}	1.95×10^{-1}
Marine ecotoxicity	kg 1,4-DB eq	3.04×10^{-2}	2.14×10^{-1}	3.75×10^{-2}	9.90×10^{-2}	5.69×10^{-4}	3.04×10^{-2}	2.14×10^{-1}
Ionizing radiation	kBq ^{235}U eq	1.16×10^{1}	2.70×10^{1}	6.15×10^{0}	1.10×10^{1}	6.57×10^{-2}	1.16×10^{1}	2.70×10^{1}
Agricultural land occupation	m^2a	7.72×10^{-2}	1.04×10^{0}	1.01×10^{-1}	7.26×10^{1}	2.28×10^{-3}	7.72×10^{-2}	1.04×10^{0}
Urban land occupation	m^2a	9.62×10^{-2}	2.13×10^{-1}	2.43×10^{-2}	5.01×10^{0}	2.52×10^{-3}	9.62×10^{-2}	2.13×10^{-1}
Natural land transformation	m^2	1.20×10^{-2}	4.80×10^{-3}	8.31×10^{-4}	5.95×10^{-3}	1.44×10^{-3}	1.20×10^{-2}	4.80×10^{-3}
Water depletion	m^3	5.86×10^{-1}	3.47×10^{0}	2.83×10^{2}	5.27×10^{1}	4.48×10^{-3}	5.86×10^{-1}	3.47×10^{0}
Metal depletion	kg Fe eq	0.00×10^{0}	0.00×10^{0}	0.00×10^{0}	0.00×10^{0}	0.00×10^{0}	0.00×10^{0}	0.00×10^{0}
Fossil depletion	kg oil eq	6.29×10^{-3}	6.01×10^{-2}	1.29×10^{-2}	4.11×10^{-2}	2.43×10^{-4}	6.29×10^{-3}	6.01×10^{-2}

[1] Abbreviations are: CFC-11: trichlorofluoromethane; 1,4-DB: 1,4-dichlorobenzene; NMVOC: non-methane volatile organic compounds.

Table 4S.4 Life cycle impact assessment (LCIA) results by life cycle stage for monoammonium phosphate (MAP) (illustrated in Figure 4.3)

Impact category	Unit[1]	MAP at storage	Heat	Electricity	Chemical plant	Transportation	Phosphoric acid
Climate change	kg CO_2 eq	0.00×10^{0}	1.62×10^{-1}	1.42×10^{-1}	3.38×10^{-1}	1.19×10^{0}	8.48×10^{0}
Ozone depletion	kg CFC-11 eq	0.00×10^{0}	2.33×10^{-8}	6.95×10^{-9}	2.29×10^{-8}	1.57×10^{-7}	7.37×10^{-7}
Terrestrial acidification	kg SO_2 eq	0.00×10^{0}	1.16×10^{-4}	5.90×10^{-4}	2.03×10^{-3}	1.08×10^{-2}	2.29×10^{-1}
Freshwater eutrophication	kg P eq	1.13×10^{-4}	2.42×10^{-6}	1.40×10^{-4}	5.36×10^{-4}	2.67×10^{-4}	2.86×10^{-3}
Marine eutrophication	kg N eq	0.00×10^{0}	4.42×10^{-6}	3.99×10^{-5}	1.02×10^{-4}	4.71×10^{-4}	1.61×10^{-3}
Human toxicity	kg 1,4-DB eq	7.04×10^{-1}	1.89×10^{-3}	8.08×10^{-2}	7.14×10^{-1}	2.09×10^{-1}	2.37×10^{0}
Photochemical oxidant formation	kg NMVOC	0.00×10^{0}	1.57×10^{-4}	2.96×10^{-4}	1.18×10^{-3}	1.22×10^{-2}	4.04×10^{-2}
Particulate matter formation	kg PM10 eq	4.95×10^{-4}	3.79×10^{-5}	1.86×10^{-4}	9.45×10^{-4}	4.02×10^{-3}	6.18×10^{-2}
Terrestrial ecotoxicity	kg 1,4-DB eq	1.73×10^{-5}	4.18×10^{-7}	3.55×10^{-6}	6.07×10^{-5}	8.11×10^{-5}	2.49×10^{-3}
Freshwater ecotoxicity	kg 1,4-DB eq	2.56×10^{-3}	1.26×10^{-5}	6.62×10^{-4}	5.17×10^{-3}	1.72×10^{-3}	1.79×10^{-2}
Marine ecotoxicity	kg 1,4-DB eq	2.07×10^{-3}	1.41×10^{-5}	6.81×10^{-4}	6.77×10^{-3}	2.83×10^{-3}	2.67×10^{-2}
Ionizing radiation	kBq ^{235}U eq	0.00×10^{0}	1.63×10^{-3}	1.12×10^{-1}	1.34×10^{-1}	2.24×10^{-1}	1.97×10^{0}
Agricultural land occupation	m^2a	0.00×10^{0}	5.65×10^{-5}	1.83×10^{-3}	7.88×10^{-2}	7.77×10^{-3}	1.86×10^{-1}
Urban land occupation	m^2a	0.00×10^{0}	6.26×10^{-5}	4.40×10^{-4}	1.23×10^{-2}	1.29×10^{-2}	1.40×10^{-1}
Natural land transformation	m^2	0.00×10^{0}	3.58×10^{-5}	1.51×10^{-5}	1.12×10^{-4}	4.37×10^{-4}	1.79×10^{-3}
Water depletion	m^3	0.00×10^{0}	1.11×10^{-4}	5.54×10^{-3}	1.09×10^{-2}	1.43×10^{-2}	1.40×10^{0}
Metal depletion	kg Fe eq	0.00×10^{0}	0.00×10^{0}	0.00×10^{0}	0.00×10^{0}	0.00×10^{0}	0.00×10^{0}
Fossil depletion	kg oil eq	0.00×10^{0}	6.03×10^{-6}	2.35×10^{-4}	5.26×10^{-4}	6.36×10^{-4}	5.55×10^{-3}

[1] Abbreviations are: CFC-11: trichlorofluoromethane; 1,4-DB: 1,4-dichlorobenzene; NMVOC: non-methane volatile organic compounds.

Table 4S.5 Processes that had high percentages of total emissions in climate change category

	Processes in life cycles[1]	Emission (kg CO_2 eq)	% of total emission
Mg-char ($Mg(OH)_2$)	Corn cobs pyrolysis	4.3×10^{1}	70
	Magnesium oxide, at plant/RER U	1.5×10^{1}	25
	Lignite, burned in power plant/DE U	2.6×10^{-1}	0.42
Mg-char (bittern)	Corn cobs pyrolysis	4.7×10^{1}	98
	Corn, at farm/US U	2.1×10^{-1}	0.44
	Natural gas, burned in industrial furnace >100kW/RER U	1.5×10^{-1}	0.32
CSH	Rice husk pyrolysis	1.5×10^{3}	79
	Quicklime, in pieces, loose, at plant/CH U	2.4×10^{2}	13
	Rice, at farm/US U	5.2×10^{1}	2.8

[1] Abbreviations in dataset names: RER, Europe; DE, Germany; US, United States; CH, Switzerland; U, unit process.

4.8.3.2 LCIA results for pH 8.5, 7.0, and pH 5.5 compared to monoammonium phosphate (MAP)

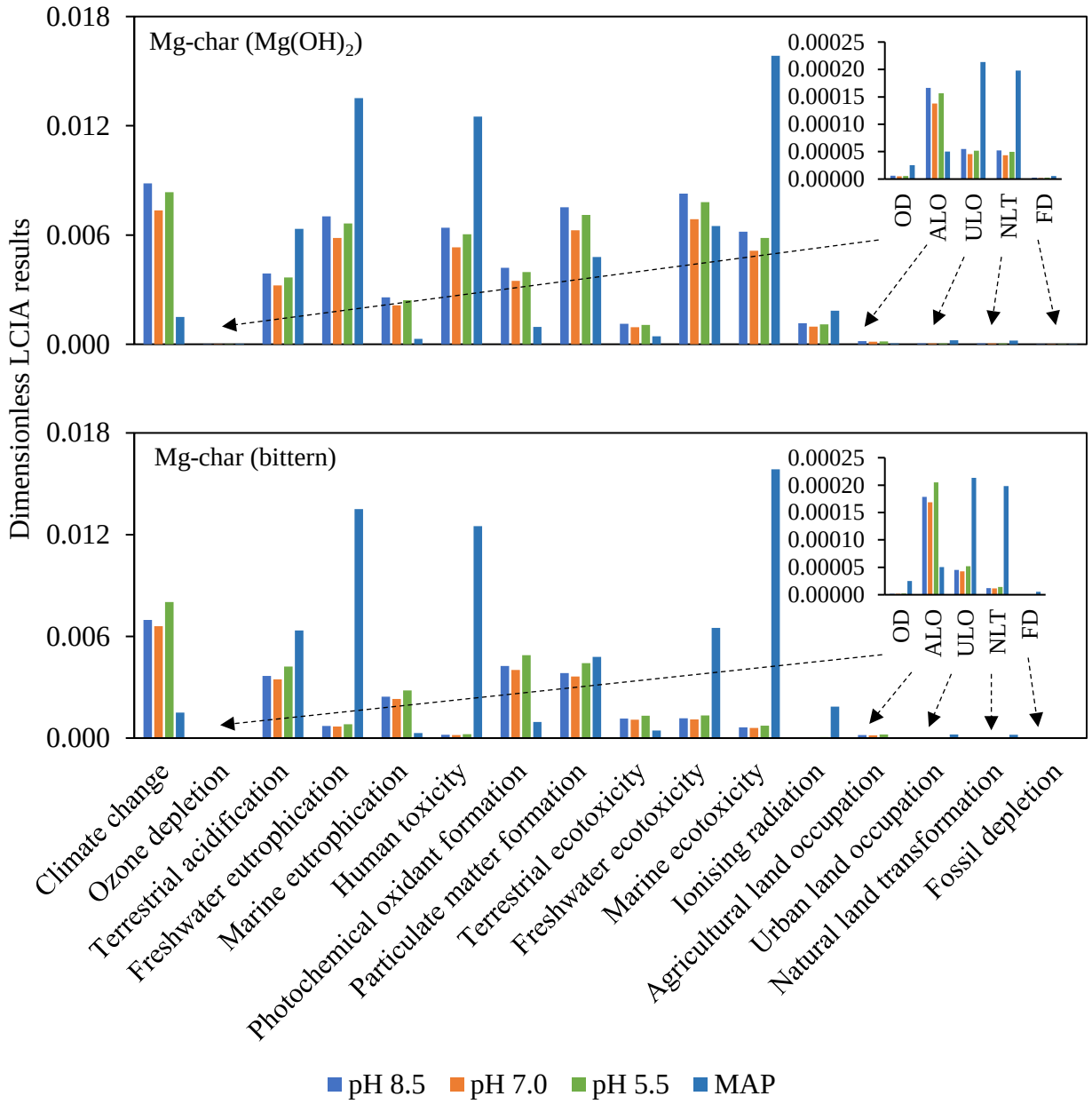

Figure 4S.5 Impacts normalized by the annual impact of one world citizen of Mg-char ($Mg(OH)_2$) and Mg-char (bittern) at pH 8.5 and 7.0, and 5.5 compared to monoammonium phosphate (MAP). Abbreviations in the insets: OD, ozone depletion; ALO, agricultural land occupation; ULO, urban land occupation; NLT, natural land transformation; FD, fossil depletion. Impact assessment values are given in Tables 4S.6 and 4S.7.

Table 4S.6 Life cycle impact assessment (LCIA) results for the two Mg-chars and monoammonium phosphate (MAP) at pH 7.0 (illustrated in Figure 4S.5)

Impact category	Unit[1]	Mg-char ($Mg(OH)_2$)	Mg-char (bittern)	MAP
Climate change	kg CO_2 eq	5.07×10^{1}	4.55×10^{1}	1.03×10^{1}
Ozone depletion	kg CFC-11 eq	1.85×10^{-7}	7.01×10^{-8}	9.47×10^{-7}
Terrestrial acidification	kg SO_2 eq	1.23×10^{-1}	1.32×10^{-1}	2.42×10^{-1}
Freshwater eutrophication	kg P eq	1.69×10^{-3}	1.96×10^{-4}	3.92×10^{-3}
Marine eutrophication	kg N eq	1.57×10^{-2}	1.70×10^{-2}	2.23×10^{-3}
Human toxicity	kg 1,4-DB eq	1.73×10^{0}	6.07×10^{-2}	4.07×10^{0}
Photochemical oxidant formation	kg NMVOC	1.98×10^{-1}	2.29×10^{-1}	5.42×10^{-2}
Particulate matter formation	kg PM10 eq	8.80×10^{-2}	5.11×10^{-2}	6.74×10^{-2}
Terrestrial ecotoxicity	kg 1,4-DB eq	5.56×10^{-3}	6.49×10^{-3}	2.65×10^{-3}
Freshwater ecotoxicity	kg 1,4-DB eq	2.96×10^{-2}	4.75×10^{-3}	2.80×10^{-2}
Marine ecotoxicity	kg 1,4-DB eq	1.27×10^{-2}	1.47×10^{-3}	3.90×10^{-2}
Ionizing radiation	kBq ^{235}U eq	1.27×10^{0}	6.38×10^{-2}	2.44×10^{0}
Agricultural land occupation	m^2a	7.49×10^{-1}	9.17×10^{-1}	2.74×10^{-1}
Urban land occupation	m^2a	3.53×10^{-2}	3.32×10^{-2}	1.66×10^{-1}
Natural land transformation	m^2	5.25×10^{-4}	1.39×10^{-4}	2.38×10^{-3}
Water depletion	m^3	2.38×10^{-1}	1.01×10^{-2}	1.43×10^{0}
Metal depletion	kg Fe eq	0.00×10^{0}	0.00×10^{0}	0.00×10^{0}
Fossil depletion	kg oil eq	2.70×10^{-3}	1.31×10^{-4}	6.95×10^{-3}

[1] Abbreviations are: CFC-11: trichlorofluoromethane; 1,4-DB: 1,4-dichlorobenzene; NMVOC: non-methane volatile organic compounds.

Table 4S.7 Life cycle impact assessment (LCIA) results for the two Mg-chars and monoammonium phosphate (MAP) at pH 5.5 (illustrated in Figure 4S.5)

Impact category	Unit[1]	Mg-char ($Mg(OH)_2$)	Mg-char (bittern)	MAP
Climate change	kg CO_2 eq	5.76×10^{1}	5.54×10^{1}	1.03×10^{1}
Ozone depletion	kg CFC-11 eq	2.10×10^{-7}	8.52×10^{-8}	9.47×10^{-7}
Terrestrial acidification	kg SO_2 eq	1.40×10^{-1}	1.61×10^{-1}	2.42×10^{-1}
Freshwater eutrophication	kg P eq	1.92×10^{-3}	2.38×10^{-4}	3.92×10^{-3}
Marine eutrophication	kg N eq	1.78×10^{-2}	2.07×10^{-2}	2.23×10^{-3}
Human toxicity	kg 1,4-DB eq	1.97×10^{0}	7.38×10^{-2}	4.07×10^{0}
Photochemical oxidant formation	kg NMVOC	2.25×10^{-1}	2.78×10^{-1}	5.42×10^{-2}
Particulate matter formation	kg PM10 eq	9.99×10^{-2}	6.21×10^{-2}	6.74×10^{-2}
Terrestrial ecotoxicity	kg 1,4-DB eq	6.32×10^{-3}	7.88×10^{-3}	2.65×10^{-3}
Freshwater ecotoxicity	kg 1,4-DB eq	3.36×10^{-2}	5.77×10^{-3}	2.80×10^{-2}
Marine ecotoxicity	kg 1,4-DB eq	1.44×10^{-2}	1.78×10^{-3}	3.90×10^{-2}
Ionizing radiation	kBq ^{235}U eq	1.44×10^{0}	7.75×10^{-2}	2.44×10^{0}
Agricultural land occupation	m^2a	8.50×10^{-1}	1.11×10^{0}	2.74×10^{-1}
Urban land occupation	m^2a	4.01×10^{-2}	4.03×10^{-2}	1.66×10^{-1}
Natural land transformation	m^2	5.96×10^{-4}	1.69×10^{-4}	2.38×10^{-3}
Water depletion	m^3	2.70×10^{-1}	1.23×10^{-2}	1.43×10^{0}
Metal depletion	kg Fe eq	0.00×10^{0}	0.00×10^{0}	0.00×10^{0}
Fossil depletion	kg oil eq	3.07×10^{-3}	1.59×10^{-4}	6.95×10^{-3}

[1] Abbreviations are: CFC-11: trichlorofluoromethane; 1,4-DB: 1,4-dichlorobenzene; NMVOC: non-methane volatile organic compounds.

4.8.3.3 LCIA results for the transportation scenario

Table 4S.8 Life cycle impact assessment (LCIA) results for two Mg-chars considering transportation (illustrated in Figure 4.4)

Impact category	Unit[1]	Mg-char ($Mg(OH)_2$)[2]			Mg-char (bittern)[2]		
		5 km	50 km	100 km	5 km	50 km	100 km
Climate change	kg CO_2 eq	6.11×10^{1}	6.23×10^{1}	6.35×10^{1}	4.82×10^{1}	4.91×10^{1}	5.00×10^{1}
Ozone depletion	kg CFC-11 eq	2.42×10^{-7}	4.17×10^{-7}	6.11×10^{-7}	8.92×10^{-8}	2.25×10^{-7}	3.69×10^{-7}
Terrestrial acidification	kg SO_2 eq	1.49×10^{-1}	1.52×10^{-1}	1.56×10^{-1}	1.40×10^{-1}	1.43×10^{-1}	1.45×10^{-1}
Freshwater eutrophication	kg P eq	2.05×10^{-3}	2.18×10^{-3}	2.32×10^{-3}	2.18×10^{-4}	3.18×10^{-4}	4.23×10^{-4}
Marine eutrophication	kg N eq	1.89×10^{-2}	1.91×10^{-2}	1.93×10^{-2}	1.80×10^{-2}	1.81×10^{-2}	1.83×10^{-2}
Human toxicity	kg 1,4-DB eq	2.10×10^{0}	2.24×10^{0}	2.40×10^{0}	7.66×10^{-2}	1.88×10^{-1}	3.06×10^{-1}
Photochemical oxidant formation	kg NMVOC	2.39×10^{-1}	2.44×10^{-1}	2.49×10^{-1}	2.42×10^{-1}	2.46×10^{-1}	2.50×10^{-1}
Particulate matter formation	kg PM10 eq	1.06×10^{-1}	1.08×10^{-1}	1.09×10^{-1}	5.41×10^{-2}	5.53×10^{-2}	5.66×10^{-2}
Terrestrial ecotoxicity	kg 1,4-DB eq	6.73×10^{-3}	6.93×10^{-3}	7.15×10^{-3}	6.88×10^{-3}	7.03×10^{-3}	7.19×10^{-3}
Freshwater ecotoxicity	kg 1,4-DB eq	3.58×10^{-2}	3.69×10^{-2}	3.82×10^{-2}	5.12×10^{-3}	6.03×10^{-3}	6.99×10^{-3}
Marine ecotoxicity	kg 1,4-DB eq	1.55×10^{-2}	1.80×10^{-2}	2.07×10^{-2}	1.77×10^{-3}	3.68×10^{-3}	5.71×10^{-3}
Ionizing radiation	kBq ^{235}U eq	1.55×10^{0}	1.72×10^{0}	1.91×10^{0}	8.25×10^{-2}	2.18×10^{-1}	3.61×10^{-1}
Agricultural land occupation	m^2a	9.04×10^{-1}	9.10×10^{-1}	9.16×10^{-1}	9.71×10^{-1}	9.76×10^{-1}	9.80×10^{-1}
Urban land occupation	m^2a	4.55×10^{-2}	7.13×10^{-2}	1.00×10^{-1}	3.73×10^{-2}	5.74×10^{-2}	7.87×10^{-2}
Natural land transformation	m^2	6.77×10^{-4}	1.09×10^{-3}	1.55×10^{-3}	1.83×10^{-4}	5.04×10^{-4}	8.43×10^{-4}
Water depletion	m^3	2.87×10^{-1}	2.96×10^{-1}	3.07×10^{-1}	1.15×10^{-2}	1.89×10^{-2}	2.67×10^{-2}
Metal depletion	kg Fe eq	0.00×10^{0}	0.00×10^{0}	0.00×10^{0}	0.00×10^{0}	0.00×10^{0}	0.00×10^{0}
Fossil depletion	kg oil eq	3.29×10^{-3}	3.68×10^{-3}	4.11×10^{-3}	1.72×10^{-4}	4.73×10^{-4}	7.92×10^{-4}

[1] Abbreviations are: CFC-11: trichlorofluoromethane; 1,4-DB: 1,4-dichlorobenzene; NMVOC: non-methane volatile organic compounds.

[2] LCIA results for no transportation are in Table 4S.1

Table 4S.9 Life cycle impact assessment (LCIA) results for calcium silicate hydrate (CSH) considering transportation

Impact category	Unit[1]	No transportation	5 km	50 km	100 km
Climate change	kg CO_2 eq	1.83×10^{3}	1.84×10^{3}	1.88×10^{3}	1.92×10^{3}
Ozone depletion	kg CFC-11 eq	2.49×10^{-5}	2.56×10^{-5}	3.17×10^{-5}	3.85×10^{-5}
Terrestrial acidification	kg SO_2 eq	1.76×10^{1}	1.76×10^{1}	1.77×10^{1}	1.78×10^{1}
Freshwater eutrophication	kg P eq	6.95×10^{-2}	7.00×10^{-2}	7.45×10^{-2}	7.95×10^{-2}
Marine eutrophication	kg N eq	1.29×10^{0}	1.29×10^{0}	1.30×10^{0}	1.30×10^{0}
Human toxicity	kg 1,4-DB eq	4.18×10^{1}	4.23×10^{1}	4.74×10^{1}	5.30×10^{1}
Photochemical oxidant formation	kg NMVOC	3.06×10^{1}	3.07×10^{1}	3.08×10^{1}	3.10×10^{1}
Particulate matter formation	kg PM10 eq	6.86×10^{0}	6.87×10^{0}	6.92×10^{0}	6.98×10^{0}
Terrestrial ecotoxicity	kg 1,4-DB eq	3.81×10^{-2}	3.88×10^{-2}	4.57×10^{-2}	5.34×10^{-2}
Freshwater ecotoxicity	kg 1,4-DB eq	3.78×10^{-1}	3.83×10^{-1}	4.23×10^{-1}	4.69×10^{-1}
Marine ecotoxicity	kg 1,4-DB eq	3.81×10^{-1}	3.91×10^{-1}	4.78×10^{-1}	5.74×10^{-1}
Ionizing radiation	kBq ^{235}U eq	5.58×10^{1}	5.64×10^{1}	6.25×10^{1}	6.93×10^{1}
Agricultural land occupation	m^2a	7.38×10^{1}	7.38×10^{1}	7.40×10^{1}	7.42×10^{1}
Urban land occupation	m^2a	5.34×10^{0}	5.44×10^{0}	6.35×10^{0}	7.36×10^{0}
Natural land transformation	m^2	2.50×10^{-2}	2.66×10^{-2}	4.11×10^{-2}	5.72×10^{-2}
Water depletion	m^3	3.40×10^{2}	3.40×10^{2}	3.41×10^{2}	3.41×10^{2}
Metal depletion	kg Fe eq	0.00×10^{0}	0.00×10^{0}	0.00×10^{0}	0.00×10^{0}
Fossil depletion	kg oil eq	1.21×10^{-1}	1.22×10^{-1}	1.36×10^{-1}	1.51×10^{-1}

[1] Abbreviations are: CFC-11: trichlorofluoromethane; 1,4-DB: 1,4-dichlorobenzene; NMVOC: non-methane volatile organic compounds.

4.8.3.4 Cost analysis results

Table 4S.10 Cost summary of producing sorbents and fertilizer that are capable of releasing 2.81 kg phosphorus after five rain/irrigation events using U.S. natural gas and electricity prices

Material	Raw material	Quantity[a]				Price ($/unit of raw material)	Cost ($)			
		pH 8.5	pH 7.0	pH 5.5	pH 8.5 + 100 km		pH 8.5	pH 7.0	pH 5.5	pH 8.5 + 100 km
Mg-char ($Mg(OH)_2$)	Corn cobs (ton)	3.7×10^{-2}	3.1×10^{-2}	3.5×10^{-2}	3.7×10^{-2}	5.60[b]	2.1×10^{-1}	1.7×10^{-1}	2.0×10^{-1}	2.1×10^{-1}
	$Mg(OH)_2$ (ton)	1.7×10^{-2}	1.4×10^{-2}	1.6×10^{-2}	1.7×10^{-2}	70.00[b]	1.2×10^{0}	9.7×10^{-1}	1.1×10^{0}	1.2×10^{0}
	Electricity (kWh)	8.1×10^{-3}	6.8×10^{-3}	7.7×10^{-3}	8.1×10^{-3}	0.16[c]	1.3×10^{-3}	1.1×10^{-3}	1.2×10^{-3}	1.3×10^{-3}
	Natural gas (m^3)	6.2×10^{-2}	5.2×10^{-2}	5.9×10^{-2}	6.2×10^{-2}	0.19[d]	1.7×10^{-2}	1.5×10^{-2}	1.6×10^{-2}	1.7×10^{-2}
	Transportation (tkm)	0.0×10^{0}	0.0×10^{0}	0×10^{0}	5.4×10^{0}	0.23[e]	0.0×10^{0}	0.0×10^{0}	0×10^{0}	1.2×10^{0}
						Total:	**$1.39**	**$1.16**	**$1.32**	**$2.64**
Mg-char (bittern)	Corn cobs (ton)	4.1×10^{-2}	3.9×10^{-2}	4.8×10^{-2}	4.1×10^{-2}	5.60[b]	2.3×10^{-1}	2.2×10^{-1}	2.7×10^{-1}	2.3×10^{-1}
	Electricity (kWh)	1.6×10^{-2}	1.5×10^{-2}	1.8×10^{-2}	1.6×10^{-2}	0.16[c]	2.6×10^{-3}	2.4×10^{-3}	3.0×10^{-3}	2.6×10^{-3}
	Natural gas (m^3)	6.9×10^{-2}	6.5×10^{-2}	7.9×10^{-2}	6.9×10^{-2}	0.19[d]	1.9×10^{-2}	1.8×10^{-2}	2.2×10^{-2}	1.9×10^{-2}
	Transportation (tkm)	0.0×10^{0}	0.0×10^{0}	0×10^{0}	4.1×10^{0}	0.23[e]	0.0×10^{0}	0.0×10^{0}	0×10^{0}	9.4×10^{-1}
						Total:	**$0.25**	**$0.24**	**$0.29**	**$1.20**
CSH	Rice husk (ton)	1.5×10^{0}			1.5×10^{0}	13.30[f]	2.0×10^{1}			2.0×10^{1}
	$Ca(OH)_2$ (ton)	3.4×10^{-1}			3.4×10^{-1}	90.00[b]	3.0×10^{1}			3.0×10^{1}
	NaOH (ton)	3.8×10^{-2}			3.8×10^{-2}	185.00[b]	7.0×10^{0}			7.0×10^{0}
	Electricity (kWh)	1.5×10^{1}			1.5×10^{1}	0.16[c]	2.4×10^{-1}			2.4×10^{-1}
	Natural gas (m^3)	2.5×10^{0}			2.5×10^{0}	0.19[d]	7.1×10^{-1}			7.1×10^{-1}
	Transportation (tkm)	0.0×10^{0}			1.9×10^{2}	0.23[e]	0.0×10^{0}			4.4×10^{1}
						Total:	**$60.48**			**$104.18**
Commercial fertilizer	MAP (ton)		6.4×10^{-3}			918.5[g]		5.9×10^{0}		
						Total:		**$5.92**		

[a] See section 4.8.2.4 for calculation details.

[b] Prices were from online vendors. Corn cobs (Alibaba 2022), $Mg(OH)_2$ (Alibaba 2023b), $Ca(OH)_2$ (Alibaba 2023a), NaOH (Alibaba 2023c).
[c] Electricity price was 2022 annual average from (U.S. Bureau of Labor Statistics; 2023).
[d] Natural gas price was 2022 annual average from (U.S. Energy Information Administration 2023).
[e] Price was from taking average price from 10 recent orders of light duty transportation (i.e., 5 ton) in Europe, i.e., $\frac{average\ price\ of\ €}{km\ per\ 5\ ton} \times \frac{1.06\ \$}{1\ €} = average\ price\ in\ \frac{\$}{tkm}$ (Della 2023). European transportation costs were used since the dataset selected for transportation was for Europe.
[f] Price was from (Thengane et al. 2020).
[g] Price was from (U.S. Department of Agriculture 2022).

Table 4S.11 Cost summary of producing sorbents and fertilizer that are capable of releasing 2.81 kg phosphorus after five rain/irrigation events using European natural gas and electricity prices

Material	Raw material	Quantity[a]				Price ($/unit of raw material)	Cost ($)			
		pH 8.5	pH 7.0	pH 5.5	pH 8.5 + 100 km		pH 8.5	pH 7.0	pH 5.5	pH 8.5 + 100 km
Mg-char ($Mg(OH)_2$)	Corn cobs (ton)	3.7×10^{-2}	3.1×10^{-2}	3.5×10^{-2}	3.7×10^{-2}	5.60[b]	2.1×10^{-1}	1.7×10^{-1}	2.0×10^{-1}	2.1×10^{-1}
	MgO (ton)	1.7×10^{-2}	1.4×10^{-2}	1.6×10^{-2}	1.7×10^{-2}	70.00[b]	1.2×10^{0}	9.7×10^{-1}	1.1×10^{0}	1.2×10^{0}
	Electricity (kWh)	8.1×10^{-3}	6.8×10^{-3}	7.7×10^{-3}	8.1×10^{-3}	0.20[c]	1.6×10^{-3}	1.4×10^{-3}	1.5×10^{-3}	1.6×10^{-3}
	Natural gas (m^3)	6.2×10^{-2}	5.2×10^{-2}	5.9×10^{-2}	6.2×10^{-2}	0.71[d]	4.4×10^{-2}	3.7×10^{-2}	4.2×10^{-2}	4.4×10^{-2}
	Transportation (tkm)	0.0×10^{0}	0.0×10^{0}	0×10^{0}	5.4×10^{0}	0.23[e]	0.0×10^{0}	0.0×10^{0}	0×10^{0}	1.2×10^{0}
						Total:	**$1.42**	**$1.18**	**$1.34**	**$2.66**
Mg-char (bittern)	Corn cobs (ton)	4.1×10^{-2}	3.9×10^{-2}	4.8×10^{-2}	4.1×10^{-2}	5.60[b]	2.3×10^{-1}	2.2×10^{-1}	2.7×10^{-1}	2.3×10^{-1}
	Electricity (kWh)	1.6×10^{-2}	1.5×10^{-2}	1.8×10^{-2}	1.6×10^{-2}	0.20[c]	3.2×10^{-3}	3.0×10^{-3}	3.7×10^{-3}	3.2×10^{-3}
	Natural gas (m^3)	6.9×10^{-2}	6.5×10^{-2}	7.9×10^{-2}	6.9×10^{-2}	0.71[d]	4.9×10^{-2}	4.6×10^{-2}	5.6×10^{-2}	4.9×10^{-2}
	Transportation (tkm)	0.0×10^{0}	0.0×10^{0}	0×10^{0}	4.1×10^{0}	0.23[e]	0.0×10^{0}	0.0×10^{0}	0×10^{0}	9.4×10^{-1}
						Total:	**$0.28**	**$0.27**	**$0.33**	**$1.23**
CSH	Rice husk (ton)	1.5×10^{0}			1.5×10^{0}	13.30[f]	2.0×10^{1}			2.0×10^{1}
	$Ca(OH)_2$ (ton)	3.4×10^{-1}			3.4×10^{-1}	90.00[b]	3.0×10^{1}			3.0×10^{1}
	NaOH (ton)	3.8×10^{-2}			3.8×10^{-2}	185.00[b]	7.0×10^{0}			7.0×10^{0}
	Electricity (kWh)	1.5×10^{1}			1.5×10^{1}	0.20[c]	2.9×10^{-1}			2.9×10^{-1}
	Natural gas (m^3)	2.5×10^{0}			2.5×10^{0}	0.71[d]	1.8×10^{0}			1.8×10^{0}
	Transportation (tkm)	0.0×10^{0}			1.9×10^{2}	0.23[e]	0.0×10^{0}			4.4×10^{1}
						Total:	**$62.16**			**$105.86**
Commercial fertilizer	MAP (ton)			6.4×10^{-3}		918.5[g]			5.9×10^{0}	
						Total:			**$5.92**	

[a] See section 4.8.2.4 for calculation details.
[b] Prices were from online vendors. Corn cobs (Alibaba 2022), $Mg(OH)_2$ (Alibaba 2023b), $Ca(OH)_2$ (Alibaba 2023a), NaOH (Alibaba 2023c).

[c] Electricity price was Europe area average for non-household consumer in the first half of 2022 from European Union (Eurostat 2022a). Price conversion: $\frac{0.1912\ €}{kWh} \times \frac{1.06\ \$}{1\ €} = \frac{0.20\ \$}{kWh}$.

[d] Natural gas price was Europe area average for non-household consumer in the first half of 2022 from European Union (Eurostat 2022b). Price conversion: $\frac{0.0636\ €}{kWh} \times \frac{10.55\ kWh}{1\ m^3 natural\ gas} \times \frac{1.06\ \$}{1\ €} = \frac{0.71\ \$}{1\ m^3 natural\ gas}$.

[e] Price was from taking average price from 10 recent orders of light duty transportation (i.e., 5 ton) in Europe, i.e., $\frac{average\ price\ of\ €}{km\ per\ 5\ ton} \times \frac{1.06\ \$}{1\ €} = average\ price\ in\ \frac{\$}{tkm}$ (Della 2023). European transportation costs were used since the dataset selected for transportation was for Europe.

[f] Price was from (Thengane et al. 2020).

[g] Price was from (U.S.Department of Agriculture 2022).

4.9 References in Supplementary Materials

Akridge, D.G. (2008) Methods for calculating brine evaporation rates during salt production. Journal of Archaeological Science 35(6), 1453-1462.

Alibaba (2022) Crushed Corn Cob. Accessed on November 15. 2022. https://www.alibaba.com/product-detail/COB-Crushed-CORN-COB-for-Mushroom_50041675651.html?spm=a2700.galleryofferlist.normal_offer.d_title.90012563IIiEWN.

Alibaba (2023a) Calcium Hydroxide. Accessed on February 5. 2023. https://www.alibaba.com/product-detail/QUality-Tope-Quality-food-grade-industrial_60649197626.html?spm=a2700.galleryofferlist.normal_offer.d_title.1faa57b2xUrCY7&s=p.

Alibaba (2023b) Magnesium Hydroxide. Accessed on March 9. 2023. https://www.alibaba.com/product-detail/Magnesium-Hydroxide-Price_60840267969.html?spm=a2700.galleryofferlist.normal_offer.d_title.7a2440ccfhrTAG&s=p.

Alibaba (2023c) Sodium Hydroxide. Accessed on February 5. 2023. https://www.alibaba.com/product-detail/Soda-Ash-Light-Double-Ring-Baking_11000006839416.html?spm=a2700.galleryofferlist.normal_offer.d_title.1a10125bbhgKTh.

Bagastyo, A.Y., Sinatria, A.Z., Anggrainy, A.D., Affandi, K.A., Kartika, S.W.T. and Nurhayati, E. (2021) Resource recovery and utilization of bittern wastewater from salt production: a review of recovery technologies and their potential applications. Environmental Technology Reviews 10(1), 295-322.

de Souza, D.F., da Guarda, E.L.A., Sauer, I.L. and Tatizawa, H. (2021) Energy Efficiency Indicators for Water Pumping Systems in Multifamily Buildings. Energies 14(21), 7152.

Della (2023) Prices for light duty transportation Europe — Europe. Accessed on February 22. 2023. https://della.eu/price/local/.

Ding, Y., Sabatini, D.A. and Butler, E.C. (2023) Effects of pH and Soil Minerals on Phosphorus Release from Agricultural Waste-Based Sorbents: A Continuous-Flow Column Study. Journal of Environmental Engineering 149(4), 04023010.

EIA (2022) Heat Content of Natural Gas Consumed. Accessed on December 19. 2022. https://www.eia.gov/dnav/ng/ng_cons_heat_a_EPG0_VGTH_btucf_a.htm.

Eurostat (2022a) Electricity price statistics. Accessed on March 6. 2023. https://ec.europa.eu/eurostat/statistics-explained/index.php?title=Electricity_price_statistics#Electricity_prices_for_non-household_consumers.

Eurostat (2022b) Natural gas price statistics. Accessed on March 6. 2023. https://ec.europa.eu/eurostat/statistics-explained/index.php?title=Natural_gas_price_statistics#Natural_gas_prices_for_non-household_consumers.

Hossain, N., Nizamuddin, S., Griffin, G., Selvakannan, P., Mubarak, N.M. and Mahlia, T.M.I. (2020) Synthesis and characterization of rice husk biochar via hydrothermal carbonization for wastewater treatment and biofuel production. Scientific reports 10(1), 18851.

IFA (2022) Fertilizer use by crop and country for the 2017-2018 period, Paris, France. Accessed on January 20. 2023. https://www.ifastat.org/consumption/fertilizer-use-by-crop. https://www.ifastat.org/consumption/fertilizer-use-by-crop.

Indexmundi (2022a) Maize (corn) Monthly Price. Accessed on November 11. 2022. https://www.indexmundi.com/Commodities/?commodity=corn&months=60.

Indexmundi (2022b) Rice Monthly Price. Accessed on November 11. 2022. https://www.indexmundi.com/Commodities/?commodity=rice&months=60.

Ippolito, J.A., Spokas, K.A., Novak, J.M., Lentz, R.D. and Cantrell, K.B. (2015) Biochar for environmental management: Science, technology and implementation, pp. 139-163.

ISO (2006) ISO 14044:2006 Environmental management — Life cycle assessment — Requirements and guidelines, Geneva, Switzerland.

Millero, F.J. (2002) Chemistry of Marine Water and Sediments. Gianguzza, A., Pelizzetti, E. and Sammartano, S. (eds), pp. 3-6, Springer Berlin Heidelberg, Berlin, Heidelberg.

Moraes, C.A., Fernandes, I.J., Calheiro, D., Kieling, A.G., Brehm, F.A., Rigon, M.R., Berwanger Filho, J.A., Schneider, I.A. and Osorio, E. (2014) Review of the rice production cycle: By-products and the main applications focusing on rice husk combustion and ash recycling. Waste Management & Research 32(11), 1034-1048.

Saft, R.J. (2007) Life cycle assessment of a pyrolysis/gasification plant for hazardous paint waste. The International Journal of Life Cycle Assessment 12(4), 230.

Sharkh, B.A., Al-Amoudi, A.A., Farooque, M., Fellows, C.M., Ihm, S., Lee, S., Li, S. and Voutchkov, N. (2022) Seawater desalination concentrate—a new frontier for sustainable mining of valuable minerals. npj Clean Water 5(1), 9.

Singh, S., Patil, T., Tekade, S.P., Gawande, M.B. and Sawarkar, A.N. (2021) Studies on individual pyrolysis and co-pyrolysis of corn cob and polyethylene: Thermal degradation behavior, possible synergism, kinetics, and thermodynamic analysis. Science of the Total Environment 783, 147004.

Thengane, S.K., Burek, J., Kung, K.S., Ghoniem, A.F. and Sanchez, D.L. (2020) Life cycle assessment of rice husk torrefaction and prospects for decentralized facilities at rice mills. Journal of Cleaner Production 275, 123177.

U.S. Bureau of Labor Statistics; (2023) Electricity price per kWh in U.S. city average. Accessed on February 5. 2023. https://data.bls.gov/timeseries/APU000072610?amp%253bdata_tool=XGtable&output_view=data&include_graphs=true.

U.S. Department of Agriculture (2022) Iowa Production Cost Report. Accessed on February 22. 2023. https://www.ams.usda.gov/mnreports/nw_gr210.txt.

U.S. Energy Information Administration (2023) United States Natural Gas Industrial Price. Accessed on February 5. 2023. https://www.eia.gov/dnav/ng/hist/n3035us3m.htm).

USGS (2023) Why is the ocean salty?. Accessed on March 6. 2023. https://www.usgs.gov/faqs/why-ocean-salty.

Wojcieszak, D., Przybył, J., Czajkowski, Ł., Majka, J. and Pawłowski, A. (2022) Effects of Harvest Maturity on the Chemical and Energetic Properties of Corn Stover Biomass Combustion. Materials 15(8), 2831.

World Bank (2022) World Population Prospects: 2022 Revision. Accessed on Decemeber 22. 2022. https://data.worldbank.org/indicator/SP.POP.TOTL?end=2021&start=1960.

Zhang, C., Chen, W.-H. and Ho, S.-H. (2022) Elemental loss, enrichment, transformation and life cycle assessment of torrefied corncob. Energy 242, 123019.

Chapter 5 Conclusions and Recommendations

5.1 Conclusions

Aiming at finding potential strategies of phosphorus recovery and reuse for closing the phosphorus cycle, this research developed a series of sorbents that can fulfill the objective using low-environmental-impact and low-cost materials. Although sorbents sharing the similar phosphorus recovery and release mechanisms have been widely studied, this research adds valuable insights on how the sorbents can be optimized to be more environmentally and economically viable compared to current nutrient management and fertilizer industry. This research evaluated multiple agricultural wastes serving as the matrix of the sorbents and verified that magnesium amendment would boost the phosphorus recovery performance (Chapter 2). Further, different naturally occurring materials were tested as alternative chemical sources as compared to commercial chemicals. Further, the proposed sorbents could effectively recover phosphorus from animal wastewater and subsequently release recovered phosphorus in modeled soils (Chapter 3). Finally, life cycle impact and cost assessments were conducted showing magnesium amended biochars can be strong candidates of substituting commercial fertilizer monoammonium phosphate with less environmental impact and overall cost (Chapter 4).

Biochar synthesized from corn cobs was found to be a porous matrix, and after the Mg amendment, the resulting MgO was distributed on the Mg-char surface for phosphorus uptake. Mg amendment considerably improved the phosphorus recovery performance compared to the pure biochar. Depending on the nature of the targeted wastewater, the phosphorus recovery mechanisms were different. Specifically, in phosphate deionized water solution without

ammonium, adsorption was predominant, but in animal wastewater containing both phosphate and ammonium, struvite precipitation was found to be the driving force of phosphorus fixation.

In animal wastewater, the phosphorus recovery performance was impacted by the initial wastewater concentration. This was because the concentrations of phosphate and ammonium had to reach the solubility product limitation before struvite formation took place. This phenomenon led the sorbents to show greater phosphorus recovery in the wastewater with higher initial concentrations. In addition, results showed that before the Mg was depleted, the resulting phosphorus concentration might be a constant value around the solubility product limit. Furthermore, through mineralogical characterization, struvite formation was confirmed. As for the optimal experimental conditions, since the struvite formation was the dominating process, more phosphorus was recovered at higher pH (i.e., pH 9 as tested in this research) corresponding to lower struvite solubility. Finally, animal wastewater often contains a high level of alkalinity, and alkalinity significantly decreased the capability of sorbents recovering phosphorus due to the carbonate competition for Mg^{2+} . For the same reason, since the Olsen-P soil test uses bicarbonate as the main reagent, Olsen-P extracted more phosphorus than Mehlich-3 and Bray and Kurtz P1 tests. This indicated that struvite recovered phosphorus can be released in calcareous soils effectively. Magnesium silicate shared all the trends and mechanisms as the Mg-chars.

Low-cost alternatives for Mg amendment were tested in the making of Mg-chars. These alternatives included brucite, periclase, dolomite, seawater, sea bittern, and desalination reject brine. And a strategy of synthesizing CSH using hydrated lime was also tested. This research found that using $Mg(OH)_2$ and bittern yielded similar phosphorus recovery compared to Mg-char produced from $MgCl_2$. And from the model animal wastewater in this research, the post-

phosphorus-exposure (spent) Mg-char ($Mg(OH)_2$) and Mg-char (bittern) can contain 182 and 198 mg phosphorus per g of the spent sorbents, respectively. Although CSH recovered phosphorus through adsorption and had lower effectiveness than Mg-chars, spent CSH can contain 46 mg phosphorus/g. The phosphorus contents in the spent Mg-chars were equal to 76% and 82% of the commercial fertilizer MAP.

The spent (phosphorus-loaded) sorbents were added to sand columns resulting a phosphorus loading at 0.9 mg phosphorus per 20 g sand (equivalent of 115 kg phosphorus per hectare), and tested for phosphorus release at pH 8.5, 7.0, and 5.5, with and without goethite or kaolinite. The two Mg-chars were excellent at phosphorus release at all pH values, achieving 83%-100% release of the recovered phosphorus in five pore volumes, which is equivalent to 240 mm rainfall or irrigation. While soil pH had insignificant influence on phosphorus release at pH 5.5 and 7.0 for two Mg-chars, at pH 8.5 the phosphorus release was obviously hindered due to the lower solubility of struvite at this pH condition. In comparison with the two Mg-chars, the spent CSH released phosphorus in a considerably slower manner. In addition, the soil minerals goethite and kaolinite retained released phosphorus to a large extent, and goethite was the greater phosphorus sink that consumed over 80% of the released phosphorus at pH 5.5 and 7.0. Soil pH had great influence on how goethite and kaolinite fixed the phosphate. At lower pH conditions such as pH 5.5 and 7.0, the surface of the minerals was more positively charged than at pH 8.5 due to their point of zero charge. Thus, at pH 8.5, the impact of the minerals on the solution phosphate concentration was lower. Overall, the sorbents showed great potential for recovering phosphorus and being used as fertilizers, and the application strategy should depend on the consideration of soil chemistry conditions to reach the fertilization goal. Namely, considering a certain amount of goethite and kaolinite minerals contained in soil, if the soil is in the acidic

region, more phosphorus would be needed compared to the alkaline soils to maintain phosphorus at a certain level.

Life cycle environmental impact and cost assessment focused on the comparison of using Mg-char ($Mg(OH)_2$), Mg-char (bittern), and CSH for phosphorus recovery and reuse versus using the commercial fertilizer MAP. The LCA revealed that the two Mg-chars had significantly lower environmental impact in most of the categories than MAP, and Mg-char (bittern) had the lowest impact. Without considering transportation of all the raw materials, the production of $Mg(OH)_2$ contributed the most to Mg-char ($Mg(OH)_2$) in more than half of the categories while corn farming was the process with the greatest impacts for Mg-char (bittern). CSH had dramatically higher impact than other sorbents and MAP from the high demand of raw materials including rice husk and chemicals due to the relatively lower phosphorus content in spent CSH than in spent Mg-chars and to the slower phosphorus release characteristics to provide the required amount of phosphorus. The three sorbents all employed pyrolysis for the synthesis of char or ash, and pyrolysis was the predominant process contributing to impacts in categories such as climate change, terrestrial acidification, marine eutrophication, and particulate matter formation. For conditions where spent materials had better phosphorus release, for instance at pH 7.0 compared to pH 8.5, impacts were proportionally lower, due to the lower material need for releasing same amount of phosphorus. When transportation was considered, the two Mg-chars continued to show better results than MAP by posing less impact in half of the modeled impact categories.

As for cost analysis, the two Mg-chars had significantly lower estimated costs than MAP in all scenarios even considering transportation. For Mg-char ($Mg(OH)_2$), $Mg(OH)_2$ accounted for the major portion of the overall cost, as high as 90%. And for Mg-char (bittern), since the

intrinsic cost was very low, the addition of transportation became responsible for much of the cost, compared to obtaining corn cobs when transportation was not considered. Additionally, chemicals contributed the most to the overall cost of CSH when no transportation was needed, and it was cost of transportation when it was added. Overall, the two Mg-chars have the potential to contribute to a more sustainable phosphorus cycle and to be used to substitute commercial fertilizer with less environmental burden and overall cost. For agricultural regions where raw biomass production, excessive phosphorus from livestock, and wastewater treatment facility are adjacent to each other, using Mg-char for phosphorus management would be ideal, especially for regions in coastal area with great supply of sea bittern.

5.2 Recommendations for future work

Future research opportunities based on this research lie in areas including but not limited to 1) evaluation of the sorbents in real animal wastewaters; 2) upscale of both the sorbents themselves and the phosphorus recovery settings; 3) consider alternative biomass treatment methods to potentially replace pyrolysis.

Although modeled animal wastewaters were used in this research containing targeted constituents such as phosphate and ammonium, as well as alkalinity, a more realistic evaluation of the sorbents in real animal wastewaters can be beneficial. There are many other constituents in animal wastewater such as Cl^-. Although they do not interact directly with phosphorus recovery, they can pose impact through determining the ionic strength of the wastewater, which affects the solubility of the precipitates. In addition, the phosphorus incorporated by plants and animals is often converted to its organic form. It was beyond the scope of this research to address the interactions between the sorbent with organic phosphorus. Therefore, more insights could come from evaluating the sorbents in real animal wastewater.

The sorbents in this research were in form of fine powders, which can potentially be problematic in larger scale industrial operations. Larger sorbent particles can be beneficial for separation from other precipitates after coagulation and flocculation. Furthermore, this research only tested the phosphorus recovery in small scale batch settings, therefore, testing the sorbents in a full-scale pilot setting can be beneficial for the realization of the strategy. Specifically, this can provide recommendations about, on the one hand, the potentially different sorption kinetics that enlarged sorbents may have which is essential for maximizing the phosphorus uptake, and on the other hand, the logistics of incorporating the strategy into common wastewater treatment practices to achieve less waste production and lower environmental impacts.

Since the environmental impact from pyrolysis was significant, alternative biomass treatment approaches should be evaluated. The preliminary study in this research tried to digest straws for silicate extraction, however, the procedure required extremely concentrated acid or base solutions. Although further phosphorus recovery and reuse, as well as LCA, did not account for this method, but if alternatives or optimizations such as using less harmful chemicals and reusing the digest solutions can be evaluated, better ways of synthesizing CSH might be found. Similarly, chemical activation of the biochar could be an optimization allowing less overall environmental impact, since biochar produced from pyrolysis coupled with chemical activation might need less energy input and result in higher product yield. Hence the research on the phosphorus recovery/release performance and associated environmental impacts of biochars with the optimized production would contribute greatly to the search for the better solution.